

## Supporting Information

### Leptochelins A-C, Cytotoxic Metallophores Produced by Geographically Dispersed *Leptothoe* Strains of Marine Cyanobacteria

Nicole E. Avalon,<sup>1+</sup> Mariana A. Reis,<sup>2+</sup> Christopher C. Thornburg,<sup>3+</sup> R. Thomas Williamson,<sup>4</sup> Daniel Petras,<sup>5,6,7</sup> Allegra T. Aron,<sup>5,8</sup> George F. Neuhaus,<sup>3</sup> Momen Al-Hindy,<sup>1</sup> Jana Mitrevska,<sup>1</sup> Leonor Ferreira,<sup>2</sup> João Morais,<sup>2</sup> Yasin El Abiead,<sup>5</sup> Evgenia Glukhov,<sup>1</sup> Kelsey L. Alexander,<sup>1,9</sup> F. Alexandra Vulpanovici,<sup>3</sup> Matthew J. Bertin,<sup>1</sup> Syrena Whitner,<sup>1</sup> Hyukjae Choi,<sup>10</sup> Gabriella Spengler,<sup>11</sup> Kirill Blinov,<sup>12</sup> Ameen M. Almohammadi,<sup>13</sup> Lamiaa A. Shaala,<sup>14</sup> William R. Kew,<sup>15</sup> Ljiljana Paša-Tolić,<sup>15</sup> Daa T. A. Youssef,<sup>16,17</sup> Pieter C. Dorrestein,<sup>5</sup> Vitor Vasconcelos,<sup>2,\*</sup> Lena Gerwick,<sup>1</sup> Kerry L. McPhail,<sup>3,\*</sup> William H. Gerwick<sup>1,5,\*</sup>

<sup>1</sup>Center for Marine Biotechnology and Biomedicine, Scripps Institution of Oceanography, UCSD, La Jolla, CA 92093, USA; <sup>2</sup> CIIMAR/CIMAR, Interdisciplinary Centre of Marine and Environmental Research, University of Porto, Matosinhos 4450-208, Portugal; <sup>3</sup>College of Pharmacy, Oregon State University, Corvallis, OR 97331, USA; <sup>4</sup>Department of Chemistry and Biochemistry, University of North Carolina Wilmington, Wilmington, NC 28403, USA; <sup>5</sup>Skaggs School of Pharmacy and Pharmaceutical Sciences, UCSD, La Jolla, CA 92093, USA; <sup>6</sup>University of California Riverside, Department of Biochemistry, Riverside, CA 92507, USA; <sup>7</sup>University of Tuebingen, CMFI Cluster of Excellence, Tuebingen 72706, Germany; <sup>8</sup> Department of Chemistry and Biochemistry, University of Denver, Denver, CO, 80210, USA; <sup>9</sup>Department of Chemistry and Biochemistry, UCSD, La Jolla, CA 92093, USA; <sup>10</sup>College of Pharmacy, Yeungnam University, Gyeongsan, Gyeong-buk 38541, South Korea; <sup>11</sup>Department of Medical Microbiology, Albert Szent-Györgyi Health Center and Albert Szent-Györgyi Medical School, University of Szeged, Szeged 6725, Hungary; <sup>12</sup>Molecule Apps, LLC, Corvallis, Oregon 97330, USA; <sup>13</sup>Department of Pharmacy Practice, Faculty of Pharmacy, King Abdulaziz University, Jeddah 21589, KSA; <sup>14</sup>Suez Canal University Hospital, Suez Canal University, Ismailia 41522, Egypt; <sup>15</sup>Environmental Molecular Sciences Laboratory, Pacific Northwest National Laboratory, Richland, WA 99354, USA; <sup>16</sup>Department of Natural Products, Faculty of Pharmacy, King Abdulaziz University, Jeddah 21589, KSA; <sup>17</sup>Department of Pharmacognosy, Faculty of Pharmacy, Suez Canal University, Ismailia 41522, Egypt

+ These authors contributed equally to the project.

\*Co-corresponding authors: William H. Gerwick, Kerry L. McPhail, and Vitor Vasconcelos

**Email:** wgerwick@health.ucsd.edu, kerry.mcphail@oregonstate.edu, vmvascon@fc.up.pt

#### This PDF file includes:

Supporting text:  
Experimental Materials and Methods  
Additional Biological Activity Results  
Physical Data  
Tables S1 to S13  
Figures S1 to S73  
SI References

<b>1. Experimental Section</b> .....	6
<b>1.1 Sampling, Cyanobacterial Isolation, and Culture Conditions</b> .....	6
<b>1.2 Genomics</b> .....	6
1.2.1 DNA Isolation and Genome Assembly .....	6
1.2.2 Phylogenetic Analysis.....	7
1.2.3 Bioinformatics for BGC Identification and Comparative Genomics .....	7
<b>1.3 Chemical Analyses</b> .....	7
1.3.1 General Chemistry Methods.....	7
1.3.2 Isolation of Leptochelins .....	8
1.3.3. UHPLC-MS <sup>2</sup> .....	9
1.3.4. 21T FT-ICR Microflow HPLC-UHR-MS <sup>2</sup> .....	9
1.3.5. Fragmentation Trees .....	9
1.3.6. Methylation Procedure for Leptochelin A.....	9
1.3.7. Hydrolysis and Marfey's Analysis .....	9
1.3.8. Post-LC Metal Infusion Metabolomics setup .....	10
<b>1.3 Copper Toxicity Assays</b> .....	10
<b>1.4 Molecular Modeling</b> .....	11
<b>1.5 Biological Activity Assays</b> .....	11
1.6.1 Cytotoxicity Assays with NCI-H460 and SF188 cell lines.....	11
1.6.2 Cytotoxicity Assays with D283-med Cell Lines.....	11
1.6.3 Cytotoxicity Assays with HCT 116 2D Monolayer Model.....	12
1.6.4 Cytotoxicity Assays using a 3D Cancer Cell Model.....	12
1.6.5 Cytotoxicity Assays with Mouse Lymphoma T-cells .....	12
1.6.6 Multidrug Resistance Reversal Assay .....	12
<b>2. Additional Biological Activity Results</b> .....	13
<b>2.1 Results of Cytotoxicity Assays using a 3D Cancer Cell Model</b> .....	13
<b>2.2. Results Discussing Cancer Multidrug Resistance Reversal</b> .....	13
<b>3. Physical Data</b> .....	13
<b>3.1 Leptochelin A (1)</b> .....	13
<b>3.2 Leptochelin B (2)</b> .....	13
<b>3.3 Leptochelin C (3)</b> .....	13
<b>3.4 Leptochelin A + Zn</b> .....	13
<b>3.5 Leptochelin B + Zn</b> .....	13

<b>3.6 Leptochelin C + Zn</b> .....	13
<b>4. Tables</b> .....	14
<b>Table S1.</b> Metadata for the collections of the three leptochelin-producing cyanobacteria of the genus <i>Leptothoe</i> .....	14
<b>Table S2.</b> 16S rRNA gene sequence partial similarity matrix .....	15
<b>Table S3.</b> NMR Data for Non-Metal Bound Leptochelins A (1), B (2), and C (3) .....	16
<b>Table S4.</b> NMR Data for Leptochelin A (1), B (2), and C (3) coordinated with zinc .....	17
<b>Table S5.</b> NMR Spectroscopic Data comparing the chemical shifts for $^{13}\text{C}$ $\delta$ for leptochelin A (1) with those of leptochelin B (2) and leptochelin C (3) .....	18
<b>Table S6.</b> NMR Spectroscopic Data comparing the chemical shifts for $^1\text{H}$ $\delta$ for leptochelin A (1), leptochelin B (2), and leptochelin C (3) .....	19
<b>Table S7.</b> Characteristics of the genome assemblies of the three leptochelin producers .....	20
<b>Table S8.</b> Comparison of the fragment masses from leptochelin A (1) and methylated leptochelin A (4) .....	21
<b>Table S9.</b> Similarity scores based on clinker analysis of the <i>lec</i> BGC from all three leptochelin producers .....	23
<b>Table S10.</b> Adenylation domain substrate specificities using antiSMASH prediction, NRPSSP, and NRPS Predictive Blast .....	27
<b>Table S11.</b> Metadata for collections of other cyanobacteria used in the copper toxicity assays .....	27
<b>Table S12.</b> Grading scale for cyanobacterial culture health and viability from the copper toxicity assays .....	28
<b>Table S13.</b> Cytotoxicity $\text{IC}_{50}$ values and standard deviations for leptochelins A (1), B (2) and C (3) .....	29
<b>5. Figures</b> .....	30
<b>Fig. S1.</b> Maximum likelihood (ML) phylogenetic tree based on 73 16S rRNA gene sequences of cyanobacterial strains .....	30
<b>Fig. S2.</b> $\text{MS}^2$ fragmentation pattern for leptochelin A (1) with major ions notated .....	31
<b>Fig. S3.</b> Fragmentation trees of the $\text{MS}^2$ CID data for leptochelin A (1) .....	32
<b>Fig. S4.</b> Fragmentation trees of the $\text{MS}^2$ HCD data for leptochelin A (1) .....	33
<b>Fig. S5.</b> $\text{MS}^2$ fragmentation pattern for methylated leptochelin A (4) .....	34
<b>Fig. S6.</b> $^{13}\text{C}$ NMR spectrum for leptochelin A (1) in $\text{CDCl}_3$ (100 MHz) .....	35
<b>Fig. S7.</b> $^1\text{H}$ NMR spectrum for leptochelin A (1) in $\text{CDCl}_3$ (400 MHz) .....	35
<b>Fig. S8.</b> Multiplicity-edited HSQC spectrum for leptochelin A (1) in $\text{CDCl}_3$ (400 MHz, 100 MHz) .....	36
<b>Fig. S9.</b> HSQC-TOCSY spectrum for leptochelin A (1) in $\text{CDCl}_3$ (400 MHz) .....	36
<b>Fig. S10.</b> HMBC spectrum for leptochelin A (1) in $\text{CDCl}_3$ (400 MHz) .....	37
<b>Fig. S11.</b> $^1\text{H}$ - $^1\text{H}$ COSY spectrum for leptochelin A (1) in $\text{CDCl}_3$ (400 MHz) .....	37
<b>Fig. S12.</b> ROESY spectrum for leptochelin A (1) in $\text{CDCl}_3$ (500 MHz) .....	38
<b>Fig. S13.</b> $^1\text{H}$ - $^{15}\text{N}$ gHMBC spectrum for leptochelin A (1) in $\text{CDCl}_3$ (500 MHz) .....	38
<b>Fig. S14.</b> $\text{MS}^3$ fragmentation series of the N-terminal fragments for leptochelin A (1) .....	39
<b>Fig. S15.</b> IR Spectrum for leptochelin A (1) .....	40

<b>Fig. S16.</b> $^{13}\text{C}$ NMR spectrum for zinc-bound leptochelin A ( <b>1</b> ) in $\text{CDCl}_3$ (150 MHz) .....	40
<b>Fig. S17.</b> $^1\text{H}$ NMR spectrum for zinc-bound leptochelin A ( <b>1</b> ) in $\text{CDCl}_3$ (600 MHz).....	41
<b>Fig. S18.</b> Multiplicity-edited HSQC spectrum for zinc-bound leptochelin A ( <b>1</b> ) in $\text{CDCl}_3$ (600 MHz).....	41
<b>Fig. S19.</b> $^1\text{H}$ - $^1\text{H}$ COSY spectrum for zinc-bound leptochelin A ( <b>1</b> ) in $\text{CDCl}_3$ (600 MHz) .....	42
<b>Fig. S20.</b> HMBC spectrum for zinc-bound leptochelin A ( <b>1</b> ) in $\text{CDCl}_3$ (600 MHz) .....	42
<b>Fig. S21.</b> $^{13}\text{C}$ NMR spectrum for leptochelin B ( <b>2</b> ) in $\text{CDCl}_3$ (200 MHz).....	43
<b>Fig. S22.</b> $^1\text{H}$ NMR spectrum for leptochelin B ( <b>2</b> ) in $\text{CDCl}_3$ (800 MHz) .....	43
<b>Fig. S23.</b> Multiplicity-edited HSQC spectrum for leptochelin B ( <b>2</b> ) in $\text{CDCl}_3$ (800 MHz) .....	44
<b>Fig. S24.</b> $^1\text{H}$ - $^1\text{H}$ COSY spectrum for leptochelin B ( <b>2</b> ) in $\text{CDCl}_3$ (800 MHz) .....	44
<b>Fig. S25.</b> HMBC spectrum for leptochelin B ( <b>2</b> ) in $\text{CDCl}_3$ (800 MHz).....	45
<b>Fig. S26.</b> $^{13}\text{C}$ NMR spectrum for zinc-bound leptochelin B ( <b>2</b> ) in $\text{CDCl}_3$ (150 MHz) .....	45
<b>Fig. S27.</b> $^1\text{H}$ NMR spectrum for zinc-bound leptochelin B ( <b>2</b> ) in $\text{CDCl}_3$ (600 MHz).....	46
<b>Fig. S28.</b> Multiplicity-edited HSQC spectrum for zinc-bound leptochelin B ( <b>2</b> ) in $\text{CDCl}_3$ (600 MHz).....	46
<b>Fig. S29.</b> $^1\text{H}$ - $^1\text{H}$ COSY spectrum for zinc-bound leptochelin B ( <b>2</b> ) in $\text{CDCl}_3$ (600 MHz) .....	47
<b>Fig. S30.</b> HMBC spectrum for zinc-bound leptochelin B ( <b>2</b> ) in $\text{CDCl}_3$ (600 MHz) .....	47
<b>Fig. S31.</b> $^{13}\text{C}$ NMR spectrum for leptochelin C ( <b>3</b> ) in $\text{CDCl}_3$ (150 MHz).....	48
<b>Fig. S32.</b> $^1\text{H}$ NMR spectrum for leptochelin C ( <b>3</b> ) in $\text{CDCl}_3$ (600 MHz).....	48
<b>Fig. S33.</b> Multiplicity-edited HSQC spectrum for leptochelin C ( <b>3</b> ) in $\text{CDCl}_3$ (600 MHz) .....	49
<b>Fig. S34.</b> $^1\text{H}$ - $^1\text{H}$ COSY spectrum for leptochelin C ( <b>3</b> ) in $\text{CDCl}_3$ (600 MHz).....	49
<b>Fig. S35.</b> HMBC spectrum for leptochelin C ( <b>3</b> ) in $\text{CDCl}_3$ (600 MHz).....	50
<b>Fig. S36.</b> $^{13}\text{C}$ NMR spectrum for zinc-bound leptochelin C ( <b>3</b> ) in $\text{CDCl}_3$ (150 MHz) .....	50
<b>Fig. S37.</b> $^1\text{H}$ NMR spectrum for zinc-bound leptochelin C ( <b>3</b> ) in $\text{CDCl}_3$ (600 MHz) .....	51
<b>Fig. S38.</b> Multiplicity-edited HSQC spectrum for zinc-bound leptochelin C ( <b>3</b> ) in $\text{CDCl}_3$ (600 MHz).....	51
<b>Fig. S39.</b> $^1\text{H}$ - $^1\text{H}$ COSY spectrum for zinc-bound leptochelin C ( <b>3</b> ) in $\text{CDCl}_3$ (600 MHz) .....	52
<b>Fig. S40.</b> HMBC spectrum for zinc-bound leptochelin C ( <b>3</b> ) in $\text{CDCl}_3$ (600 MHz).....	52
<b>Fig. S41.</b> Fragmentation trees of leptochelin B ( <b>2</b> ) CID $\text{MS}^2$ scan .....	53
<b>Fig. S42.</b> Fragmentation trees of leptochelin B ( <b>2</b> ) HCD $\text{MS}^2$ scan.....	54
<b>Fig. S43.</b> $\text{MS}^3$ fragmentation series of the N-terminal fragments for leptochelin B ( <b>2</b> ).....	55
<b>Fig. S44.</b> Differences in $^{13}\text{C}$ chemical shifts between metal-free leptochelins and differences in $^1\text{H}$ chemical shifts of free and Zn-bound leptochelin A ( <b>1</b> ) .....	56
<b>Fig. S45.</b> Retrobiosynthetic analysis of leptochelin A ( <b>1</b> ) .....	57
<b>Fig. S46.</b> Phylogenetic tree of the <i>lec</i> TE domain with select TE domains from BGCs linked to known natural products.....	58
<b>Fig. S47.</b> Determination of the absolute configuration of the D-serine residue in leptochelin A ( <b>1</b> ).....	59

<b>Fig. S48.</b> Determination of the absolute configuration of the L-bromophenylalanine residue in leptochelin A (1) .	59
<b>Fig. S49.</b> Determination of the absolute configuration of the 2-Me-L-cysteine residue in leptochelin A (1) .....	60
<b>Fig. S50.</b> Newman projections reflecting the NOE correlations that were key in determining the relative configuration from C-9 to C-11 in leptochelin A (1) .....	60
<b>Fig. S51.</b> Molecular modeling of zinc-bound leptochelin A (1) .....	61
<b>Fig. S52.</b> Overview of the methods used to determine the absolute configuration of leptochelin A (1) .....	61
<b>Fig. S53.</b> Early molecular network from GNPS revealing the potential for leptochelin analogues with metal binding properties .....	62
<b>Fig. S54.</b> UV chromatogram of <i>Leptothoe</i> extracts in iron replete and iron deplete media.....	62
<b>Fig. S55.</b> Extracted ion chromatograms from metal-binding studies using pure leptochelin B (2).....	63
<b>Fig. S56.</b> Extracted ion chromatograms from metal-binding studies using a mixture of leptochelins A (1) and B (2) .....	63
<b>Fig S57.</b> Extracted ion chromatograms from metal-binding studies using semipure leptochelin A (1) under pH adjusted conditions. ....	63
<b>Fig. S58.</b> Summary of copper toxicity assay reflecting organism health at Day 14 post-inoculation for <i>Leptothoe</i> sp. ISB3NOV94-8A and four <i>Leptolyngbya</i> spp. ....	64
<b>Fig. S59.</b> Copper toxicity assay results for <i>Leptothoe</i> sp. ISB3NOV94-8A.....	64
<b>Fig. S60.</b> Copper toxicity assay results for <i>Leptolyngbya</i> sp. ISB3NOV94-8B .....	65
<b>Fig. S61.</b> Copper toxicity assay results for <i>Leptolyngbya</i> sp. PAP09SEP10-2A.....	65
<b>Fig. S62.</b> Copper toxicity assay results for <i>Leptolyngbya</i> sp. ASX22JUL14-2.....	66
<b>Fig. S63.</b> Photographs of <i>Leptothoe</i> sp. ISB3NOV94-8A cultures on Day 14 of the copper toxicity assays .....	67
<b>Fig. S64.</b> Photographs of <i>Leptolyngbya</i> sp. ISB3NOV94-8B cultures on Day 14 of the copper toxicity assays....	68
<b>Fig. S65.</b> Photographs of <i>Leptolyngbya</i> sp. PAP09SEP10-2A cultures on Day 14 of the copper toxicity assays .	69
<b>Fig. S66.</b> Photographs of <i>Leptolyngbya</i> sp. ASX22JUL14-2 cultures on Day 14 of the copper toxicity assays ....	70
<b>Fig. S67.</b> LC-MS tracings showing no significant change in ion abundance for the [M + H] <sup>+</sup> of leptochelin A (1) with varying concentrations of copper in the growth media .....	71
<b>Fig. S68.</b> Zinc-bound leptochelins A (1) and C (3) reverse multidrug resistance phenotype .....	72
<b>Fig. S69.</b> The dose response curve for leptochelin A (1) in NCI-H460 cell line with three biological replicates ....	73
<b>Fig. S70.</b> The dose response curves for leptochelin A (1) and Zn-bound leptochelin A in human NCI-H460 and HeLa cervical carcinoma cell lines .....	73
<b>Fig. S71.</b> The dose response curves for leptochelin A (1) in human D283-med medulloblastoma cell lines.....	74
<b>Fig. S72.</b> The dose response curves for leptochelin A (1) in human SF188 glioblastoma cell lines.....	74
<b>Fig. S73.</b> Biological activity of the leptochelins in HCT 116 spheroids.....	75
<b>6. SI Appendix References</b> .....	76

# 1. Experimental Section

## 1.1 Sampling, Cyanobacterial Isolation, and Culture Conditions

Sampling of cyanobacteria was performed in November of 1994 at the North end of the island of Sulawesi in Indonesia (**SI Appendix, Table S1**). The original specimen of *Leptothoe* sp. ISB3NOV94-8A (original collection code of ISN3NOV94-8) was obtained by hand collection while scuba diving. The culture was subsequently inoculated into a Fernback flask with 1.5 L of SWBG11 medium (artificial sea water) and grown at 26 – 28°C with a 16 h light/8 h dark regimen. A mono-cyanobacterial culture was later established and has been maintained in the Gerwick Lab culture collection.

A mat-forming cyanobacterium was hand collected via SCUBA from hard coral substrate in the Red Sea in May of 2007 (**SI Appendix, Table S1**). The glycerol-preserved subsample was revived using an enrichment medium (1), resulting in several live isolates of cyanobacteria. The monoclonal isolate (RS02), characterized as as a *Leptothoe* sp., was isolated microscopically from serial dilutions of enrichment cultures in which strong growth was present and maintained in liquid medium. This isolate was given the strain code EHU-05/26/07-4 based on the original sample collection code.

A sampling campaign was carried out in April 2018 on the island of São Vicente, which is part of the archipelago of Cape Verde, located in the Atlantic Ocean, off the West African coast. One of the samples was obtained from the intertidal zone in Baía das Gatas (**SI Appendix, Table S1**) by scraping the surface of a rock with a clean knife blade. The sample was kept in a polypropylene tube with Z8 medium supplemented with 25 g l<sup>-1</sup> of synthetic sea salts (Tropic Marine) and 10 µg ml<sup>-1</sup> vitamin B12 (Sigma Aldrich, Merck, Saint Louis, MO, USA) until further analysis. After arrival at the laboratory, the environmental sample was observed under Leica DMLB light microscope coupled to a Leica ICC50 HD digital camera (Leica Microsystems, Germany). The original sample was clearly dominated by a large, reddish brown cyanobacterial filament (tentatively a "*Lyngbya*" = *Moorena*) mixed with other thinner filaments of cyanobacteria. The sample was enriched in Z8 medium and maintained under controlled temperature conditions (21-23°C), a photoperiod of 14h light/10h dark cycles and a light intensity of 20 µmol photons m<sup>-2</sup> s<sup>-1</sup>. After 2-3 weeks of growth, aliquots were transferred onto solid Z8 medium plates with 1.5% agarose using an inoculation loop. When isolated filaments were detected, these were picked with the help of a sterile surgical blade and transferred to 50 mL culture flasks with liquid medium, growing under the conditions as described above. This sample led to the isolation of the strain *Leptothoe* sp. LEGE 181152 that has been deposited and kept at the Blue Biotechnology and Ecotoxicology Culture Collection (LEGE-CC) - <https://lege.ciimar.up.pt/>.

## 1.2 Genomics

### 1.2.1 DNA Isolation and Genome Assembly

***Leptothoe* sp. ISB3NOV94-8A:** Total genomic DNA was extracted using the QIAGEN Genomic DNA extraction kit (Qiagen, Valencia, CA, #13323), following the protocol for 20/G Genomic-tip columns with slight modifications. Protocol modifications included the use of 10 µL of Proteinase K solution and increased incubation times for a total of two hours total for both the 37°C and 50°C incubations during cell lysis stages to optimize DNA recovery. The final DNA product was dissolved overnight in deionized water at 4°C according to protocol. DNA was then quantified using a Qubit fluorometer 3.0 and 260/280 nm scores were checked using a Nanodrop 2000c spectrophotometer. Libraries were then prepared using the Oxford Nanopore Ligation Sequencing kit (Oxford Nanopore Technologies, UK, #SQK-LSK110), and sequences using Oxford Nanopore Technologies MinION device using the Flongle cells (Oxford Nanopore Technologies, UK, #EXP-FLP002, #EXP-WSH002). Raw nanopore sequencing data was first basecalled using Guppy v3.2.2, and subsequently evaluated using FastQC (2) to assess sequence quality. Following initial quality checks, Nanopore reads were combined with reads previously sequenced using Illumina technology, and a hybrid genome assembly was performed using Unicycler v0.4.8 (3) with default parameters. The contigs and scaffolds obtained from the assembly were subjected to genome binning using MetaBAT2 (4) in order to separate cyanobacterial genomes from other bacterial strains present in co-culture. The quality of the resulting genome bins were assessed using CheckM v1.1.2. (5) Cyanobacterial genome bins were then identified and used for biosynthetic gene cluster annotation using antiSMASH v7.0 (6). The genome assembly associated with the *Leptothoe* sp. ISB3NOV94-8A genome were deposited in NCBI GenBank under accession number SAMN38524433.

***Leptothoe* sp. EHU-05/26/07-4:** Cells were added from 6-well cultures to a glass fiber filter and washed with sterile instant ocean (IO). The washed cells were added to a 15 mL Falcon tube containing 10 mL sterile IO, sonicated and vortexed for 10 minutes, and washed once more with sterile IO. These washed cells were placed in a mortar and liquid N<sub>2</sub> was added to freeze the cells. The cells were then ground into a fine powder and added to 1.5 mL Eppendorf tube. Total genomic DNA was extracted using the Promega Wizard Genomic DNA extraction protocol for plant tissues with slight modifications. After initial incubation with 600 µL lysis solution (65 °C x 15 min), the cells became gel-like and an additional 600 µL of the lysis solution was added and the incubation period at 65 °C was repeated. Due to coloration of the DNA pellet, a Qiagen spin column was used to clean up the DNA before storage at -80 °C. Sequencing was performed using Oxford Nanopore Technologies, UK) with a PromethION system, (MinKNOW v.22.05.10, Bream v.7.1.4, Configuration v.5.1.5, MinKNOW Core v.5.1.0). Raw nanopore sequencing data was basecalled using Guppy v.6.1.5 (7). Following quality checks, duplex chimeric reads were split using duplex\_tools. NanoFlit v2.7.1 (8) was used to preprocess reads and read length was filtered using Porechop v0.6.7 (9). Genomic assembly was performed with Flye v2.9.1 (10). Binning was performed using Metabat v2.12.1 (4) to separate cyanobacterial genomes from other bacterial strains present in co-culture and the appropriate bin was selected based on the similarity to the *Leptothoe* sp. ISB3NOV94-8A genome assembly. The biosynthetic gene clusters in the resulting cyanobacterial genome were annotated using antiSMASH v7.0 (6). The genome assembly associated with *Leptothoe* sp. EHU-05/26/07-4 was deposited in NCBI GenBank under accession number SAMN38764028.

***Leptothoe* sp. LEGE181152:** Marine cyanobacteria cultures were vacuum filtered using sterile culture techniques and subsequently dried by blotting filtered cultures on a Kim-Wipe tissue to remove excess salt and media. Once adequately dried, cyanobacteria cells were placed in a chilled mortar, flash frozen using liquid nitrogen, and subject to mechanical lysis using a pestle until cells were pulverized into a fine powder. The resulting powder was promptly scraped into a sterile 2 mL Eppendorf tube for DNA extraction. Total genomic DNA was extracted from a fresh pellet of 50 mL of culture of the filamentous cyanobacterial

strain *Leptothoe* sp. LEGE 181152 using the commercial NZY Plant/Fungi gDNA Isolation kit (NZYTech), according to the manufacturer's instructions. Quality of the gDNA was evaluated in a DS-11 FX Spectrophotometer (DeNovix) and 1% agarose gel electrophoresis, before genome sequencing. The genome of *Leptothoe* sp. LEGE 181152 was sequenced at MicrobesNG using Illumina platform with 2 × 250 bp paired-end libraries. Because the cyanobacterial culture was not axenic, the contigs obtained were analyzed using the binning tool MaxBin2 (V2.2.4) (11) and CheckM (v1.0.18) (5) within Kbase software (12) to obtain only cyanobacterial contigs. Sequence data associated with *Leptothoe* sp. LEGE 181152 genome were deposited in NCBI GenBank under accession number JASATU000000000 (BioProject - PRJNA960947).

### 1.2.2 Phylogenetic Analysis

A total of 73 sequences were used in the final phylogenetic analysis, including *Gloeobacter violaceus* PCC 7421 as the outgroup. This included 70 cyanobacterial sequences, including type and reference strains retrieved from GenBank (National Center for Biotechnology Information, NCBI, Bethesda, MD, USA), and three 16S rRNA gene sequences obtained from LEGE 181152, ISB3NOV94-8A and EHU-05/26/07-4 genomes. Multiple sequence alignment was constructed using MAFFT v7.450 (13, 14) and sequences were manually proofread and edited. The best substitution model for ML-based analyses was chosen using jModelTest 2 software (15) using the Akaike information criterion. Maximum likelihood (ML) analysis was carried out using substitution model GTR+G+I with 1000 bootstrap resampling replicates using the IQ-TREE 2 software (16). The final phylogenetic tree was edited on iTOL (Interactive Tree of Life) (17) and Inkscape 1.2 (18).

### 1.2.3 Bioinformatics for BGC identification and Comparative Genomics

The putative biosynthetic gene cluster for the leptochelins was identified using automated annotation and manual bioinformatic tools. Enzymatic reactions and biosynthetic logic were based on homology analysis. The BGCs in the genomes of each of the leptochelin producers in this study were identified using antiSMASH (v.7.0-beta) (6) using the suite of annotation options. These annotations were expanded using active site and motif identification, protein family homology analysis, and searches for conserved domains. Additionally, BLASTP searches were used for confirmation of enzymatic domain identification. Adenylation specificity was analyzed using antiSMASH (6), NRPSp (19), and NRPS Predictive Blast (20). Comparison of the BGCs from the three producing *Leptothoe* strains was performed using Clinker and visualized using clustermap.js (21). The default parameters were used for synteny evaluation with visualization of links in Fig. 4B increased to a threshold of 0.5. For evaluation of thioesterase domains, MIBiG v.3.0 (22) was used to obtain the amino acid sequences of thioesterase domains of BGCs with compound links that led to either hydrolytic release of a linear compound or cyclization and release of the compound. A multiple sequence alignment was created in Geneious Prime v.2023.2.1 with ClustalOmega. A Jukes-Cantor Genetic Distance Model was used to create a Neighbor-Joining Tree with bootstrap resampling with 1000 replicates and a support threshold of 50%. A condensation domain from the *lec* BGC (4\_149) was used as the outgroup.

## 1.3 Chemical Analyses

### 1.3.1 General Chemistry Methods

Optical rotations were measured using a P-2000 polarimeter (JASCO International Co. Ltd., Tokyo, Japan) with SpectraManager 2.14.02 software. Infrared spectra were collected on a Nicolet iS5 FTIR spectrometer (ThermoScientific) with OMNIC 9.8.372 software. The UV-Vis spectrum was acquired on a 1600PC spectrophotometer (VWR) with a 1 cm path length quartz cuvette.

NMR acquisition at University of California San Diego: 1D NMR and 2D NMR spectra were acquired using a Bruker Avance Neo 800 NMR with a triple resonance TXO cryoprobe connected to a Linux workstation for instrument control and data processing. NMR spectra were referenced to residual solvent CDCl<sub>3</sub> signals ( $\delta_{\text{H}}$  7.26 and  $\delta_{\text{C}}$  77.16) as internal standards. NMR spectra were analyzed using MestReNova v.14.3.0-30573 (Mestrelab, Santiago de Compostela, Spain). <sup>1</sup>H and <sup>13</sup>C NMR chemical shifts are expressed in  $\delta$  (ppm) and the proton coupling constants *J* in hertz (Hz).

NMR acquisition at Oregon State University: 1D NMR and 2D NMR spectra were acquired in CDCl<sub>3</sub> on a Bruker Avance III 700 MHz spectrometer equipped with a 5 mm <sup>13</sup>C cryogenic probe, and Bruker DRX600 and AM400 spectrometers. NMR spectra were analyzed using MestReNova v.14.3.0-30573 (Mestrelab, Santiago de Compostela, Spain). NMR spectra were referenced to residual solvent CDCl<sub>3</sub> signals ( $\delta_{\text{H}}$  7.26 and  $\delta_{\text{C}}$  77.2) as internal standards. <sup>1</sup>H and <sup>13</sup>C NMR chemical shifts are expressed in  $\delta$  (ppm) and the proton coupling constants *J* in hertz (Hz).

NMR acquisition at University of Porto: NMR spectra were acquired as a service of the Materials Center of the University of Porto (CEMUP): 1D and 2D NMR data were recorded on a Bruker Avance III HD (<sup>1</sup>H 600 MHz, <sup>13</sup>C 151 MHz) equipped with a 5 mm cryoprobe and controlled by TopSpin 3.6.1 or on a Bruker Avance III (<sup>1</sup>H 400 MHz, <sup>13</sup>C 101 MHz) controlled by TopSpin 3.2. NMR spectra were referenced to residual solvent CDCl<sub>3</sub> signals ( $\delta_{\text{H}}$  7.26 and  $\delta_{\text{C}}$  77.16) as internal standards. <sup>1</sup>H and <sup>13</sup>C NMR chemical shifts are expressed in  $\delta$  (ppm) and the proton coupling constants *J* in hertz (Hz).

NMR acquisition at University of North Carolina Wilmington: 1D NMR and 2D NMR spectra were acquired in CDCl<sub>3</sub> on a Bruker Avance 500 MHz spectrometer equipped with a H/F C/N TCI 5 mm Prodigy Cryoprobe. NMR spectra were analyzed using MestReNova v.14.3.0-30573 (Mestrelab, Santiago de Compostela, Spain). NMR spectra were referenced to residual solvent CDCl<sub>3</sub> signals ( $\delta_{\text{H}}$  7.26 and  $\delta_{\text{C}}$  77.2) as internal standards. <sup>1</sup>H and <sup>13</sup>C chemical shifts are expressed in  $\delta$  (ppm) and the proton coupling constants *J* in hertz (Hz).

MS acquisition at University of California, San Diego: Low resolution-LCMS data were collected on a Thermo Finnigan Surveyor Autosampler/LC-Pump-Plus/PDA-Plus with a Thermo Finnigan Advantage Max mass spectrometer equipped with a Kinetex 5 $\mu$  C18 100 analytical column (100 Å, 4.6 mm, 5  $\mu$ m, Phenomenex). HRLCMS data were obtained using a Vanquish HPLC system coupled to a Q-Exactive Orbitrap mass spectrometer or Orbitrap Elite (Thermo Fisher Scientific). LC-MS/MS data were analyzed using Xcalibur Qual Browser v.1.4 SR1 (Thermo Fisher Scientific, Inc.) and the GNPS Dashboard.(23)

MS acquisition at University of Porto: Liquid chromatography-high resolution electrospray ionization tandem mass spectrometry (LC-HRESIMS/MS) were performed on a Vanquish HPLC system with a C18 porous core column ACE UltraCore 2.5 SuperC18 column (75 × 2.1 mm, ACE, Reading, UK) coupled to an Orbitrap Exploris 120 mass spectrometer and controlled by Q Exactive Focus Tune 2.9 and Xcalibur 4.1 (Thermo Fisher Scientific, Waltham, MA, USA). MS data were processed using Xcalibur software (ThermoFisher Scientific).

MS acquisition at Pacific Northwest National Laboratory: A Waters Acquity UHPLC system (Agilent Zorbax SB-C18 5  $\mu$ m, 150  $\times$  0.5 mm column) coupled to a 21 Tesla FT-ICR mass spectrometer was used for ultra-high mass resolution data acquisition. The 21 Tesla instrument is comprised of a Velos Pro Dual Linear Ion Trap front-end with a heated electrospray ionization (HESI) source and custom built ICR spectrometer containing a Window ICR cell.

Medium-pressure liquid chromatography (MPLC) was performed on a Teledyne ISCO CombiFlash Rf using RediSep Gold HP silica columns or on a Büchi Pure C-850 FlashPrep using silica or C18 SiliaSep flash cartridges (SiliCycle, Inc). Column chromatography for LC-MS preparation was performed using C18 solid-phase extraction (SPE) with 1 g of Bond Elut-C18. Analytical and semipreparative HPLC purification was carried out with a Thermo Scientific Dionex UltiMate 3000 LC system interfaced to a DAD detector (Dionex, Thermo Fisher Scientific Company, Waltham, MA, USA) equipped with a Kinetex 5  $\mu$ m C18 100 using Chromeleon software.

Solvents used for extraction, purification, and LC-MS/MS analysis were purchased from Fisher Chemical. All solvents were HPLC or LC-MS grade. Deuterated solvents were purchased from Cambridge Isotope Laboratories or Eurisotop.

### 1.3.2 Isolation of Leptocheilins

Leptothoe sp. ISB3NOV94-8A. Cultures of *Leptothoe* sp. ISB3NOV94-8A were grown until stationary phase (4 weeks – 6 months depending on the experiment) and were harvested by filtration using Whatman #1 filter paper with a Buchner funnel under vacuum. As one example, the biomass (5.63 g) was extracted in organic solvent ( $\text{CH}_2\text{Cl}_2$ -MeOH, 2:1) affording 811 mg of organic extract. A DCM:H<sub>2</sub>O partition was performed and the resulting extract from the organic layer was then subjected to normal phase vacuum liquid chromatography (NP VLC) with stationary phase silica gel in a stepped solvent gradient of hexanes to EtOAc to 25% MeOH in EtOAc to 100% MeOH to produce 9 fractions (A through I). Fraction H (25% MeOH in EtOH; 194 mg) was then further purified using iterations of reverse-phase high performance liquid chromatography (RP HPLC) first using a combined isocratic and gradient profile (column: Synergi Hydro-RP 80  $\text{\AA}$ , 10  $\times$  250 mm, 3.5 mL/min) with 30% ACN-H<sub>2</sub>O for 3.5 min, increasing to 90% ACN-H<sub>2</sub>O for 31.5 min, isocratic mixture at 90% ACN-H<sub>2</sub>O for 5 minutes, followed by isocratic mixture at 30% ACN-H<sub>2</sub>O for 7 minutes. The fraction containing the leptocheilins (35.8 mg) was then subjected to an additional round of RP HPLC using a combined isocratic and gradient profile (column: Kinetex<sup>®</sup> 5  $\mu$ m C18 100  $\text{\AA}$ , 10  $\times$  250 mm, 1.0 mL/min) with 30% ACN-H<sub>2</sub>O for 3 min, increasing to 50% ACN-H<sub>2</sub>O for 2 min, isocratic at 50% ACN-H<sub>2</sub>O for 12 minutes, an increase to 90% ACN-H<sub>2</sub>O over 5 minutes, held for 3 minutes, followed by an isocratic mixture at 30% ACN-H<sub>2</sub>O for 4 minutes. This resulted in the isolation of 1.3 mg of pure leptocheilin A ( $t_R$  = 6.78 min).

Approximately 3 L of medium obtained from vacuum filtration of the cultures was placed in a 4 L flask along with 40 g of conditioned XAD-16 resin and allowed to gently shake at room temperature overnight. The resin was collected by vacuum filtration and twice extracted with  $\text{CH}_2\text{Cl}_2$ -MeOH (2:1) and once with 100% MeOH. The extracts were combined and solvents evaporated in vacuo to provide 1.49 g of organic extract. A H<sub>2</sub>O:EtOAc partition provided an organic layer that was subjected to purification using normal phase medium pressure liquid chromatography (NP MPLC) (column: Silica, 24 g RediSep Gold High Performance, 40 mL/min) and a combined isocratic and gradient profile with 100% hexanes for 5 minutes, 0 to 100% hexanes-EtOAc over 25 minutes and then 100% EtOAc for 7 minutes, followed by elution with 25% MeOH in EtOAc for 13 minutes, gave an initial purification of leptocheilin B. A strong UV signal was observed with the introduction of 25% MeOH ( $t_R$  = 39.0 min) consistent with a fraction enriched in leptocheilins (17 mg). RP HPLC of this fraction using the analytical method described above afforded 0.9 mg of pure leptocheilin B (**2**) ( $t_R$  = 9.17 min).

Leptothoe sp. EHU-05/26/07-4 (RS02). Cultures of *Leptothoe* sp. EHU-05/26/07-4 (10  $\times$  1.5 L cultures grown for 6 months) were harvested by filtration on glass-fiber filters and extracted in organic solvents ( $\text{CH}_2\text{Cl}_2$ -MeOH, 2:1) to afford 2.05 g of extract. The organic extract was subjected to bioassay-guided fractionation via NP VLC using a stepped solvent gradient of hexanes to EtOAc to MeOH to produce six fractions (A, C, E, G, H and I). The fraction eluting with 25% MeOH-EtOAc (H) was moderately toxic to brine shrimp and further separated by RP<sub>18</sub> SPE using a stepped solvent gradient of MeOH-H<sub>2</sub>O from 50% MeOH-H<sub>2</sub>O to 100% MeOH, followed by 100%  $\text{CH}_2\text{Cl}_2$ . The RP<sub>18</sub> SPE fraction eluting in 85% MeOH was subjected to RPHPLC using a combined isocratic and gradient profile (column: Synergi Polar-RP, 10  $\times$  250 mm, 75% MeOH-H<sub>2</sub>O for 30 min, increasing to 100% MeOH for 30 min, 3.0 mL/min) to yield Zn-leptocheilin A (1.1 mg,  $t_R$  = 46.8 min). LC-MS profiling (Synergi Fusion-RP, 2  $\times$  100 mm, 0.2 mL/min, 70% MeOH in 0.1% (v/v) aqueous formic acid) of fraction H also showed an ion cluster for  $[\text{M} - 4\text{H} + \text{Fe} + \text{Na}]^+$  at  $m/z$  947/949/951/953 suggesting the presence of Fe-leptocheilin. Furthermore, a cluster spanning  $m/z$  955 to 965  $[\text{M} - 2\text{H} + \text{X} + \text{Na}]^+$ , where X = Zn(II) or Cu(II), suggested the presence of two overlapping ion clusters for Zn<sup>2+</sup> and Cu<sup>2+</sup> bound species. However, only the Zn-bound form was isolated in this HPLC protocol.

Leptothoe sp. LEGE181152. Cultures of *Leptothoe* sp. LEGE181152 were grown up to 40 L with constant aeration and at the exponential phase cells were harvested, frozen and freeze-dried. The biomass (36.3 g) was exhaustively extracted with 4.75 L of MeOH, yielding 12.5 g of extract. To concentrate the chemical components in different polarities, the crude was subjected to NP VLC using 360 g of silica gel-60 (0.015–0.040 mm) with the mobile phase being a step gradient of hexanes-EtOAc (9:1 to 0:1; 0.5 L each mixture) to EtOAc-MeOH (7:3 to 0:1; 0.5 L each), resulting in 10 fractions. The subsequent fractionations were guided by bioactivity results from cytotoxic assays on the HCT 116 cell line and LC-MS data. Fraction G2 (1.68 g) eluted at EtOAc: MeOH (7:3) was separated by flash chromatography (Pure C-850 FlashPrep, Buchi), using as stationary phase SiO<sub>2</sub> (SiliCycle 25 g cartridge), and as mobile phase mixtures of hexanes-EtOAc (5:5 to 0:1) and EtOAc-MeOH (1:0 to 0:1) with a flow rate of 10 mL/min, yielding 15 fractions. Fractions G2\_8 and G2\_9 were pooled (745.5 mg) and separated by reverse phase flash chromatography (Pure C-850 FlashPrep, Buchi), with a C18 40 g cartridge (SiliCycle) using a mixture of H<sub>2</sub>O/MeOH (3:2 to 0:1), from which resulted in subfractions A – K. The three most bioactive fractions, G2\_8+9\_DEF, were pooled (92 mg) and fractionated by normal phase flash chromatography (Pure C-850 FlashPrep, Buchi), on a 4 g silica cartridge (SiliCycle) with a gradient of hexanes/acetone (4:1 to 0:1). Given the peculiar appearance of a bright blue band on TLC viewed at 254 nm, fraction 3 (18 mg) was separated by preparative TLC with an elution mixture of  $\text{CH}_2\text{Cl}_2$ :MeOH (96:4), resulting in 3 fractions (3A-3C). Fraction 3B was subjected to RP HPLC, using a semi-preparative ACE Excel C18-AR column (100  $\text{\AA}$  pore size; 10  $\mu$ m particle size, 250  $\times$  10 mm; ACE, Reading, UK), eluent with an isocratic mixture of H<sub>2</sub>O/MeCN (47:53). This separation yielded 0.8 mg of zinc-bound leptocheilin C ( $R_t$  = 6.2 min) and 6 mg of zinc-bound leptocheilin A ( $R_t$  = 7.0 min). Fraction 3C was separated using similar HPLC conditions, but with an isocratic mixture of H<sub>2</sub>O/MeCN (2:3) as eluent, yielding 1 mg of zinc-bound leptocheilin B ( $R_t$  = 3.1



min). Given that these isolation procedures led to the purification of zinc-bound leptochelins, an additional attempt to isolate these compounds without metal was implemented following a similar approach. The substitution of commercial LC-MS grade water for the previously used on-site deionized water was used for all reverse-phase procedures. The final purification step, using semi-preparative HPLC with an ACE Excel C18-AR column and an isocratic mixture of H<sub>2</sub>O-ACN (1:1), resulted in the purification of the free leptochelins. This yielded 0.3 mg of leptochelin B (R<sub>t</sub> = 6.8 min), 0.9 mg of leptochelin C (R<sub>t</sub> = 7.8 min), and 0.4 mg of leptochelin A (R<sub>t</sub> = 8.8 min).

### 1.3.3 UHPLC-MS<sup>2</sup>

A 5  $\mu$ l aliquot of sample was injected into a Vanquish HPLC system coupled to a Q-Exactive Orbitrap mass spectrometer or Orbitrap Elite (Thermo Fisher Scientific). A C18 porous core column (Kinetex polar C18, 150  $\times$  2.1 mm, particle size of 1.7  $\mu$ m, pore size of 100  $\text{\AA}$ , Phenomenex) was used for chromatography. For gradient elution, a high-pressure binary gradient system was used. The mobile phase consisted of solvent A (H<sub>2</sub>O + 0.1% formic acid (FA)) and solvent B (acetonitrile (ACN) + 0.1% FA). The flow rate was set to 0.5 mL/min. After injection, the samples were eluted with one of the following linear gradients: 0–1 min, 5% B, 1–11 min 5–100% B, followed by a 2-min washout phase at 100% B and a 3-min re-equilibration phase at 5% B. Data-dependent acquisition (DDA) as well as targeted MS<sup>2</sup> spectra were acquired in positive mode. ESI parameters were set to a sheath gas flow of 53 AU, auxiliary gas flow of 14 AU, sweep gas flow of 0 AU and auxiliary gas temperature of 400 °C, while the spray voltage was set to 3.5 kV, the inlet capillary to 320 °C, and a S-lens RF level 50 was applied. The MS scan range was set to 200–2000  $m/z$  with a resolution at  $m/z$  200 ( $R_{m/z}$  200) of 140,000 with one micro-scan. The maximum ion injection time was set to 100 ms with an automated gain control (AGC) target of  $5.0 \times 10^5$ . Up to five MS<sup>2</sup> spectra per MS<sup>1</sup> survey scan were recorded in DDA mode with  $R_{m/z}$  200 of 17,500 with one micro-scan. The maximum ion injection time for MS<sup>2</sup> scans was set to 100 ms with an AGC target of  $5.0 \times 10^5$  ions. The MS<sup>2</sup> precursor isolation window was set to  $m/z$  1 or  $m/z$  4 for MS<sup>3</sup> experiments. For HCD experiments, the normalized collision energy was set to a stepwise increase from 20 to 30 to 40% with  $z = 1$  as default charge state. MS<sup>2</sup> scans were triggered at the apex of chromatographic peaks within 2 to 15 s from their first occurrence. Dynamic precursor exclusion was set to 10 s. Ions with unassigned charge states were excluded from MS<sup>2</sup> acquisition as well as isotope peaks. For targeted MS<sup>3</sup> experiments, precursor ions were isolated in the linear ion trap of the Orbitrap elite and further fragmented using first CID for MS<sup>2</sup>, followed by CID or HCD for MS<sup>3</sup>. Collision energies were individually adjusted to yield optimal fragmentation.

### 1.3.4 21T FT-ICR. Microflow HPLC-UHR-MS<sup>2</sup>

A 21 Tesla FT-ICR mass spectrometer as previously described was used for ultra-high mass resolution measurements (24). Briefly, the 21 Tesla instrument comprises a Velos Pro Dual Linear Ion Trap front-end and custom built ICR spectrometer containing a Window ICR cell (25). This instrument, with a heated electrospray ionization (HESI) source, was coupled to a Waters Acquity UHPLC system. A 10  $\mu$ l aliquot of sample was injected onto an Agilent Zorbax SB-C18 (5  $\mu$ m, 150  $\times$  0.5 mm) column. Gradient elution was performed with solvents A) H<sub>2</sub>O + 0.1% FA and B) methanol + 0.1% FA. The gradient program was performed at a flow rate of 20  $\mu$ l/min with initial conditions of 95% A for 0-2 min, then ramping to 5% A from 2-25 min, followed by return to 95% A from 25-26 min, and final re-equilibration until 40 min.

HESI parameters included sheath gas of 7 AU with no aux or sweep gas, the source heater at 40 °C and ion inlet capillary at 275 °C, with an applied 3.6 kV ESI voltage. Analysis was performed in positive ion mode. Automatic gain control (AGC) was enabled with a target of  $2.0 \times 10^5$  charges and max ion injection time of 500 ms for both MS<sup>1</sup> and MS<sup>2</sup> levels. MS<sup>1</sup> spectra were acquired between  $m/z$  220-1000 with a transient length of 3.1 s (resolving power target of 1.2M at  $m/z$  400). MS<sup>2</sup> spectra were acquired with data-dependent acquisition and a transient length of 1.5 s (resolving power target 600k at  $m/z$  400). For DDA, the top two most intense precursors were selected for fragmentation after a single micro-scan MS<sup>1</sup> acquisition, using CID fragmentation with a normalized collision energy of 35 and mass isolation window of 2  $m/z$ .

### 1.3.5 Fragmentation Trees

Fragmentation trees were generated via SIRIUS 5.6.3 using a mass accuracy of 8 ppm. The formula and adduct were manually set as previously determined. All other parameters were set to the Orbitrap default and trees were exported as json files. Structural annotations for fragmentation tree nodes were generated via MS-FINDER 2.52. MS<sup>2</sup> tolerance was set to 8 ppm and Tree depth was set to 3, with the other parameters left at default. In cases where SIRIUS and MS-FINDER aligned regarding molecular formula annotations of fragments, the structural annotation was annotated with the respective node using R 4.2.2. The final trees were visualized using Cytoscape 3.9.1 and edited using Adobe Illustrator 27.6.1.

### 1.3.6 Methylation Procedure for Leptochelin A

The carboxylic acid terminus of leptochelin A (**1**) was methylated with diazomethane to yield methylated leptochelin A (**4**) following a procedure modified from reference (26). In a double neck round bottom flask attached to a condenser, a solution of N-methyl-N'-nitro-N-nitrosoguanidine dissolved in diethyl ether was added to a 6 M aqueous solution of KOH and stirred at RT for 30 min. The resulting organic phase was separated and added gradually to a vial containing leptochelin dissolved in methanol with vigorous stirring at 0 °C. The resulting solution was evaporated to dryness under low pressure.

### 1.3.7 Hydrolysis and Marfey's Analysis

To determine the absolute configuration of the bromophenylalanine residue in **1**, 0.3 mg of leptochelin was reconstituted in 0.5 mL of 6 N HCl and stirred in an oil bath at 120 °C for 15 h. The hydrolysate was dried under N<sub>2</sub> and reconstituted in 300  $\mu$ l of 1 M NaHCO<sub>3</sub> and treated with 160  $\mu$ l of a 0.1% solution of N- $\alpha$ -(2,4-dinitro-5-fluorophenyl)-L-valinamide (L-FDVA) in acetone. The reaction mixture was stirred at 40 °C for 1 h and quenched with 50  $\mu$ l of 2 N HCl. The hydrolysate was dried under N<sub>2</sub> to an oil and reconstituted in 250  $\mu$ l of 50% CH<sub>3</sub>CN-H<sub>2</sub>O. The hydrolysate, a standard of L-FDVA derivatized D,L-bromophenylalanine, and L-FDVA derivatized L-bromophenylalanine were subjected to LC-MS analysis (10% CH<sub>3</sub>CN/90% H<sub>2</sub>O to 50% CH<sub>3</sub>CN-H<sub>2</sub>O over 90 min; Phenomenex Kinetex C18 column, 100  $\times$  4.6 mm, flow 0.4 mL/min). Examination of retention times clearly showed

that L-bromophenylalanine was present in **1**. Standard for D-bromophenylalanine had an  $t_R$  of 87.95 min, standard for L-bromophenylalanine had an  $t_R$  of 94.32 min, and the compound liberated from leptochelin had an  $t_R$  of 94.30 min (**Fig. S48**).

To determine the absolute configuration of the serine residue of the oxazoline ring, the enhanced Marfey's reagent 1-fluoro-2,4-dinitrophenyl-5-D-leucine-*N,N*-dimethylethylenediamine-amide (D-FDLDA) was prepared according to Kuranaga, et al (27).

**Synthesis of Marfey's standards of serine:** To a 1 mg/mL solution of amino acid (L-Ser or D/L-Ser) in H<sub>2</sub>O (100  $\mu$ L), saturated NaHCO<sub>3</sub> (100  $\mu$ L) was added, followed by a 10 mg/mL solution of D-FDLDA in acetone (50  $\mu$ L). The reaction was heated to 40 °C and allowed to stir for 1 h before being quenched with 1 M HCl (240  $\mu$ L) and concentrated under reduced pressure. For LC-MS analysis, the crude reaction mixture was dissolved in MeOH (2 mL), filtered through a 0.2  $\mu$ m filter, and diluted 100-fold.

**Analysis of leptochelin:** 250  $\mu$ g of leptochelin A (**1**) was transferred to a reaction flask and dissolved in 1,4-dioxane (50  $\mu$ L). D<sub>2</sub>O (250  $\mu$ L) was added followed by 35% DCl in D<sub>2</sub>O (250  $\mu$ L). The reaction was heated to 110 °C for 8 h in an oil bath, concentrated under reduced pressure and dissolved in H<sub>2</sub>O (200  $\mu$ L), to which saturated NaHCO<sub>3</sub> (200  $\mu$ L) was added, followed by 10 mg/mL D-FDLDA solution in acetone (100  $\mu$ L). The reaction was heated to 40 °C for 1 h before quenching with 2 M HCl (100  $\mu$ L) and concentrating under reduced pressure. The remaining residue was dissolved in MeOH (1 mL), filtered through a 0.2  $\mu$ m filter, diluted 10-fold and analyzed by LC-MS.

**LC-MS method:** All samples were analyzed on an Agilent 1260 infinity II LC coupled to a 6545 QToF MS with an Agilent Zorbax C3 column (5  $\mu$ m, 3  $\times$  250 mm). The solvent system included ultra-pure H<sub>2</sub>O with 0.1% formic acid (**A**) and ACN with 0.1% formic acid (**B**). The gradient used was 0-10 min 30% **B** followed by ramping to 60% **B** over 40 min, then holding at 60% **B** for an additional 5 min before re-equilibration. Electrospray ionization (ESI) parameters were set to a gas temperature of 325 °C, gas flow of 10 L/min, nebulizer 20 psi, sheath gas temperature of 270 °C, and a sheath gas flow of 12 L/min. The spray voltage was set to 600 V. MS scan range was set to  $m/z$  100-3000 and the scan rate was 10 spectra/sec. EICs of the HR mass of the standards were analyzed in Agilent MassHunter Quantitative Analysis. The D-FDLDA standard for D-serine had an  $t_R$  of 10.88 min, the D-FDLDA standard for L-serine had an  $t_R$  of 15.23 min, and the compound liberated from leptochelin had an  $t_R$  of 10.90 min (**Fig. S47**).

To determine the absolute configuration of the 2-Me-cysteine residue of the thiazoline ring, an oxidation of leptochelin A was performed to generate 2-Me-cysteic acid for subsequent analysis (28). Multiple reactions were required due to low ionization of the expected Marfey's product from leptochelin A samples. The use of both D-FDLDA and *N*- $\alpha$ -(2,4-dinitro-5-fluorophenyl)-L-leucinamide (L-FDLA) resulted in reversal of the elution order of standards between the pairs of products obtained for the two reagents, which is consistent with the result obtained using both configurations of the same Marfey's reagent, given the co-elution of enantiomeric product pairs.

**Synthesis of 2-Me-cysteic acid standards:** Amino acids (0.5mg; 2-Me-L-cysteine or 2-Me-D-cysteine) were dissolved in 0.5 mL of H<sub>2</sub>O<sub>2</sub>-HCO<sub>2</sub>H (1:1) and heated to 70°C for 30 mins. The mixture was then allowed to cool and solvent was removed under reduced pressure. The remaining residue was then dissolved in H<sub>2</sub>O (100  $\mu$ L) and saturated NaHCO<sub>3</sub> (100  $\mu$ L) was added, followed by a 10 mg/mL solution of Marfey's reagent (D-FDLDA or L-FDLA) in acetone (50  $\mu$ L). The reaction was heated to 40 °C and allowed to stir for 1 h before being quenched with 2 M HCl (100  $\mu$ L) and concentrated under reduced pressure. For LC-MS analysis, the crude reaction mixtures were dissolved in MeOH (1 mL), filtered through a 0.2  $\mu$ m filter, and diluted 2-fold.

**Analysis of leptochelin:** 250  $\mu$ g of leptochelin A was transferred to a reaction flask, dissolved in 2 mL of CH<sub>2</sub>Cl<sub>2</sub> and O<sub>3</sub> was bubbled through the solution at RT for 30 min. The DCM was then removed under reduced pressure and the remaining residue was dissolved in 0.5 mL of H<sub>2</sub>O<sub>2</sub>-HCO<sub>2</sub>H (1:1) and heated to 70°C for 30 min. The mixture was then allowed to cool and solvent was removed under reduced pressure. The remaining residue was then dissolved in D<sub>2</sub>O (500  $\mu$ L) and 35% DCl in D<sub>2</sub>O (500  $\mu$ L) was added before the reaction was heated to 110 °C overnight in an oil bath. The reaction was then concentrated under reduced pressure and dissolved in H<sub>2</sub>O (100  $\mu$ L), to which saturated NaHCO<sub>3</sub> (100  $\mu$ L) was added, followed by 10 mg/mL solution of Marfey's reagent (D-FDLDA or L-FDLA) in acetone (50  $\mu$ L). The reaction was heated to 40 °C for 1 h before quenching with 2 M HCl (100  $\mu$ L) and concentrating under reduced pressure. The remaining residue was dissolved in MeOH (1 mL), filtered through a 0.2  $\mu$ m filter, and analyzed by LC-MS.

**LC-MS method:** The MS parameters, eluent system, and HPLC column used was the same as the above analysis of the serine residue. For the D-FDLDA derivatized samples, the gradient used was 0-20 min at 20% **B** followed by ramping to 50% **B** over 30 min, then holding at 50% **B** for additional 7 min before a wash at 75% **B** and re-equilibration. For the L-FDLA derivatized samples, the gradient used was 0-5 min at 20% **B** followed by ramping to 50% **B** over 30 min, then holding at 50% **B** for additional 5 min before a wash at 75% **B** and re-equilibration. The D-FDLDA standard for 2-Me-D-cysteic acid had an  $t_R$  of 43.05 min, the D-FDLDA standard for 2-Me-L-cysteic acid had an  $t_R$  of 40.15 min, and the compound liberated from leptochelin had an  $t_R$  of 40.11 min (**Fig. S49**, panel A). The L-FDLA standard for 2-Me-D-cysteic acid had an  $t_R$  of 21.31 min, the L-FDLA standard for 2-Me-L-cysteic acid had an  $t_R$  of 23.19 min, and the compound liberated from leptochelin had an  $t_R$  of 23.30 min (**Fig. S49**, panel B).

### 1.3.8 Post-LC Metal Infusion Metabolomics Setup

A 100 mM solution of each metal (FeCl<sub>3</sub>, CuSO<sub>4</sub>, Co(OAc)<sub>2</sub>, ZnSO<sub>4</sub>) was prepared as the stock solution for metal infusion. Each metal stock was diluted to a final concentration of 1 mM for individual experiments and 200  $\mu$ M for the mixed metal infusion. Metal solutions were infused post-LC at a flow rate of 5  $\mu$ L/min from an external syringe pump (29).

## 1.4 Copper Toxicity Assays

For the copper toxicity assays, 10 L of standard SWBG11 media(30, 31) was prepared and autoclaved without the copper-containing component (BG#8, which typically contains copper in the form of CuSO<sub>4</sub>•5H<sub>2</sub>O). 500 mL of BG#8 was prepared following standard procedure for all required components except CuSO<sub>4</sub>•5H<sub>2</sub>O. This solution was sonicated for 40 min at room temperature. Using a portion of the described culture media, CuSO<sub>4</sub>•5H<sub>2</sub>O was dissolved to create a 100 mg/5 mL stock solution,

which was sonicated for 10 min. A confirmed volume of copper-free BG#8 was allocated into prelabeled falcon tubes and the appropriate volume of the stock solution was added to create solutions of desired concentration with a total volume of 40 mL. These modified BG#8 components were filter sterilized. The complete modified SWBG11 media for each concentration was achieved by then adding the modified BG#8 with each desired concentrations of copper to the medium containing all of the other components [BG#1-7, 9-11 + vitamin mix (note: the vitamin mix was added in a sterile fashion after the medium returned to RT after being autoclaved)] to ensure that other than the varying levels of copper, the media components were maintained as per the standard SWBG11 recipe.

Three additional strains of cyanobacteria were selected for this copper toxicity experiment based on taxonomic similarity to *Leptothoe* sp. ISB3NOV94-8A (for which a 16S rRNA gene was identified). The taxonomic similarity was based on identifications from microscopic images and colony morphology. These included *Leptolyngbya* sp. ISB3NOV94-8B, *Leptolyngbya* sp. PAP09SEP10-2A, and *Leptolyngbya* sp. ASX22JUL14-2. The genomes were annotated for secondary biosynthetic gene clusters using antiSMASH v.7.0(6) and the presence of genes associated with siderophore production was noted. The different strains were grown in 50 mL culture tubes using the culture media as described above. For each concentration of added copper there were three replicates for each strain. After inoculation, the cultures were monitored daily, and culture health and viability were assessed on Days 0, 2, 4, 7, 9, 10, and 14 using a predesigned five-point system (**SI Appendix, Table S12**).

On Day 14, the cultures of *Leptothoe* sp. ISB3NOV94-8A were harvested through vacuum filtration, the biomass was lyophilized, and the media was frozen. Both the biomass and media were stored at -20 °C. After lyophilization, 1 mg of sulfamethoxazole (SMZ) was added as an internal standard to each biomass sample. After thawing the frozen media, 0.1 mg of SMZ was added as an internal standard to each media sample. The biomass was extracted using DCM:MeOH (2:1) with 1 min sonication followed by 20 min steeping x 5 rounds of extraction. The resultant organic extract was evaporated to dryness using a rotary evaporator. The media was extracted using liquid-liquid extraction with EtOAc x 5. The organic layer was evaporated to dryness using a rotary evaporator. The resulting extracts were resuspended and approximately 1.5 mg of sample was loaded on a 100 mg C-18 SepPak columns (Bond Elut C18, 100 mg, 1 mL) using MeOH 1 mL x 3 to elute. The sample was dried under N<sub>2</sub> (g) and resuspended at 1 mg/mL. The samples were run in technical triplicates with appropriate blanks and QC using UPLC with the reverse phase solvent system coupled with an Orbitrap QE as described above in **1.3.3**. LC-MS/MS data were analyzed using Xcalibur Qual Browser v.1.4 SR1 (Thermo Fisher Scientific, Inc.) and the GNPS Dashboard (23).

## 1.5 Molecular Modeling

As the first step of this effort, conformational searches were performed using the OPLS4 forcefield as implemented in the Schrödinger MacroModel® software package. During this search distance constraint of 3.5 +/- 1 angstrom was applied between H-27 and C-13 to reflect a strong ROE correlation between H<sub>3</sub>-13 and the H-27 protons. The lowest energy model satisfying all ROE constraints observed for Zn-complexed leptochelin A was selected from the resulting ensemble and this structure was transferred to MOE for further refinement using the same singular constrain and a Zn<sup>2+</sup> atom that was allowed to energy optimize using the Molecular Operating Environment (MOE) v.2022.02. Amber10:EHT forcefield with Gas Phase solvation was implemented in MOE. Fix Hydrogens and Fix Charges were selected after the zinc was assigned a +2 formal charge. The H<sub>3</sub>-13 and H-27 atoms were constrained before the energy minimization calculation was performed. The resultant energy minimization model was reviewed and consistent with the expected pseudo-cyclic conformation (see Fig. S51). Additionally, the atoms with ROE correlations observed by NMR were confirmed to have distances well within 5 Å of one another in the molecular model.

## 1.6 Biological Activity Assays

### 1.6.1 Cytotoxicity Assays with NCI-H460 and SF188 Cell Lines

Colorimetric cell viability assays were performed using SF188 (glioblastoma, Sigma Cat. #SCC282) and NCI-H460 (lung carcinoma, ATCC HTB-177™) cell lines. For SF188, Minimum Essential Medium (MEM, Sigma, Cat. M2279) was supplemented with 10% fetal bovine serum (Sigma, ES-009-B), 2 mM L-glutamine (Sigma, TMS-002-C) was used. For NCI-H460, RPMI-1640 medium (Cellgro, 10-040-CV) was supplemented with 10% fetal bovine serum (ATCC 30-2020), 1 nM sodium pyruvate, and 0.15% sodium bicarbonate. Both media contained 1% Pen/Strep mixture (Hyclone, SV-300-10). Cells were dislodged with either accutase (SF188) or trypsin (NCI-H460), respectively, and then seeded at 3.33 × 10<sup>4</sup> cells/mL of complete MEM or RPMI-1640 medium into clear flat bottom Falcon 96 well plates, 180 µL/well. Plates were incubated overnight and exposed to leptochelin A or positive controls. Compounds were dissolved initially in DMSO then diluted 20-fold with complete medium and further diluted to obtain 9 half logarithmic dilutions. The resulting samples were added as 20 µL/well in duplicate and on three separate plates. Quisinstat or doxorubicin served as positive controls, respectively for SF188 and NCI-H460 cells, and were processed in the same way as for the leptochelin A sample. Plates were incubated for an additional 48 h before staining with 3-(4,5-dimethylthiazol-2-yl)-2,5-diphenyl-2H-tetrazolium bromide (MTT, 0.83 mg/mL) for 60 or 25 min and analyzed in comparison with the negative control (100% complete medium set to represent 100% cell viability) at 570 nm. Absorption at 630 nm was subtracted as the background. The percentage of cell viability was calculated as expressed in **Equation 1**, and IC<sub>50</sub> values were calculated as log(inhibitor) vs normalized response – variable slope on GraphPad Prism 10.

$$\% \text{ viability} = \left( \frac{(\bar{x} \text{ absorbance compound at } 570 \text{ nm}) - (\bar{x} \text{ absorbance compound at } 630 \text{ nm})}{(\bar{x} \text{ absorbance medium control at } 570 \text{ nm}) - (\bar{x} \text{ absorbance medium control at } 630 \text{ nm})} \times 100 \right)$$

**Equation 1.** Calculation for percent viability using the NCI-H460 and SF188 cell lines.

### 1.6.2 Cytotoxicity Assays with D283-med Cell Lines

A luminescent cell viability assay was performed using the D283-med (medulloblastoma, ATCC, Cat HTV-185) cell line. The cells were grown in non-treated tissue culture flasks at 37 °C, 5% CO<sub>2</sub> with complete Eagle's Minimum Essential Medium (EMEM,

ATCC 30-2002) was supplemented with 10% fetal bovine serum (ATCC 30-2020) and 1% Pen/Strep mixture (Hyclone, SV-300-10). The cells were dissociated with accutase and then seeded at  $1.8 \times 10^5$  cells/mL into BRANDplates (EW-07903-59) white round-bottomed 96 well plates, 75  $\mu$ L/well. After one hour either leptochelin A or the positive control quisinostat was added. Compounds were dissolved initially in DMSO, then diluted 50-fold with complete medium, and then further diluted to obtain 9 half logarithmic dilutions. The resulting samples were added as 25  $\mu$ L/well in duplicate on three separate plates. Then plates were incubated for 48 h, after which the cells were lysed in darkness with Reconstituted CellTiter-Glo® Reagent (Promega G7572) for 10 min and luminometry signals were measured against a negative control (100% complete EMEM medium set to represent 100% cell viability). Colorimetric and luminometric signals were measured using a SpectraMax M3 microplate reader (Molecular Devices). The percentage of cell viability was calculated as expressed in **Equation 2**, and IC<sub>50</sub> values were calculated as log(inhibitor) vs normalized response – variable slope on GraphPad Prism 10.

$$\% \text{ viability} = \left( \frac{\bar{x} \text{ luminescence compound}}{\bar{x} \text{ absorbance medium control}} \times 100 \right)$$

**Equation 2.** Calculation for percent viability using the D283-med cell lines.

### 1.6.3 Cytotoxicity Assays with HCT 116 2D Monolayer Model

The human colon carcinoma cell line HCT116 (ATCC, USA) was maintained in McCoy's 5A modified media (Merck Life Science S.L.U., Algés, Portugal), complemented with 10% fetal bovine serum (Biocrom, Berlin, Germany), 1% penicillin/streptomycin (Biocrom, Berlin, Germany), and 0.1% amphotericin B (GE Healthcare, Little Chafont, United Kingdom). All cell lines were incubated in a humidified atmosphere at 37°C and in 5% CO<sub>2</sub>. HCT 116 cells were seeded on 96-well plates at a density of  $3.3 \times 10^4$  cells/mL, and after adherence were incubated with the compounds for 48 h with a concentration gradient up to 100  $\mu$ M. DMSO (0.5%) (Sigma, USA) was used as the solvent and staurosporine served as the positive control. After the experimental exposure, MTT was added at a final concentration of 200  $\mu$ g/mL per well for 3 h. Formazan crystals were dissolved in 100  $\mu$ L of DMSO, and the absorbance measured at 550 nm using a Synergy HT microplate reader (Biotek, Germany). Data were obtained from two independent assays with three replicates in each, and was transformed to log scale and normalized to the negative solvent control. IC<sub>50</sub> values were calculated as log(inhibitor) vs normalized response – variable slope on GraphPad Prism 7.

### 1.6.4 Cytotoxicity Assays using a 3D Cancer Cell Model

To prepare 3D spheroids, HCT 116 cells at a concentration of 50,000 cells/mL were seeded on an Ultra-Low Attachment round bottom 96-well plate (Costar, Corning, New York, NY, USA) and then incubated for 5 days until forming spheroids. Concentrations of pure compounds ranging up to 100  $\mu$ M (1% DMSO) were tested on the spheroids for 96 h. CellTiter-Glo® 3D cell (Promega, Madison, USA), a cell viability kit formulated to quantify ATP in 3D cultures, was used according to manufacturer instructions. Luminescence was read on microplate reader (Synergy HT, Biotek, Bart Frederick Shahr, Germany) with an integration time of 0.6 seconds and gain of 125. Data were retrieved from two independent assays with three replicates in each and was transformed to log scale and normalized to the negative solvent control. IC<sub>50</sub> values were calculated as log(inhibitor) vs normalized response – variable slope on GraphPad Prism 7. Bright field images of spheroids at 24 h and 96 h after exposure were taken on a Cytation 5 Cell Imaging Multimode Reader (Biotek) with 2.5x magnification. ImageJ was used for image analysis and Inkscape for image treatment.

### 1.6.5 Cytotoxicity Assays with Mouse Lymphoma T-cells

Mouse T-cell lymphoma cells L5178Y (ECACC Cat. No. 87111908, FDA, Silver Spring, MD, USA) and the ABCB1-transfected multidrug resistant subline L5178Y-MDR were cultured in McCoy's 5A media supplemented with 10% heat-inactivated horse serum, 100 U/L L-glutamine, and 100 mg/L penicillin–streptomycin mixture, (Sigma-Aldrich Kft, Budapest, Hungary). Colchicine (Sigma-Aldrich Chemie GmbH, Steinheim, Germany) was used at the concentration of 60 ng/mL to preserve the MDR phenotype of L5178Y-MDR cells. All cell lines were incubated in a humidified atmosphere at 37°C and in 5% CO<sub>2</sub>. Cytotoxicity against mouse lymphoma T-cells was accessed by MTT assay after 24 h of exposure. Compounds were diluted in media and then cells at a concentration of  $1 \times 10^4$  cells/mL were added to each well, except for medium control wells. Wells containing only cells and no test compounds were used as the negative control. At the end of the exposure time, MTT was added to each well (final concentration of 0.5 mg/mL), incubated for 4 h, and then 100  $\mu$ L of sodium dodecyl sulfate (SDS) (10% in 0.01 N HCl) was added to each well and left overnight. Optical density was measured at 540/630 nm with a Multiscan EX ELISA reader (Thermo Labsystems, Cheshire, WA, USA). The percentage of cell viability was calculated as expressed in **Equation 3** below, and IC<sub>50</sub> values were calculated as log(inhibitor) vs normalized response – variable slope on GraphPad Prism 7.

$$\% \text{ viability} = \left( \frac{(\bar{x} \text{ absorbance compound}) - (\bar{x} \text{ absorbance medium control})}{(\bar{x} \text{ absorbance cell control}) - (\bar{x} \text{ absorbance medium control})} \times 100 \right)$$

**Equation 3.** Calculation for percent viability using mouse lymphoma T-cells.

### 1.6.6 Multidrug Resistance Reversal Assay

The zinc forms of leptochelins A or C and P-glycoprotein (ABCB1), L5178Y-MDR cells were incubated along with the ABCB1 substrate rhodamine 123. Cells at a concentration of  $2 \times 10^6$  cells/mL were resuspended in 500  $\mu$ L of serum-free McCoy's 5A medium and then incubated for 10 min at room temperature with the test compounds at the concentrations of 0.2, 2 and 20  $\mu$ M. DMSO (2%) was used as solvent control and Tariquidar (0.2  $\mu$ M) as the positive control. The fluorescent dye rhodamine 123 was added at a concentration of 5.2  $\mu$ M, and then incubated at 37 °C for 20 min. Cells were washed twice with PBS and then transferred to flow cytometry tubes. Fluorescence was measured with a CyFlow® flow cytometer (Partec, Münster, Germany). The intracellular accumulation of rhodamine 123 was quantified by the fluorescence activity ratio (FAR), calculated by dividing the mean fluorescence intensity (FL-1) of treated MDR cells against the FL-1 of untreated cells (**Fig. S68**).

## 2. Additional Biological Activity Results

### 2.1 Results of Cytotoxicity Assays using a 3D Cancer Cell Model

In the HCT 116 spheroid model, the leptochelins (1-3) in their free form were more toxic than those bound to zinc, with IC<sub>50</sub> values ranging from 8.6 to 16.5 μM, similar to the 2D results (*SI Appendix, Table S13*). When complexed with zinc, leptochelin B (2) lost its cytotoxic effect entirely. The concentration required to cause cytotoxicity in spheroids was higher than in the 2D cultures (*SI Appendix, Table S13*). The results obtained for leptochelins (1-3) are consistent with previous findings for other cytotoxic cyanobacterial compounds (portoamides A and B and nocuolin A).<sup>(32, 33)</sup> Furthermore, after 96 h of exposure to leptochelins A-C (1-3), there was a clear decrease in the layers of proliferating and quiescent cells and an increase in the necrotic core (**Fig. S73**). Leptochelin C (3) was the most active molecule in both HCT 116 2D and 3D assays (*SI Appendix, Table S13*). The results indicate that the absence of the alpha-methyl of the thiazoline in 3 may contribute to this increased cytotoxicity, whereas the presence of both Br and Cl (2) instead of two Br atoms (1) results in decreased cytotoxicity.

### 2.2. Results Discussing Cancer Multidrug Resistance Reversal

Cancer multidrug resistance (MDR) is a major constraint in the success of chemotherapy treatment. One possible approach for overcoming MDR involves inhibition of the ATP- dependent efflux pump ABCB1 or P-glycoprotein. In cancer cells this transmembrane transporter is often overexpressed, which consequently reduces the intracellular concentration of cytotoxic drugs like paclitaxel, vinblastine, and doxorubicin, leading to the development of drug resistance. To investigate if leptochelins could have MDR reversing properties, the zinc-bound forms of leptochelins A (1) and C (3) were tested against two different phenotypes: L5178Y mouse lymphoma cells transfected with human-ABCB1 gene (L5178Y-MDR) and its parental counterpart (L5178Y-PAR).

Only leptochelin C (3) showed a cytotoxic effect, however, with equal potency towards both the MDR phenotype and parental strain, indicating that it overcame this mechanism of drug resistance (*SI Appendix, Table S13*). To probe whether this was due to inhibition of the ABCB1 efflux pump, compounds 1 and 3 were tested in a rhodamine-123-based functional assay. This fluorescent dye is an efflux substrate for the ABCB1 pump, and hence its cytoplasmic accumulation is a direct measure of inhibition of ABCB1 transport activity. Fluorescence data revealed that both leptochelin A (1) and C (3) could revert the MDR phenotype (*SI Appendix, Table S13* and **Fig. S68**), with a fluorescence activity ratio (FAR) of 36.4 at 20 μM for compound 1 and 46.4 at 2 μM for compound 3.

## 3. Physical Data

**3.1 Leptochelin A.** C<sub>35</sub>H<sub>40</sub>Br<sub>2</sub>N<sub>6</sub>O<sub>8</sub>S<sub>2</sub>; Optical Rotation:  $[\alpha]_D^{24} = -21.4$  (c 0.05, MeOH); See **Table 1** of Main Text for NMR Data; UV/Vis (MeOH): λ<sub>max</sub> (ε) = 353 (1058), 255 (2814), 221.5 (8084), 204.5 (8563). See *SI Appendix, Fig. S14* for IR Data; HRMS (ESI): *m/z* 895.0790 [M + H]<sup>+</sup> (calcd for C<sub>35</sub>H<sub>41</sub>Br<sub>2</sub>N<sub>6</sub>O<sub>8</sub>S<sub>2</sub><sup>+</sup>; 895.0794; Δ -0.45 ppm).

**3.2 Leptochelin B.** C<sub>35</sub>H<sub>40</sub>BrClN<sub>6</sub>O<sub>8</sub>S<sub>2</sub>;  $[\alpha]_D^{22} = +12.1$  (c 0.05 in MeOH); See *SI Appendix, Table S3* for NMR Data UV/Vis (MeOH): λ<sub>max</sub> (ε) = 349.5 (1201), 255 (3441), 222 (9547), 205 (9582). HRMS (ESI): *m/z* 851.1294 [M + H]<sup>+</sup> (calcd for C<sub>35</sub>H<sub>41</sub>BrClN<sub>6</sub>O<sub>8</sub>S<sub>2</sub><sup>+</sup>; 851.1299; Δ -0.61 ppm).

**3.3 Leptochelin C.** C<sub>34</sub>H<sub>38</sub>Br<sub>2</sub>N<sub>6</sub>O<sub>8</sub>S<sub>2</sub>;  $[\alpha]_D^{22} = -17.3$  (c 0.05 in MeOH); See *SI Appendix, Table S3* for NMR Data UV/Vis (MeOH): λ<sub>max</sub> (ε) = 352 (2310), 255.5 (5550), 223 (15358), 204 (14049). HRMS (ESI): *m/z* 881.0643 [M + H]<sup>+</sup> (calcd for C<sub>34</sub>H<sub>39</sub>Br<sub>2</sub>N<sub>6</sub>O<sub>8</sub>S<sub>2</sub><sup>+</sup>; 881.0638; Δ 0.62 ppm).

**3.4 Leptochelin A + Zn.** C<sub>35</sub>H<sub>39</sub>Br<sub>2</sub>N<sub>6</sub>O<sub>8</sub>S<sub>2</sub>Zn;  $[\alpha]_D^{24} = -89.4$  (c 0.1 in CH<sub>2</sub>Cl<sub>2</sub>); See *SI Appendix, Table S4* for NMR Data; UV/Vis (MeOH): λ<sub>max</sub> (ε) = 353.5 (1647), 233.5 (2747), 196 (955). HRMS (ESI): *m/z* 956.9927 [M + Zn - H]<sup>+</sup> (calcd for C<sub>35</sub>H<sub>39</sub>Br<sub>2</sub>N<sub>6</sub>O<sub>8</sub>S<sub>2</sub>Zn<sup>+</sup>; 956.9929; Δ -0.21 ppm).

**3.5 Leptochelin B + Zn.** C<sub>35</sub>H<sub>39</sub>BrClN<sub>6</sub>O<sub>8</sub>S<sub>2</sub>Zn;  $[\alpha]_D^{22} = +17.1$  (c 0.1 in MeOH); See *SI Appendix, Table S4* for NMR Data; UV/Vis (MeOH): λ<sub>max</sub> (ε) = 350 (684), 261 (2490), 219 (7224), 205.5 (8706). HRMS (ESI): *m/z* 913.0421 [M + Zn - H]<sup>+</sup> (calcd for C<sub>35</sub>H<sub>39</sub>BrClN<sub>6</sub>O<sub>8</sub>S<sub>2</sub>Zn<sup>+</sup>; 913.0434; Δ -1.44 ppm).

**3.6 Leptochelin C + Zn.** C<sub>34</sub>H<sub>37</sub>Br<sub>2</sub>N<sub>6</sub>O<sub>8</sub>S<sub>2</sub>Zn;  $[\alpha]_D^{24} = -31.3$  (c 0.08 in CH<sub>2</sub>Cl<sub>2</sub>); See *SI Appendix, Table S4* for NMR Data; UV/Vis (MeOH): λ<sub>max</sub> (ε) = 353.5 (2829), 233.5 (3414), 218 (3207). HRMS (ESI): *m/z* 942.9762 [M + Zn - H]<sup>+</sup> (calcd for C<sub>34</sub>H<sub>37</sub>Br<sub>2</sub>N<sub>6</sub>O<sub>8</sub>S<sub>2</sub>Zn<sup>+</sup>; 942.9772; Δ -1.11 ppm).

#### 4. Tables

**Table S1.** Metadata for the collections of the three leptochelin-producing cyanobacteria of the genus *Leptothoe*.

<b>Lab ID: Culture Isolate</b>	<b>Collection Date</b>	<b>Lab ID: Field Collection</b>	<b>GPS Coordinates of Collection Site</b>	<b>Collection Site</b>
<b>ISB3NOV94-8A</b>	3 November 1994	ISB3NOV94-8A	1°45'17.978"N 124°59' 9.484"E	North End of Sulawesi, Indonesia, Pacific Ocean
<b>EHU-05/26/07-4</b>	26 May 2007	RS02	27°10'16.1"N 33°57'3.6"E	El Aruk near Hurgada, Egypt, Red Sea
<b>JM1C</b>	14 April 2018	LEGE 181152	16°54'11.2"N 24°54'16.9"W	Baía das Gatas; São Vicente Island; Republic of Cabo Verde, Atlantic Ocean

**Table S2.** 16S rRNA gene sequence partial similarity matrix. A partial similarity matrix (P-distance) generated using 16S rRNA gene sequences of strains used in this work from and other characterized strains of the *Leptothoe* clade.

Sequence	1	2	3	4	5	6	7	8	9	10	11	12	13	14	15	16	17	18	19	20	21	22	23	24	25	26	27	28	29	30	31	32		
1.JASATU0000000000 <i>Leptothoe</i> sp. LEGE 181152																																		
2.JAXSQV0000000000 <i>Leptothoe</i> sp. EHu-05/26/07-4	99.9																																	
3.JAXSQW0000000000 <i>Leptothoe</i> sp. ISB3NOV94-8A	100	99.9																																
4.NR_177056.1 <i>Adonisia_turfae</i> CCMR0081	100	99.9	100																															
5.ON311285.1 <i>Leptothoe</i> sp. LEGE 181153	99.1	99.1	99.1	99.1																														
6.OM732258.1 <i>Leptothoe</i> sp. BACA0637	98.2	98.1	98.2	98.2	98.7																													
7.KY744812 <i>Leptothoe_kymatousa</i> TAU-MAC 1215	96.9	96.8	96.9	96.9	97.2	97																												
8.MH982247 <i>Leptothoe_kymatousa</i> TAU-MAC 1615	97.8	97.8	97.8	97.8	98.2	97.9	99																											
9.KY744809 <i>Leptothoe_sithoniana</i> TAU-MAC 0915	97.5	97.4	97.5	97.5	97.8	97.5	96.2	97.1																										
10.KY744810 <i>Leptothoe_spongobia</i> TAU-MAC 1015	97.7	97.8	97.7	97.7	98	97.3	95.8	96.8	96.9																									
11.KY744811 <i>Leptothoe_spongobia</i> TAU-MAC 1115	96.1	96	96.1	96.1	96.3	96.6	94.8	95.8	96.1	96.4																								
12.KU951663.1 <i>Leptolyngbya</i> aff. <i>ectocarpi</i> LEGE 11473	97.2	97.1	97.2	97.2	97.4	97.8	96.3	97.3	97.2	96.6	95.6																							
13.OK586770.1 <i>Leptolyngbya_ectocarpi</i> ULC424	99.3	99.2	99.3	99.3	99.4	98.2	96.9	97.8	97.2	97.7	96	97.1																						
14.AB039011 <i>Leptolyngbya_ectocarpi</i> PCC 7375	99	99.1	99	99	99.2	97.8	96.6	97.5	97	97.6	95.7	96.8	99.6																					
15.KU951732.1 <i>Leptolyngbya</i> cf. <i>ectocarpi</i> LEGE 11479	98.1	98	98.1	98.1	98.4	98.9	97	98	97.9	97.1	96.2	97.8	98.1	97.8																				
16.KU951733.1 <i>Leptolyngbya_ectocarpi</i> LEGE 11474	98	97.9	98	98	98.3	98.8	97	97.9	97.8	97	96.1	97.8	98	97.7	99.9																			
17.KC469578.1 <i>Leptolyngbya_ectocarpi</i> SAG 60.90	99.2	99.1	99.2	99.2	99.3	98	96.7	97.7	97.1	97.6	95.9	97	99.8	99.5	97.9	97.8																		
18.ON133562.1 <i>Leptolyngbya_ectocarpi</i> BEA 1211B	97.9	97.8	97.9	97.9	98.3	98.6	96.7	97.7	97.7	96.9	96	98	97.8	97.4	99.3	99.2	97.6																	
19.EF654085.1 <i>Pseudanabaena_persicina</i> SAG 80.79	99.3	99.4	99.3	99.3	99.4	98.1	96.8	97.8	97.2	97.9	95.9	97	99.8	99.8	98	97.9	99.8	97.7																
20.AB115963.1 <i>Pseudanabaena_persicina</i>	98.8	98.9	98.8	98.8	99.1	97.8	96.5	97.4	96.9	97.4	95.6	96.6	99.4	99.3	97.7	97.6	99.3	97.4	99.5															
21.JF518829 <i>Leptolyngbya</i> sp. RS03	97.5	97.4	97.5	97.5	98.2	98.5	96.6	97.5	97.6	96.8	96.3	97.5	97.5	97.3	98.4	98.3	97.4	98.9	97.5	97.2														
22.EF110975 <i>Leptolyngbya</i> sp. FLKBBD1	98.2	98.1	98.2	98.2	98.2	97.5	96.5	97.4	96.9	96.9	95.2	98.1	98.2	97.9	98.4	98.3	98.1	97.9	98.2	97.7	97.1													
23.EU249128.1 <i>Leptolyngbya</i> sp. HBC2	98.4	98.3	98.4	98.4	98.6	97.8	96.5	97.4	97.2	97.2	95.5	98	98.6	98.4	98.5	98.4	98.6	98.2	98.6	98.2	97.5	99.4												
24.EF372581.1 <i>Leptolyngbya</i> sp. P2b-2	98.2	98.1	98.2	98.2	98.2	97.5	96.5	97.4	96.9	96.9	95.2	98.1	98.2	97.9	98.4	98.3	98.1	97.9	98.2	97.7	97.1	99.8	99.4											
25.OP902253.1 <i>Leptolyngbya</i> sp. MACC29	97.5	97.4	97.5	97.5	97.8	97.3	96.1	97	96.2	96.3	95.6	96.8	97.9	97.7	97.3	97.2	97.8	96.8	97.9	97.6	96.7	97.8	98.2	97.8										
26.DQ917868.1 Uncultured <i>Leptolyngbya</i> sp. clone ME54	98.6	98.6	98.6	98.6	98.6	97.9	96	97	97.1	97.2	95.6	97.3	98.8	98.6	98.5	98.4	98.7	98.2	98.8	98.3	97.4	98.9	99	98.9	97.5									
27.DQ917878.1 Uncultured <i>Leptolyngbya</i> sp. clone ME90	97.9	97.8	97.9	97.9	97.8	97.2	96.2	97.1	96.7	96.7	94.9	97.8	97.9	97.6	98.1	98	97.8	97.6	97.9	97.4	96.8	99.5	99	99.5	97.5	98.6								
28.MN833627.1 <i>Rhodoploca_sivonenia</i> TAU-MAC 1815	93.9	93.8	93.9	93.9	94.3	94.4	92.7	93.5	93.1	93.1	92.6	93.8	94.1	93.8	94	93.9	93.9	93.9	94	93.7	93.5	93.8	93.8	93.8	93.3	93.9	93.5							
29.KU958136.1 <i>Salileptolyngbya</i> sp. <i>Phormidium</i> sp. BDU 141041	93.7	93.7	93.7	93.7	93.9	93.7	92.5	93.3	92.8	92.8	91.9	92.7	93.7	93.4	93.7	93.7	93.5	93.4	93.7	93.3	93.1	93.2	93	93.1	92.9	93.3	92.8	93.6						
30.MF614799.1 <i>Salileptolyngbya</i> diazotrophicum SC5IO 43686	94.1	94	94.1	94.1	94.3	94.4	93.4	94.2	92.9	92.9	92.1	92.9	94.1	93.8	94.2	94.1	93.9	93.7	94	93.7	93.7	93.4	93.5	93.4	93.2	93.7	93.1	93.6	96.5					
31.MN833626 <i>Cymatolege_isodiametrica</i> TAU-MAC 1715	93	93	93	93	93.2	92.9	92.3	93.3	92.6	91.9	91.4	92.9	92.8	92.6	92.9	92.9	92.6	93	92.9	92.7	92.5	92.5	93	92.5	92.5	92.8	92.2	92	91	92				
32. KY744813 <i>Cymatolege_spiroides</i> TAU-MAC 1315	92.1	92.2	92.1	92.1	92.5	92.6	91.8	92.7	91.9	91.4	92.3	92.2	92.1	91.9	91.9	91.9	91.9	92	92.2	92	92.3	91.5	91.9	91.5	91.5	91.8	91.2	91.4	91.1	91.2	96.4			

**Table S3.** NMR Data for Non-Metal Bound Leptochelins A (1), B (2), and C (3). Leptochelin A, <sup>1</sup>H (400 MHz) and <sup>13</sup>C (101 MHz) NMR Spectroscopic Data (δ), spectra recorded in Chloroform-d; Leptochelin B, <sup>1</sup>H (800 MHz) and <sup>13</sup>C (200 MHz) NMR Spectroscopic Data (δ), spectra recorded in Chloroform-d; Leptochelin C, <sup>1</sup>H (600 MHz) and <sup>13</sup>C (151 MHz) NMR Spectroscopic Data (δ), spectra recorded in Chloroform-d.

Leptochelin A (1)			Leptochelin B (2)			Leptochelin C (3)		
Position	δC	δH, mult (J in Hz)	Position	δC	δH, mult (J in Hz)	Position	δC	δH, mult (J in Hz)
1	178.9, C	-	1	178.9, C	-	1	176.7	-
2	85.4, C	-	2	85.3, C	-	2	78.4	5.16, dd (11.7, 9.3)
3a	41.8, CH <sub>2</sub>	3.43, d (11.7)	3a	41.8, CH <sub>2</sub>	3.43, d (11.7)	3a	35.0	3.67, m
3b		3.58, d (11.7)	3b		3.58, d (11.7)	3b		3.83, m
4	176.8, C	-	4	176.8, C	-	4	178.1	-
5	61.5, C	-	5	61.5, C	-	5	61.9	-
6	64.4, CH	3.68, d (7.8)	6	64.5, CH	3.56, d (8.0)	6	64.7	3.64, m
7	75.4, CH	3.93*	7	75.5, CH	3.92*	7	74.9	4.03, dt (10.2, 8.3)
8a	37.8, CH <sub>2</sub>	3.72*	8a	37.8, CH <sub>2</sub>	3.71, t (9.6)	8a	38.3	3.78, dd (11.5, 8.2)
8b		3.88*	8b		3.91*	8b		3.92, t (10.8)
9	186.5, C	-	9	186.5, C	-	9	185.1	-
10	62.7, C	-	10	62.7, C	-	10	61.9	-
NH <sub>2</sub> -10a		not observed	NH <sub>2</sub> -10a		not observed	NH <sub>2</sub> -10a		1.68
NH <sub>2</sub> -10b		not observed	NH <sub>2</sub> -10b		not observed	NH <sub>2</sub> -10b		3.55, d (11.0)
11	77.9, CH	3.83, bs	11	77.9, CH	3.83, bs	11	78.2	3.85, m
12	50.2, CH	4.51*	12	50.1, CH	4.52, m	12	50.6	4.52, td (7.6, 3.0)
NH-12		10.08, d (7.7)	NH-12	NH	10.11, d (7.8)	NH-12		10.10, d (7.7)
13	22.9, CH <sub>3</sub>	1.46, s	13	22.8, CH <sub>3</sub>	1.45, s	13	21.4	1.54, s
14	21.1, CH <sub>3</sub>	1.57, s	14	21.0, CH <sub>3</sub>	1.55, s	14	29.9	1.56, s
15	31.1, CH <sub>3</sub>	1.53, s	15	31.2, CH <sub>3</sub>	1.53, s	15	15.9	1.18, d (7.5)
16	15.4, CH <sub>3</sub>	1.14, d (7.4)	16	15.4, CH <sub>3</sub>	1.14, d (7.6)	16	175.3	-
17	175.2, C	-	17	175.2, C	-	17	58.1	4.41, m
18	57.8, CH	4.40*	18	57.9, CH	4.40*	NH-17		7.95, d (6.9)
NH-18		8.06, d (7.0)	NH-18	NH	8.05, d (7.4)	18a	37.2	2.92, dd (14.3, 11.5)
19a	37.1, CH <sub>2</sub>	2.91, dd (14.3, 11.5)	19a	37.1, CH <sub>2</sub>	2.92, dd (14.2, 11.8)	18b		3.25, dd (14.2, 3.6)
19b		3.24, dd (14.3, 4.1)	19b		3.24, dd (14.2, 3.8)	19	135.7	-
20	135.7, C	-	20	135.7, C	-	20/24	131.0	7.22, d (8.2)
21/25	130.9, CH	7.22, d (8.3)	21/25	130.9, CH	7.23, d (7.9)	21/23	132.1	7.46, d (8.3)
22/24	131.9, CH	7.46, d (8.3)	22/24	131.9, CH	7.46, d (7.9)	22	121.3	-
23	121.0, C	-	23	121.0, C	-	25	172.7	-
26	173.0, C	-	26	173.0, C	-	26	67.5	4.58, m
27	67.4, CH	4.57*	27	67.5, CH	4.49*	27a	69.2	4.33, t (8.4)
28a	69.4, CH <sub>2</sub>	4.33, t (7.8)	28a	69.4, CH <sub>2</sub>	4.33, t (8.8)	27b		4.44, m
28b		4.45*	28b		4.45, t (8.8)	28	170.8	-
29	171.0, C	-	29	171.0, C	-	29	118.6	-
30	118.0, C	-	30	118.0, C	-	30	165.7	-
31	165.0, C	-	31	164.06, C	-	31	109.9	-
32	111.2, C	-	32	111.4, C	-	32	137.8	7.57, dd (1.5, 1.8)
33	137.5, CH	7.58, dd (7.9, 1.8)	33	134.2, CH	7.38, m	33	113	6.28, t (7.8)
34	112.8, CH	6.29, t (7.9)	34	112.0, CH	6.35, t (7.8)	34	130.6	7.60, dd (8.1, 1.9)
35	130.2, CH	7.61, dd (7.9, 1.8)	35	129.4, CH	7.56, d (7.8)			

\* Signals partially overlapped



**Table S4.** NMR Data for Leptochelin A (1), B (2), and C (3) coordinated with zinc. Leptochelin A + Zn, <sup>1</sup>H (400 MHz) and <sup>13</sup>C (101 MHz) NMR Spectroscopic Data ( $\delta$ ), spectra recorded in Chloroform-d; Leptochelin B + Zn and Leptochelin C + Zn, <sup>1</sup>H (600 MHz) and <sup>13</sup>C (151 MHz) NMR Spectroscopic Data ( $\delta$ ), spectra recorded in Chloroform-d.

Leptochelin A + Zn			Leptochelin B + Zn			Leptochelin C + Zn		
Position	$\delta$ C	$\delta$ H, mult ( <i>J</i> in Hz)	Position	$\delta$ C	$\delta$ H, mult ( <i>J</i> in Hz)	Position	$\delta$ C	$\delta$ H, mult ( <i>J</i> in Hz)
1	178.9, C	-	1	179.1	-	1	176.3 <sup>a</sup>	-
2	84.3, C	-	2	84.4	-	2	78.4	5.16, dd (11.8, 9.3)
3a	42.1, CH <sub>2</sub>	3.43, d (11.7)	3a	42.2	3.42, d (11.6)	3a	34.9	3.66, m*
3b		3.58, d (11.7)	3b		3.57, m*	3b		3.84, m*
4	176.2, C	-	4	176.3	-	4	176.7	-
5	61.5, C	-	5	61.7/61.9	-	5	61.9	-
6	64.3, CH	3.71, d (8.4)	6	64.6	3.57, m*	6	64.7	3.64, m*
7	75.0, CH	4.0, dt, (9.9, 8.4)	7	75.2	3.98, m	7	74.9	4.02, dt (10.0, 8.1)
8a	37.2, CH <sub>2</sub>	3.78, dd (11.4, 8.4)	8a	38.2	3.78, m	8a	38.3	3.78, dd (11.4, 8.2)
8b		3.92, dd, (11.4, 9.9)	8b		3.92, m	8b		3.92, t (10.8)
9	185.0, C	-	9	185.4	-	9	184.9	-
10	61.7, C	-	10	61.7/61.9	-	10	61.8	-
NH <sub>2</sub> -10a		1.63	NH <sub>2</sub> -10a	NH <sub>2</sub>	3.84, brs	NH <sub>2</sub> -10a		1.67
NH <sub>2</sub> -10b		3.54	NH <sub>2</sub> -10b		4.51, m	NH <sub>2</sub> -10b		3.55, d (11.1)
11	77.9, C	3.85, d, (3.4)	11	78.1	1.44, s	11	78.2	3.86, m*
		4.51, ddq (10.7, 7.6, 3.4 Hz)	12	50.4	1.48, s	12	50.6	4.53, dt (8.1, 4.0)
12	50.2, CH	10.15, d (7.6)	NH-12			NH-12		10.09, d (7.6)
13	22.6, CH <sub>3</sub>	1.46, s	13	22.8	1.53, s	13	21.4	1.53, s
14	20.9, CH <sub>3</sub>	1.53, s	14	20.9	1.63	14	30.4	1.55, s
15	30.8, CH <sub>3</sub>	1.53, s	15	31.0	3.58, m*	15	15.9	1.17, d (7.5)
16	15.5, CH <sub>3</sub>	1.15, d (7.6)	16	15.6	1.15, d (7.5)	16	175.3	-
17	175.2, C	-	17	175.3	-	17	58.1	4.41, m*
18	58.0, CH	4.40, ddd (11.3, 7.0, 3.7)	18	58.2	4.40, m	NH-17		7.95, d (7.1)
NH-18		8.26, d (7.0)	NH-18		8.27, brs	18a	37.2	2.92, dd (14.3, 11.5)
19a	37.0, CH <sub>2</sub>	2.92, dd (14.3, 11.3)	19a	37.1	2.92, m	18b		3.25, dd (14.2, 3.6)
19b		3.24, dd (14.3, 3.7)	19b		3.24, dd (14.2, 3.6)	19	135.7	-
20	135.6, C	-	20	135.7	-	20/24	131.0	7.22, d (8.3)
21/25	130.9, CH	7.23, d (8.)	21/25	131.1	7.23, m	21/23	132.1	7.46, d (8.3)
22/24	131.9, CH	7.46, d (8.3)	22/24	132.0	7.46, d (8.3)	22	120.9	-
23	121.0, C	-	23	121.2	-	25	172.7	-
26	172.8, C	-	26	173.0	-	26	67.5	4.57, m
27	67.1, CH	4.56, dd (9.5, 8.3)	27	67.4	4.55, m	27a	69.2	4.32, t (8.4)
28a	69.0, CH <sub>2</sub>	4.33, t, (8.3)	28a	69.2	4.32, brt (8.8)	27b		4.44, m*
28b		4.45, t (9.5)	28b		4.46, m	28	170.8	-
29	170.5, C	-	29	170.7	-	29	118.2	-
30	118.4, C	-	30	110.1	-	30	165.5	-
31	165.5, C	-	31	165.4	-	31	109.7	-
32	109.7, C	-	32	126.4 <sup>a</sup>	-	32	137.8	7.57, m
33	137.6, CH	7.58, dd (7.8, 1.9)	33	134.4	7.37, m	33	113.0	6.28, t (7.8)
34	112.8, CH	6.29, t (7.8)	34	112.2	6.33, t (7.8)	34	130.6	7.59, dd (8.1, 2.0)
35	130.4, CH	7.61, dd (7.8, 1.9)	35	129.7	7.55, m			

<sup>a</sup> Value was derived from the HMBC spectrum.

\* Signals partially overlapped

**Table S5.** NMR Spectroscopic Data comparing the chemical shifts for  $^{13}\text{C}$   $\delta$  for leptochelin A (1) with those of leptochelin B (2) and leptochelin C (3). Red font depicts significant chemical shift differences, indicating point of structural difference between leptochelin A vs B and A vs C.

Leptochelin A (1)		Leptochelin B (2)			Leptochelin C (3)		
Position	$\delta\text{C}$	Position	$\delta\text{C}$	$\text{delta } \delta\text{C (1)-(2)}$	Position	$\delta\text{C}$	$\text{delta } \delta\text{C (1)-(3)}$
1	178.9	1	178.9	0	1	176.7	2.2
2	85.4	2	85.3	0.1	2	78.4	7.0
3	41.8	3	41.8	0	3	35	6.8
4	176.8	4	176.8	0	4	178.1	-1.3
5	61.5	5	61.5	0	5	61.9	-0.4
6	64.4	6	64.5	-0.1	6	64.7	-0.3
7	75.4	7	75.5	-0.1	7	74.9	0.5
8	37.8	8	37.8	0	8	38.3	-0.5
9	186.5	9	186.5	0	9	185.1	1.4
10	62.7	10	62.7	0	10	61.9	0.8
11	77.9	11	77.9	0	11	78.2	-0.3
12	50.2	12	50.1	0.1	12	50.6	-0.4
13	22.93	13	22.83	0.1	-	-	-
14	21.13	14	21.03	0.1	13	21.43	-0.3
15	31.13	15	31.23	-0.1	14	29.93	1.2
16	15.43	16	15.43	0	15	15.93	-0.5
17	175.2	17	175.2	0	16	175.3	-0.1
18	57.8	18	57.9	-0.1	17	58.1	-0.3
19	37.1	19	37.1	0	18	37.2	-0.1
20	135.7	20	135.7	0	19	135.7	0
21	130.9	21	130.9	0	20	131	-0.1
22	131.9	22	131.9	0	21	132.1	-0.2
23	121.0	23	121.0	0	22	121.3	-0.3
24	131.9	24	131.9	0	23	132.1	-0.2
25	130.9	25	130.9	0	24	131	-0.1
26	173	26	173	0	25	172.7	0.3
27	67.4	27	67.5	-0.1	26	67.5	-0.1
28	69.4	28	69.4	0	27	69.2	0.2
29	171	29	171	0	28	170.8	0.2
30	118	30	118	0	29	118.6	-0.6
31	165	31	164.1	0.9	30	165.7	-0.7
32	111.2	32	111.4	-0.2	31	109.9	1.3
33	137.5	33	134.2	3.3	32	137.8	-0.3
34	112.8	34	112	0.8	33	113	-0.2
35	130.2	35	129.4	0.8	34	130.6	-0.4

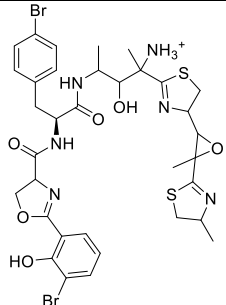
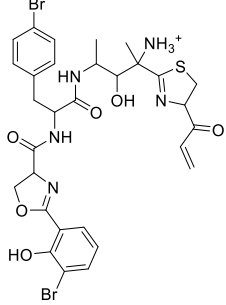
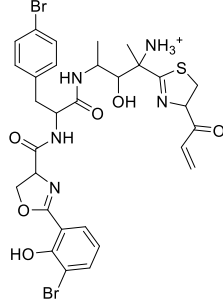
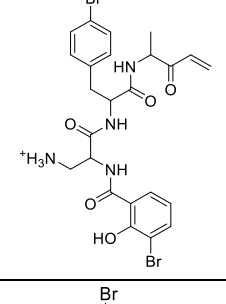
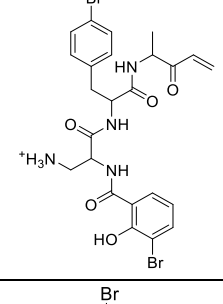
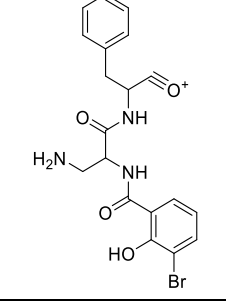
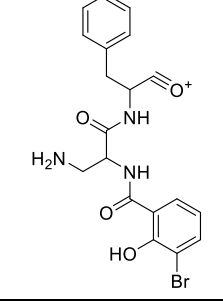
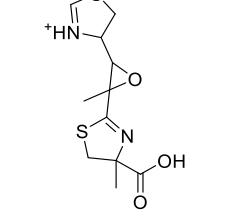
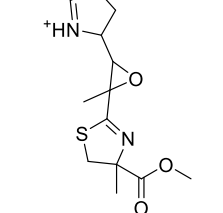
**Table S6.** NMR Spectroscopic Data comparing the chemical shifts for  $^1\text{H}$   $\delta$  for leptochelin A (1), leptochelin B (2), and leptochelin C (3).

Leptochelin A (1)		Leptochelin B (2)			Leptochelin C (3)		
Position	$\delta H$	Position	$\delta H$	$\delta C$ (1)-(2)	Position	$\delta H$	$\delta C$ (1)-(3)
2	-	2			2	5.16	-
3a	3.43	3a	3.43	0	3a	3.67	-0.24
3b	3.58	3b	3.58	0	3b	3.83	-0.25
6	3.68	6	3.56	0.12	6	3.64	0.04
7	3.93	7	3.92	0.01	7	4.03	-0.1
8a	3.72	8a	3.71	0.01	8a	3.78	-0.06
8b	3.88	8b	3.91	-0.03	8b	3.92	-0.04
11	3.83	11	3.83	0	11	3.85	-0.02
12	4.51	12	4.52	-0.01	12	4.52	-0.01
13	1.46	13	1.45	0.01	-	-	-
14	1.57	14	1.55	0.02	13	1.54	0.03
15	1.53	15	1.53	0	14	1.56	-0.03
16	1.14	16	1.14	0	15	1.18	-0.04
18	4.4	18	4.4	0	17	4.41	-0.01
19a	2.91	19a	2.92	-0.01	18a	2.92	-0.01
19b	3.24	19b	3.24	0	18b	3.25	-0.01
21	7.22	21	7.23	-0.01	20	7.22	0
22	7.46	22	7.46	0	21	7.46	0
24	7.46	24	7.46	0	23	7.46	0
25	7.22	25	7.23	-0.01	24	7.22	0
27	4.57	27	4.49	0.08	26	4.58	-0.01
28a	4.33	28a	4.33	0	27a	4.33	0
28b	4.45	28b	4.45	0	27b	4.44	0.01
33	7.58	33	7.38	0.2	32	7.57	0.01
34	6.29	34	6.35	-0.06	33	6.28	0.01
35	7.61	35	7.56	0.05	34	7.6	0.01

**Table S7.** Characteristics of the genome assemblies of the three leptochelin producers.

<i>Strain_Code</i>	<i>Genome_Size (bp)</i>	<i>Number of Contigs</i>	<i>Largest Contig</i>	<i>Degree of completeness</i>	<i>Contamination level</i>	<i>GC Content (%)</i>	<i>N50</i>	<i>N90</i>	<i>L50</i>	<i>L90</i>	<i>Number of transposases</i>	<i>Number of CDSs</i>	<i>No. of rRNA</i>	<i>No. of tRNA</i>	<i>No. of CRISPRS</i>	<i>Coding Ratio (%)</i>	<i>Number of BGCs</i>
<i>Leptothoe sp.</i> ISB3NOV94-8A	8505043	8	7062414	99.46	1.36	47.38	7062414	410881	1	3	49	6932	6	60	11	83.1	18
<i>Leptothoe sp.</i> EHU-05/26/07-4	8850636	11	2036160	99.73	1.09	47.4	1320978	416923	3	8	103	7091	6	59	10	82.7	20
<i>Leptothoe sp.</i> LEGE 181152	8362023	68	839842	99.73	0.82	47.35	273977	98196	11	31	51	6773	3	58	14	82.9	19
<i>Software_used</i>	Quast   Dfast	Quast   Dfast	Quast	CheckM	CheckM	Quast   Dfast	Quast   Dfast	Quast	Quast	Quast	Geneious	Dfast	Dfast	Dfast	Dfast	Dfast	antiSMASH

**Table S8.** Comparison of the fragment masses from leptochelin A (1) and methylated leptochelin A (4). Methylation of the carboxylic acid at C-1 was performed to confirm the linear nature of leptochelin A.

Fragment No.	Fragment Before methylation		Fragment After methylation		
	Structure	Exact mass	Proposed Structure	Observed Major Fragment Mass	Exact Mass
i.		851.09	There is no corresponding Fragment	NA	NA
ii.		750.06		750.07	750.06
iii.		609.03		609.01	609.03
iv.		509.97		510.06	509.97
v.		287.05		301.12	301.07

vi.		386.12		400.04	400.14
ix.		463.94		464.87	463.94
x.		330.09		344.19	344.11

**Table S9.** Similarity scores based on clinker analysis of the *lec* BGC from all three leptochelin producers. For all of the core biosynthetic and tailoring genes, the identity and similarity are at least 0.94.

***Leptothoe* sp. ISB3NOV94-8A vs *Leptothoe* sp. EHU-05/26/07-4**

Query	Target	Identity	Similarity
<i>ctg4_126</i>	<i>ctg9_114</i>	0.97	0.97
<i>ctg4_127</i>	<i>ctg9_113</i>	1	1
<i>ctg4_127</i>	<i>ctg9_94</i>	0.32	0.45
<i>ctg4_128</i>	<i>ctg9_112</i>	1	1
<i>ctg4_129</i>	<i>ctg9_111</i>	1	1
<i>ctg4_130</i>	<i>ctg9_110</i>	1	1
<i>ctg4_131</i>	<i>ctg9_109</i>	1	1
<i>ctg4_132</i>	<i>ctg9_108</i>	1	1
<i>ctg4_133</i>	<i>ctg9_107</i>	1	1
<i>ctg4_134</i>	<i>ctg9_106</i>	1	1
<i>ctg4_135</i>	<i>ctg9_105</i>	1	1
<i>ctg4_135</i>	<i>ctg9_84</i>	0.45	0.55
<i>ctg4_136</i>	<i>ctg9_104</i>	0.99	1
<i>ctg4_136</i>	<i>ctg9_89</i>	0.31	0.43
<i>ctg4_137</i>	<i>ctg9_103</i>	0.99	0.99
<i>ctg4_138</i>	<i>ctg9_102</i>	1	1
<i>ctg4_139</i>	<i>ctg9_101</i>	0.94	0.94
<i>ctg4_140</i>	<i>ctg9_100</i>	1	1
<i>ctg4_141</i>	<i>ctg9_99</i>	1	1
<i>ctg4_142</i>	<i>ctg9_98</i>	1	1
<i>ctg4_143</i>	<i>ctg9_97</i>	0.77	0.77
<i>ctg4_144</i>	<i>ctg9_96</i>	1	1
<i>ctg4_145</i>	<i>ctg9_95</i>	1	1
<i>ctg4_146</i>	<i>ctg9_113</i>	0.32	0.45
<i>ctg4_146</i>	<i>ctg9_94</i>	1	1
<i>ctg4_147</i>	<i>ctg9_93</i>	1	1
<i>ctg4_148</i>	<i>ctg9_92</i>	1	1
<i>ctg4_148</i>	<i>ctg9_89</i>	0.34	0.46
<i>ctg4_148</i>	<i>ctg9_85</i>	0.49	0.65
<i>ctg4_149</i>	<i>ctg9_91</i>	0.99	0.99
<i>ctg4_150</i>	<i>ctg9_90</i>	1	1
<i>ctg4_150</i>	<i>ctg9_88</i>	0.48	0.63
<i>ctg4_151</i>	<i>ctg9_104</i>	0.31	0.44
<i>ctg4_151</i>	<i>ctg9_92</i>	0.34	0.46
<i>ctg4_151</i>	<i>ctg9_89</i>	0.99	0.99
<i>ctg4_151</i>	<i>ctg9_85</i>	0.41	0.52
<i>ctg4_152</i>	<i>ctg9_90</i>	0.48	0.63
<i>ctg4_152</i>	<i>ctg9_88</i>	1	1
<i>ctg4_153</i>	<i>ctg9_87</i>	1	1

ctg4_154	ctg9_86	1	1
ctg4_155	ctg9_92	0.49	0.65
ctg4_155	ctg9_89	0.4	0.51
ctg4_155	ctg9_85	1	1
ctg4_156	ctg9_105	0.45	0.56
ctg4_156	ctg9_84	1	1
ctg4_157	ctg9_83	1	1
ctg4_158	ctg9_82	0.95	0.98
ctg4_159	ctg9_81	0.97	0.99
ctg4_160	ctg9_80	0.99	1
ctg4_161	ctg9_79	1	1
ctg4_162	ctg9_77	1	1
ctg4_163	ctg9_76	1	1
ctg4_164	ctg9_75	0.94	0.96

**Leptothoe sp. ISB3NOV94-8A vs Leptothoe sp. LEGE 181152**

Query	Target	Identity	Similarity
ctg4_126	ctg3_15	1	1
ctg4_127	ctg3_16	1	1
ctg4_127	ctg3_35	0.32	0.45
ctg4_128	ctg3_17	1	1
ctg4_129	ctg3_18	1	1
ctg4_130	ctg3_19	1	1
ctg4_131	ctg3_20	0.99	1
ctg4_132	ctg3_21	1	1
ctg4_133	ctg3_22	1	1
ctg4_134	ctg3_23	1	1
ctg4_135	ctg3_24	1	1
ctg4_135	ctg3_45	0.45	0.55
ctg4_136	ctg3_25	1	1
ctg4_136	ctg3_40	0.31	0.44
ctg4_137	ctg3_26	1	1
ctg4_138	ctg3_27	1	1
ctg4_139	ctg3_28	0.94	0.95
ctg4_140	ctg3_29	1	1
ctg4_141	ctg3_30	1	1
ctg4_142	ctg3_31	1	1
ctg4_143	ctg3_32	0.77	0.77
ctg4_144	ctg3_33	1	1
ctg4_145	ctg3_34	1	1
ctg4_146	ctg3_16	0.32	0.45
ctg4_146	ctg3_35	1	1
ctg4_147	ctg3_36	1	1



<i>ctg4_148</i>	<i>ctg3_37</i>	1	1
<i>ctg4_148</i>	<i>ctg3_40</i>	0.34	0.46
<i>ctg4_148</i>	<i>ctg3_44</i>	0.49	0.65
<i>ctg4_149</i>	<i>ctg3_38</i>	0.99	0.99
<i>ctg4_150</i>	<i>ctg3_39</i>	0.99	1
<i>ctg4_150</i>	<i>ctg3_41</i>	0.48	0.63
<i>ctg4_151</i>	<i>ctg3_25</i>	0.31	0.44
<i>ctg4_151</i>	<i>ctg3_37</i>	0.34	0.46
<i>ctg4_151</i>	<i>ctg3_40</i>	1	1
<i>ctg4_151</i>	<i>ctg3_44</i>	0.41	0.52
<i>ctg4_152</i>	<i>ctg3_39</i>	0.48	0.63
<i>ctg4_152</i>	<i>ctg3_41</i>	1	1
<i>ctg4_153</i>	<i>ctg3_42</i>	1	1
<i>ctg4_154</i>	<i>ctg3_43</i>	1	1
<i>ctg4_155</i>	<i>ctg3_37</i>	0.49	0.65
<i>ctg4_155</i>	<i>ctg3_40</i>	0.4	0.51
<i>ctg4_155</i>	<i>ctg3_44</i>	1	1
<i>ctg4_156</i>	<i>ctg3_24</i>	0.45	0.55
<i>ctg4_156</i>	<i>ctg3_45</i>	1	1
<i>ctg4_157</i>	<i>ctg3_46</i>	1	1
<i>ctg4_158</i>	<i>ctg3_47</i>	0.96	0.98
<i>ctg4_159</i>	<i>ctg3_48</i>	0.97	0.99
<i>ctg4_160</i>	<i>ctg3_49</i>	0.99	1
<i>ctg4_161</i>	<i>ctg3_50</i>	1	1
<i>ctg4_162</i>	<i>ctg3_51</i>	0.63	0.63
<i>ctg4_163</i>	<i>ctg3_52</i>	1	1
<i>ctg4_164</i>	<i>ctg3_53</i>	1	1

***Leptothoe* sp. EHU-05/26/07-4 vs *Leptothoe* sp. LEGE 181152**

Query	Target	Identity	Similarity
<i>ctg9_114</i>	<i>ctg3_15</i>	0.97	0.97
<i>ctg9_113</i>	<i>ctg3_16</i>	1	1
<i>ctg9_113</i>	<i>ctg3_35</i>	0.32	0.45
<i>ctg9_112</i>	<i>ctg3_17</i>	1	1
<i>ctg9_111</i>	<i>ctg3_18</i>	1	1
<i>ctg9_110</i>	<i>ctg3_19</i>	1	1
<i>ctg9_109</i>	<i>ctg3_20</i>	0.99	1
<i>ctg9_108</i>	<i>ctg3_21</i>	1	1
<i>ctg9_107</i>	<i>ctg3_22</i>	1	1
<i>ctg9_106</i>	<i>ctg3_23</i>	1	1
<i>ctg9_105</i>	<i>ctg3_24</i>	1	1
<i>ctg9_105</i>	<i>ctg3_45</i>	0.45	0.56
<i>ctg9_104</i>	<i>ctg3_25</i>	0.99	1

<i>ctg9_104</i>	ctg3_40	0.31	0.44
<i>ctg9_103</i>	ctg3_26	0.99	0.99
<i>ctg9_102</i>	ctg3_27	1	1
<i>ctg9_101</i>	ctg3_28	0.99	1
<i>ctg9_100</i>	ctg3_29	1	1
<i>ctg9_99</i>	ctg3_30	1	1
<i>ctg9_98</i>	ctg3_31	1	1
<i>ctg9_97</i>	ctg3_32	1	1
<i>ctg9_96</i>	ctg3_33	1	1
<i>ctg9_95</i>	ctg3_34	1	1
<i>ctg9_94</i>	ctg3_16	0.32	0.45
<i>ctg9_94</i>	ctg3_35	1	1
<i>ctg9_93</i>	ctg3_36	1	1
<i>ctg9_92</i>	ctg3_37	1	1
<i>ctg9_92</i>	ctg3_40	0.34	0.46
<i>ctg9_92</i>	ctg3_44	0.49	0.65
<i>ctg9_91</i>	ctg3_38	0.99	1
<i>ctg9_90</i>	ctg3_39	1	1
<i>ctg9_90</i>	ctg3_41	0.48	0.63
<i>ctg9_89</i>	ctg3_25	0.31	0.43
<i>ctg9_89</i>	ctg3_37	0.34	0.46
<i>ctg9_89</i>	ctg3_40	0.99	0.99
<i>ctg9_89</i>	ctg3_44	0.41	0.51
<i>ctg9_88</i>	ctg3_39	0.48	0.63
<i>ctg9_88</i>	ctg3_41	1	1
<i>ctg9_87</i>	ctg3_42	1	1
<i>ctg9_86</i>	ctg3_43	1	1
<i>ctg9_85</i>	ctg3_37	0.49	0.65
<i>ctg9_85</i>	ctg3_40	0.41	0.52
<i>ctg9_85</i>	ctg3_44	1	1
<i>ctg9_84</i>	ctg3_24	0.45	0.55
<i>ctg9_84</i>	ctg3_45	1	1
<i>ctg9_83</i>	ctg3_46	1	1
<i>ctg9_82</i>	ctg3_47	0.99	0.99
<i>ctg9_81</i>	ctg3_48	1	1
<i>ctg9_80</i>	ctg3_49	1	1
<i>ctg9_79</i>	ctg3_50	1	1
<i>ctg9_77</i>	ctg3_51	0.63	0.63
<i>ctg9_76</i>	ctg3_52	1	1
<i>ctg9_75</i>	ctg3_53	0.94	0.96

**Table S10.** Adenylation domain substrate specificities predicted for the *lec* BGC using antiSMASH, NRPSSP, and NRPS Predictive Blast.

Adenylation domain gene	Adenylation domain location	antiSMASH prediction	NRPSSP	NRPSSP score	Fallout	NRPS predictive blast	NRPS predictive blast
CTG4_136	c1799..3010	cys	Cysteine	709.9	0.0764	AdpB-M3-Thr	D L Y N I G I I
CTG4_141	c8970..10133	N/A	Phenylalanine	198.1	0.1511	N/A	none detected
CTG4_148	20727..21944	cys	threonine	733.7	0.0611	no prediction	D L Y N I G X X
CTG4_149	25331..26539	leu	Leucine	690.1	0.0812	no prediction	D P L X L G N V
CTG4_149	28517..29716	gly	Glycine	706.2	0.0763	MbtB-M1-Ser/Thr	D M V X L G L V
CTG4_151	37979..39184	cys	Cysteine	804.4	0.0243	PchE-M1-Cys	D L F N L S L I
CTG4_155	50848..52059	cys	Cysteine	802.5	0.0243	Irp2-M1-Cys	D L Y N M S L I

**Table S11.** Metadata for collections of organisms used in the copper toxicity assays.

Lab ID: Field Collection	Collection Date	Collection Site	GPS Coordinates	Taxonomy based on Morphology
ISB3NOV94-8B	3 November 1994	North end of Sulawesi, Indonesia	N 1°45'17.978" E 124°59' 9.484"	<i>Leptolyngbya</i> sp.
PAP09SEP10-2A	9 September 2010	Salmedina Reef, Portobello, Panama	N 9° 33' 15.012" W 79° 41' 29.111"	<i>Leptolyngbya</i> sp.
ASX22JUL14-2	22 July 2014	Faga'itua Bay, American Samoa	S 14°16' 7.824" W 170° 36'53.964"	<i>Leptolyngbya</i> sp.

**Table S12.** Grading scale for cyanobacterial culture health and viability from the copper toxicity assays.

<b>Visual Grade</b>	<b>Gross Morphologic Characteristics of Culture Health</b>
<b>5</b>	Healthy and vibrant cultures with no sign of bleaching or color loss
<b>4</b>	Edges of biomass with some bleaching or color loss noted
<b>3</b>	Heterogeneous appearing tissue with some bleaching or color loss noted
<b>2</b>	Edges of biomass with near complete bleaching or color loss noted
<b>1</b>	Complete bleaching or color loss noted

**Table S13.** Cytotoxicity IC<sub>50</sub> values and standard deviations for leptochelins A (1), B (2) and C (3). Cytotoxicity was measured as the half maximal inhibitory concentration (IC<sub>50</sub>) against a panel of human cancer cell lines and a multidrug-resistant cancer model. The Fluorescence Activity Ratios (FAR) were used to determine ABCB1-mediated reversal of multidrug resistance. Data on each positive control and Zn-bound leptochelins (when available) are also provided for comparison.

Cell line	Leptochelin A (1)		Leptochelin B (2) <sup>e</sup>		Leptochelin C (3) <sup>e</sup>		ZnCl <sub>2</sub> IC <sub>50</sub> (μM ± SD)	Staurosporine IC <sub>50</sub> (nM ± SD)	Tariquidar FAR <sup>a</sup>	
	IC <sub>50</sub> (μM ± SD)		IC <sub>50</sub> (μM ± SD)		IC <sub>50</sub> (μM ± SD)					FAR <sup>a</sup> +Zn
	Free	+Zn	Free	+Zn	Free	+Zn				
NCI-H460 (2013)	0.153 ± 0.086	0.073 ± 0.040								
HeLa	1.071 ± 0.563	0.239 ± 0.089								
SF188	> 3.4									
NCI-H460 (2023)	1.60 ± 0.19									
D283-med	0.39 ± 0.02									
HCT 116 2D	0.40 ± 0.06	4.4 ± 2.3	0.52 ± 0.04	3.0 ± 0.90	0.13 ± 0.04	2.80 ± 0.30	>100	0.50 ± 0.14	-	
HCT 116 3D	12.4 ± 1.3	19.7 ± 0.02	16.50 ± 0.10	>100	8.60 ± 3.10	18.50 ± 0.40	>100	36.70 ± 12.80	-	
L5178Y-PAR		>100				2.0 ± 1.80				
L5178Y-MDR		>100	36.40 <sup>b</sup>						85.64 <sup>d</sup>	

<sup>a</sup> FAR (fluorescence activity ratio); <sup>b</sup> FAR value at 20 μM; <sup>c</sup> FAR value at 2 μM; <sup>d</sup> FAR value at 0.2 μM; <sup>e</sup> These compounds may be more active as these samples contained small amounts of grease.

5. Figures:

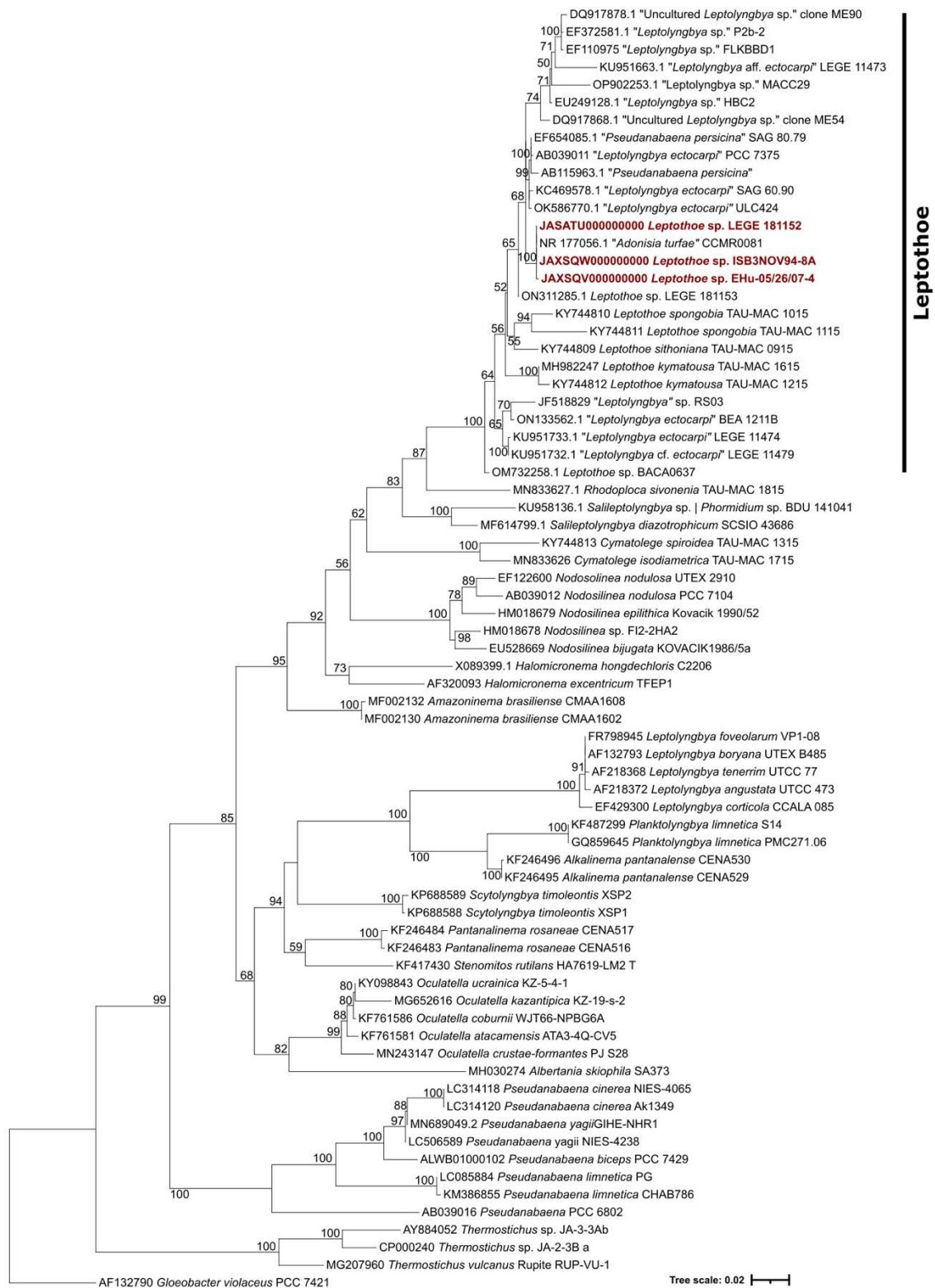
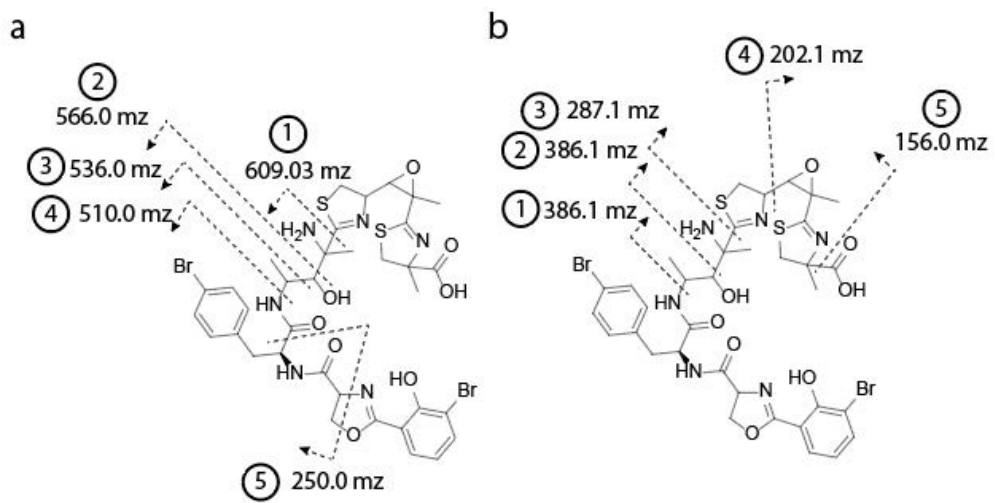
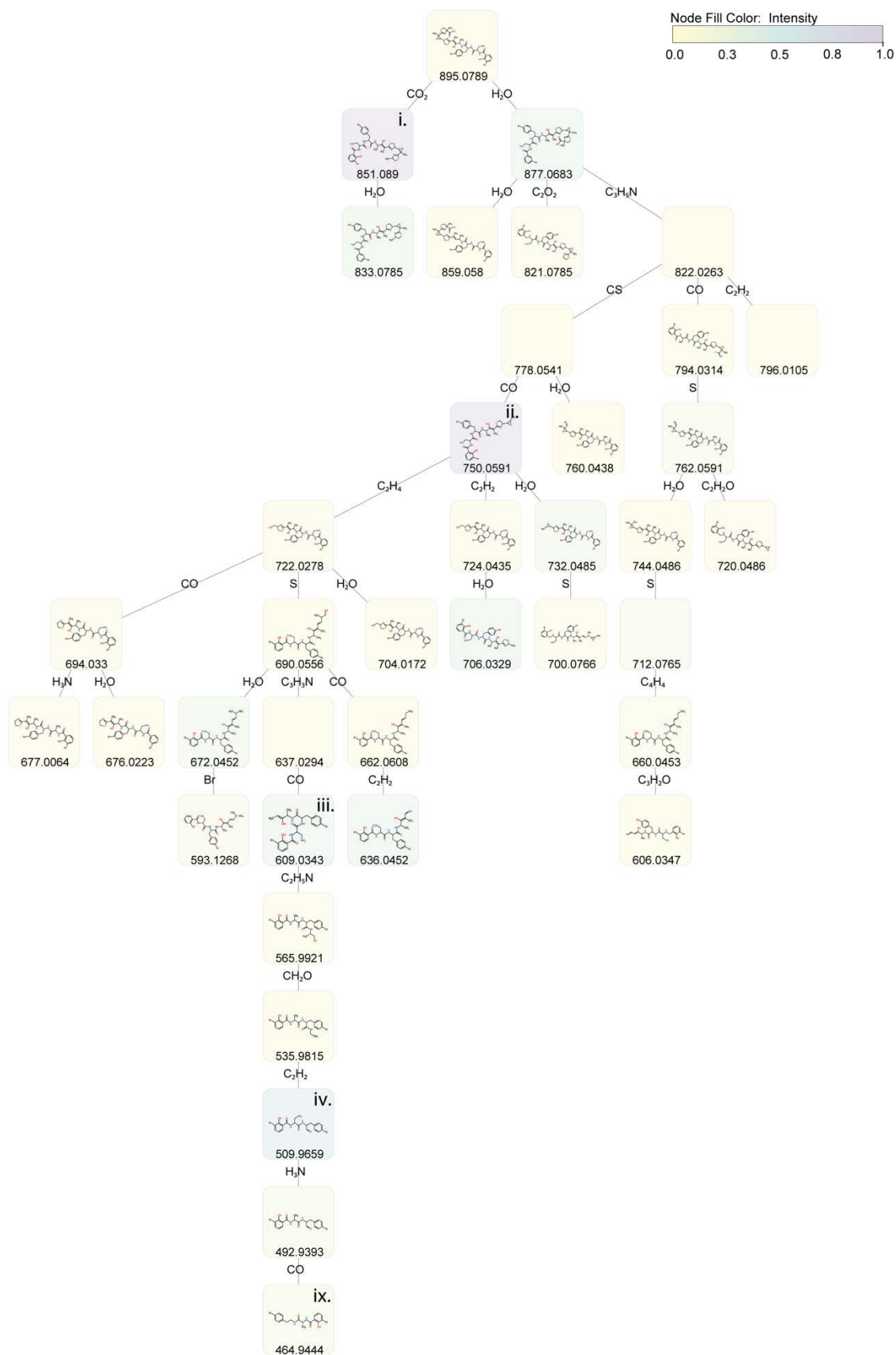


**Fig. S1.** Maximum likelihood (ML) phylogenetic tree based on 73 16S rRNA gene sequences of cyanobacterial strains belonging to the orders Gloeobacterales, Thermostrictales, Pseudanabaenales, Oculatellales, Nodosilineales, Leptolyngbyales and Synechococcales. *Gloeobacter violaceus* PCC 7421 was used as the outgroup. Phylogenetic positions of *Leptothoe* sp. LEGE 181152, *Leptothoe* sp. ISB3NOV94-8A and *Leptothoe* sp. EHU-05/26/07-4 are indicated in bolded red font. Bootstrap values over 50% are indicated at the nodes. Names of strains in quotation marks correspond to GenBank labels.



SI Fig. S2. MS<sup>2</sup> fragmentation pattern for leptochelin A (1) with major ions notated.



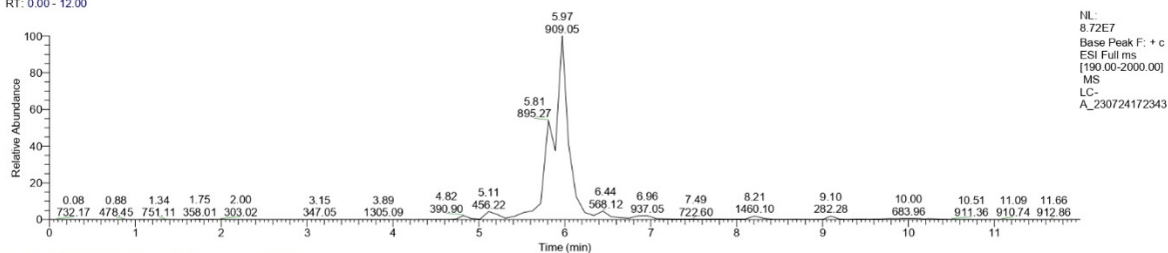
**SI Fig. S3.** Fragmentation trees of the MS<sup>2</sup> CID data for leptochelin A (1). Edges were labeled with the molecular formulas of neutral losses (from MS-FINDER) and nodes with the fragment *m/z* values and annotated structures (from MS-FINDER), and roman numerals referencing the respective structures in Fig. 3. It should be noted that MS-FINDER structures do not account for hydrogen losses and might differ from manually annotated structures given in Fig. 3. Nodes were colored by the respective fragment intensity.



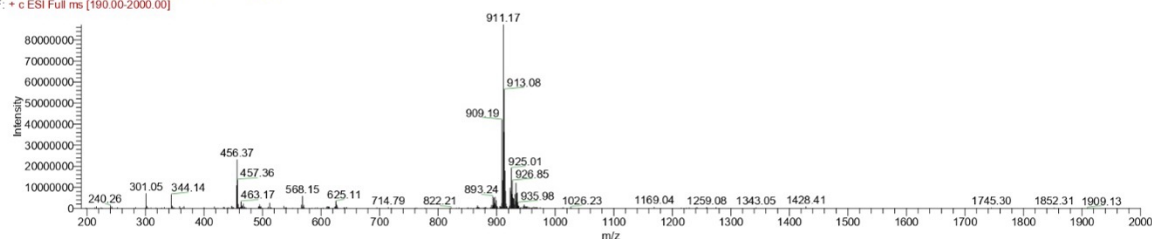


C:\Users\...LC-A\_230724172343

RT: 0.00 - 12.00



LC-A\_230724172343 #237 RT: 5.97 AV: 1 NL: 8.72E7  
F: + c ESI Full ms [190.00-2000.00]



LC-A\_230724172343 #239 RT: 6.01 AV: 1 NL: 1.28E6  
F: + c ESI d Full ms2 909.05@cid35.00 [240.00-920.00]

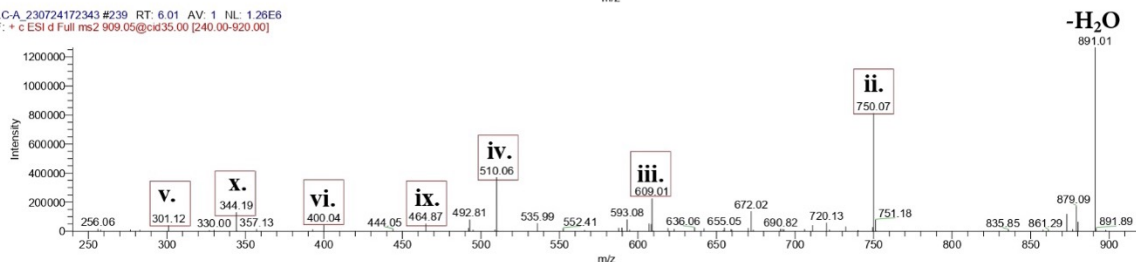


**Fig. S5.** MS<sup>2</sup> fragmentation pattern for methylated leptochelein A (**4**). The top panel shows the base peak chromatogram of leptochelein A after methylation, two major peaks are presented: 895.10 (Rt 5.81) and 909.05 (Rt 5.97) corresponding to unmethylated leptochelein A and methylated leptochelein A, respectively (See **Fig. 3** in main text for numbering of fragment ions). The second panel represents the MS<sup>1</sup> spectrum of the methylated leptochelein A. The bottom panel represents the MS<sup>2</sup> spectrum of the methylated leptochelein A (**4**). Fragments that do not contain a carboxylic acid group (ii., iii., iv., and ix.) maintain their same mass after methylation, while fragments that contain the free carboxylic acid group before methylation (v., vi., and x.) exhibit increased mass due to the addition of a methyl group to the free carboxylic acid.

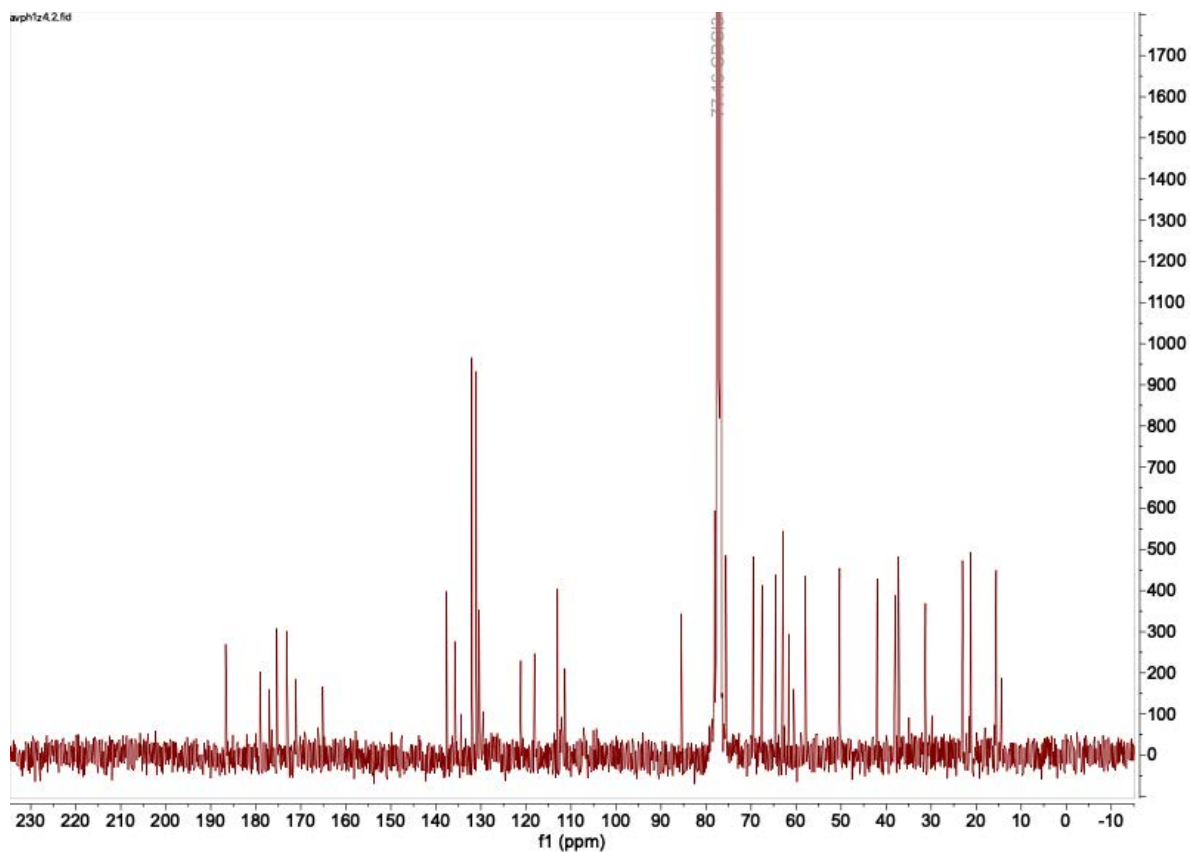


Fig. S6.  $^{13}\text{C}$  NMR spectrum for leptochelin A (1) in  $\text{CDCl}_3$  (100 MHz).

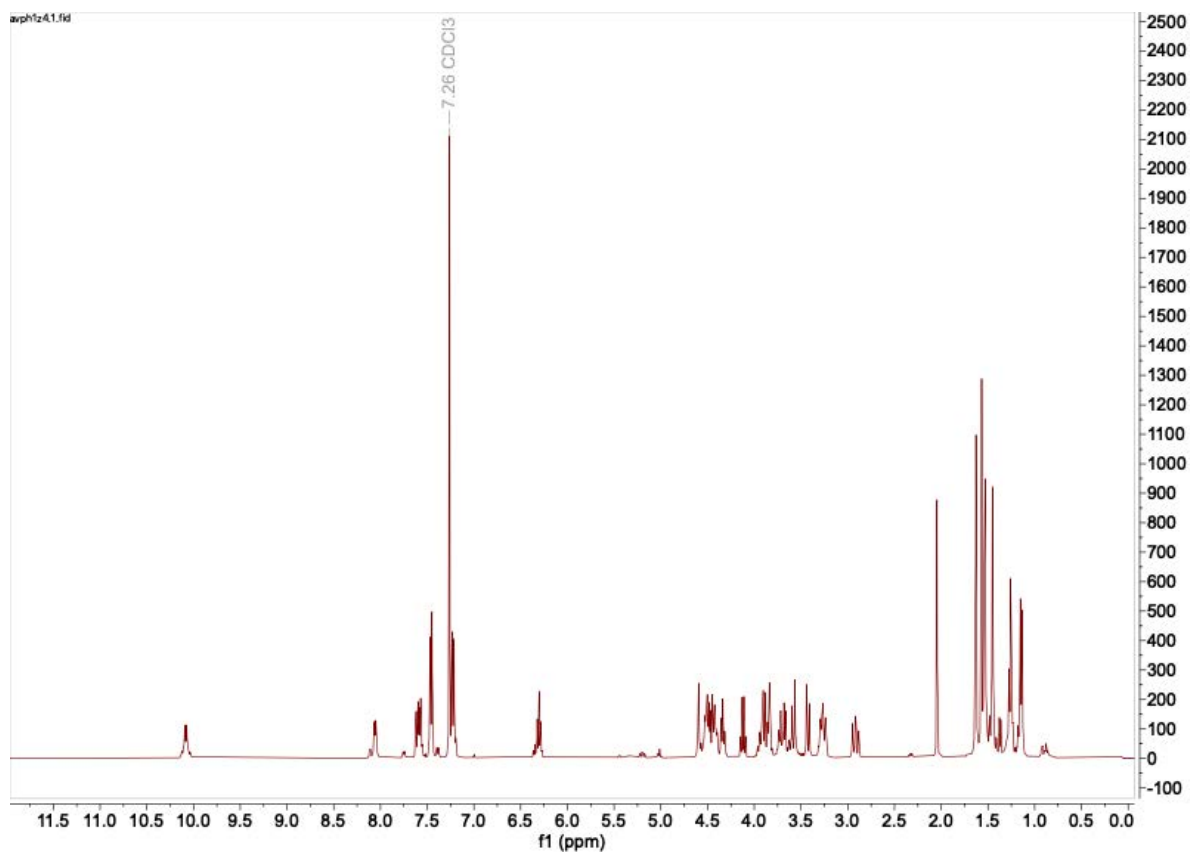


Fig. S7.  $^1\text{H}$  NMR spectrum for leptochelin A (1) in  $\text{CDCl}_3$  (400 MHz).

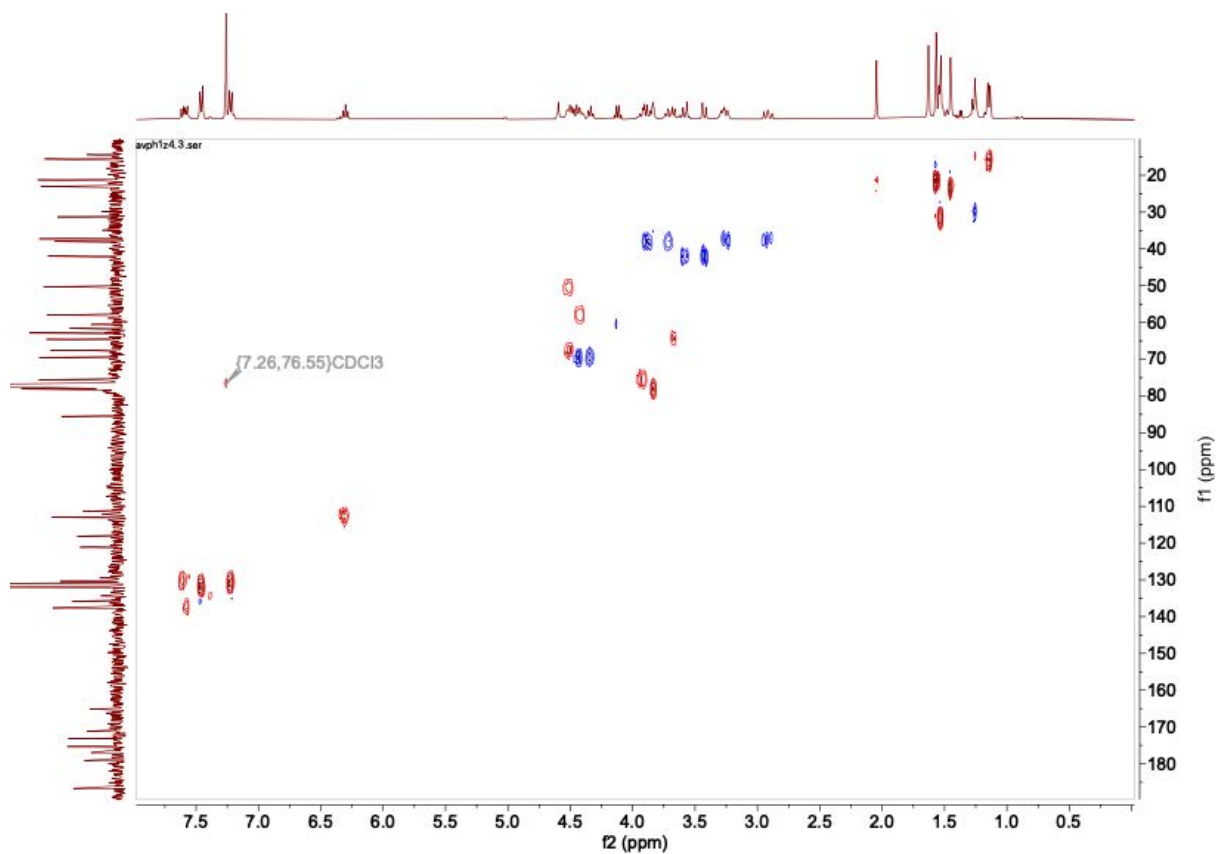


Fig. S8. Multiplicity-edited HSQC spectrum for leptochelin A (**1**) in  $\text{CDCl}_3$  (400 MHz, 100 MHz).

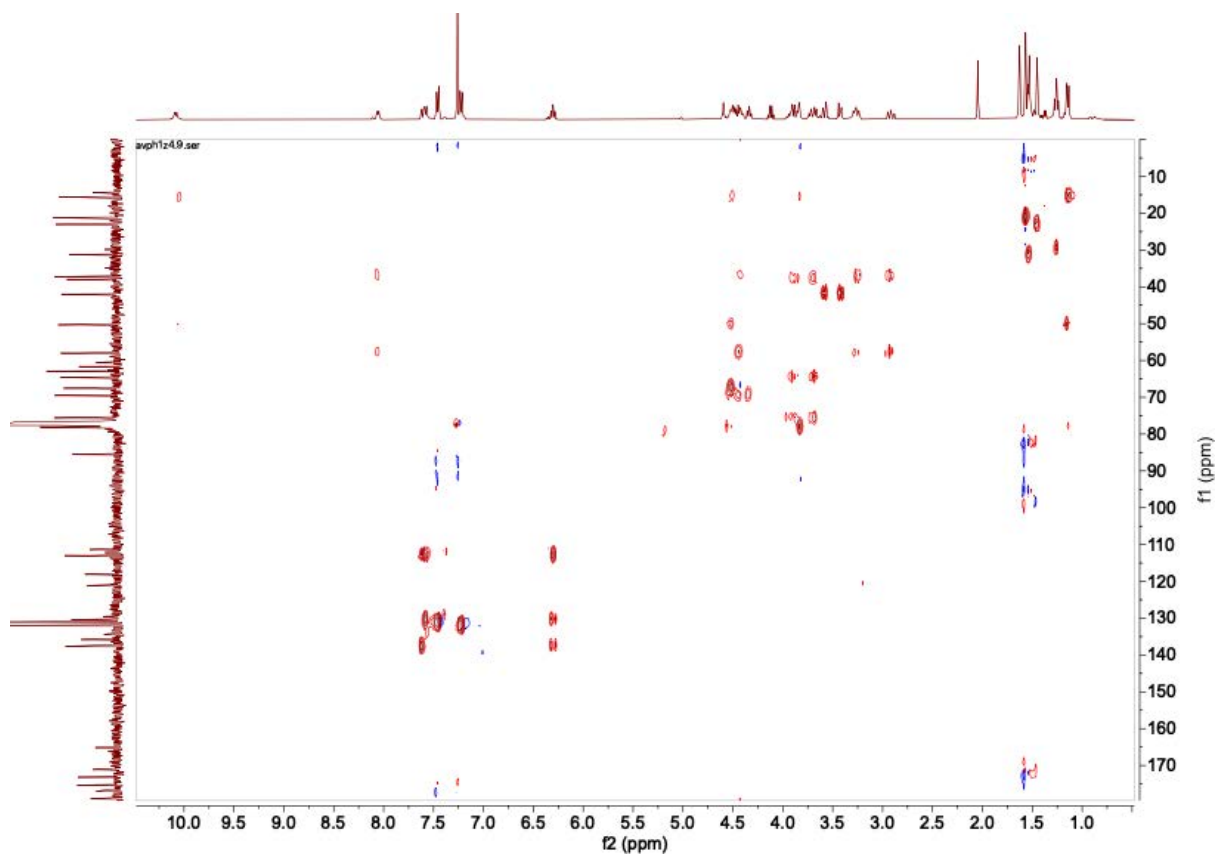


Fig. S9. HSQC-TOCSY spectrum for leptochelin A (**1**) in  $\text{CDCl}_3$  (400 MHz).

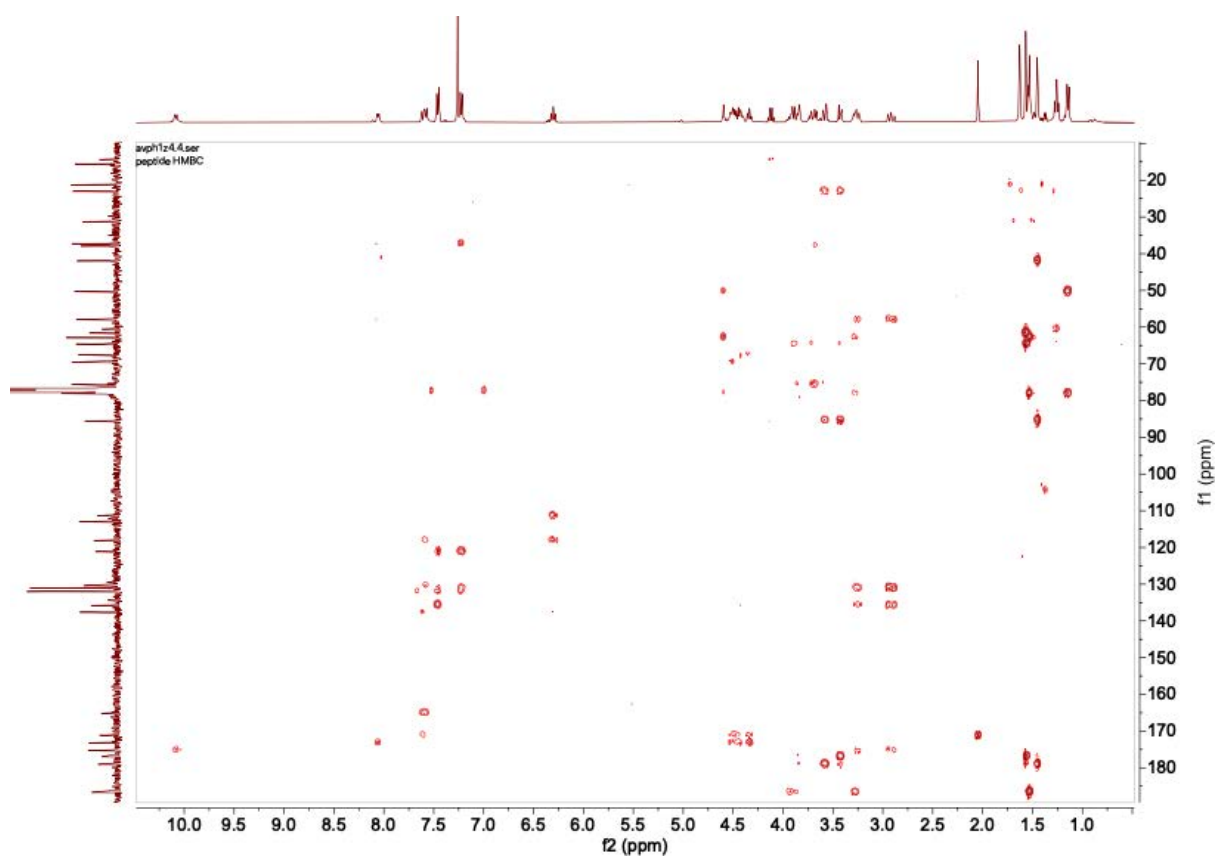


Fig. S10. HMBC spectrum for leptochelin A (1) in CDCl<sub>3</sub> (400 MHz).

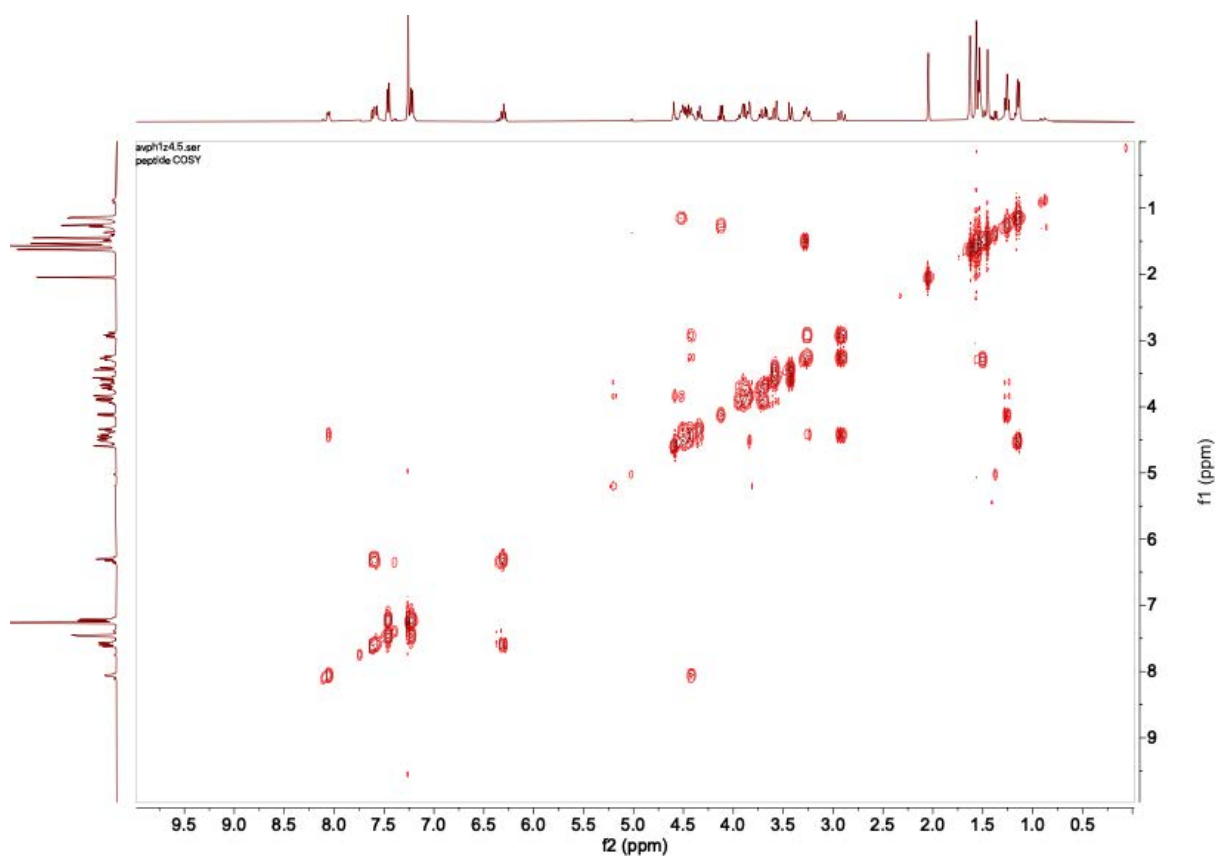
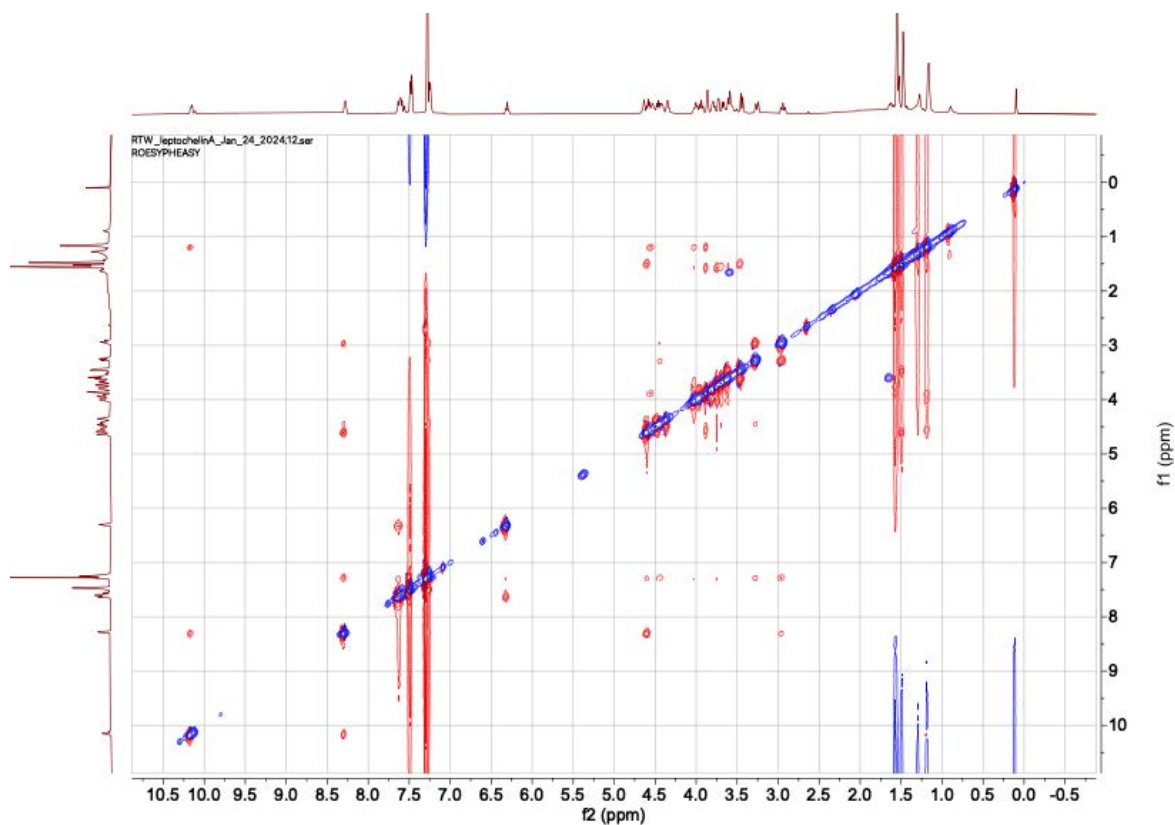
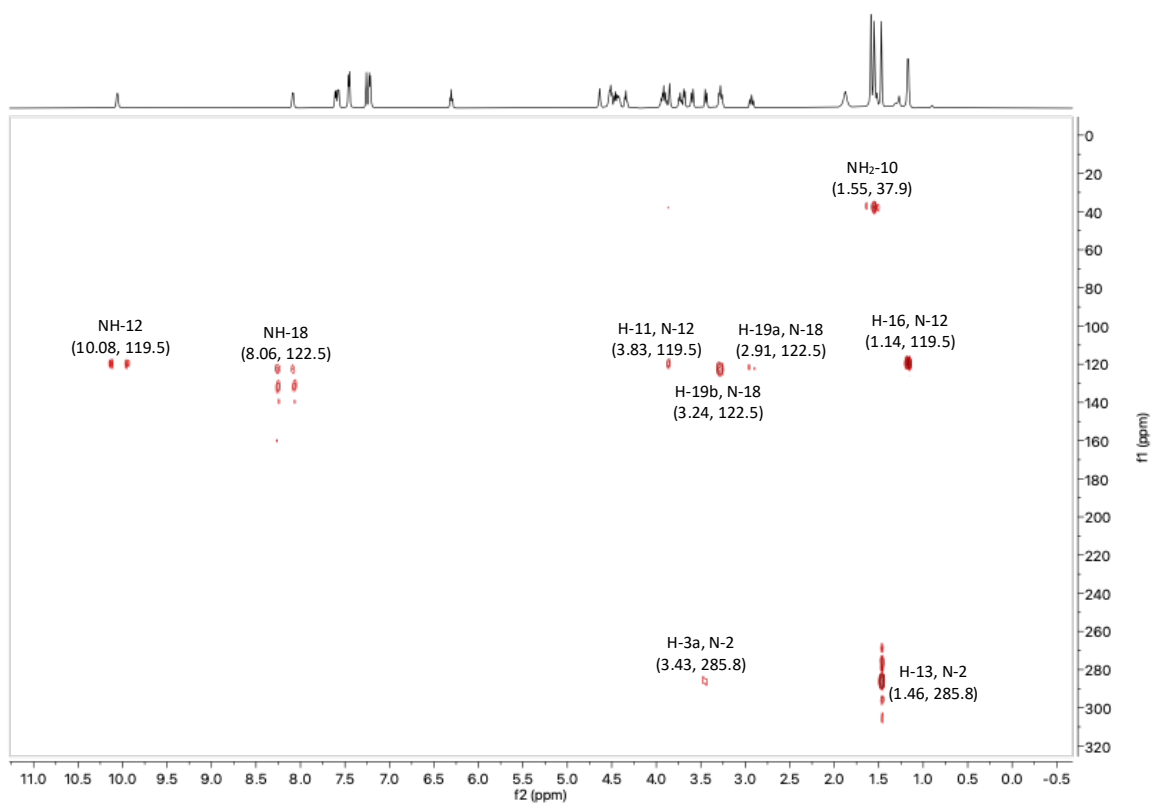


Fig. S11. <sup>1</sup>H-<sup>1</sup>H COSY spectrum for leptochelin A (1) in CDCl<sub>3</sub> (400 MHz).



**Fig. S12.** ROESY spectrum for leptochelin A (**1**) in  $\text{CDCl}_3$  (500 MHz).



**Fig. S13.**  $^1\text{H}$ - $^{15}\text{N}$  gHMBC spectrum for leptochelin A (**1**) in  $\text{CDCl}_3$  (500 MHz). The spectrum was acquired without a lowpass J filter, allowing for observation of 1-bond correlations ( $\text{NH}_2$ -10, NH-12, and NH-18) in addition to the 2- and 3-bond HMBC correlations.

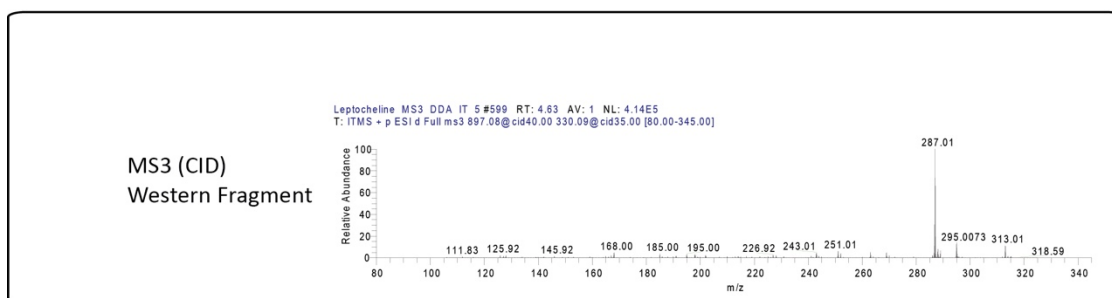
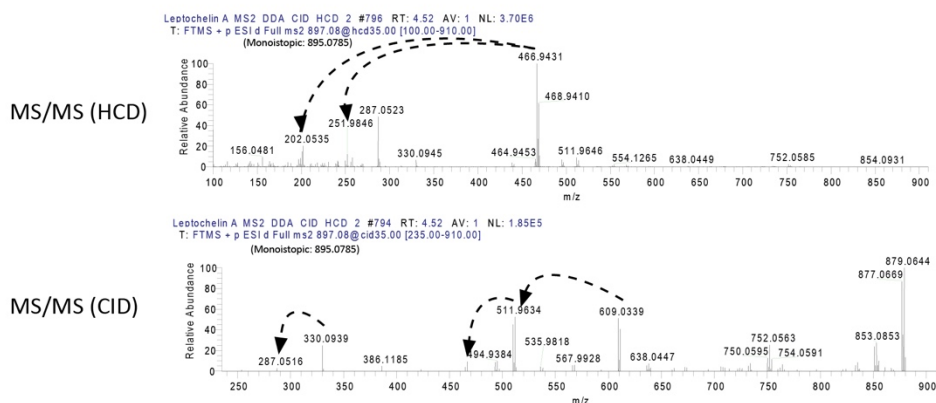
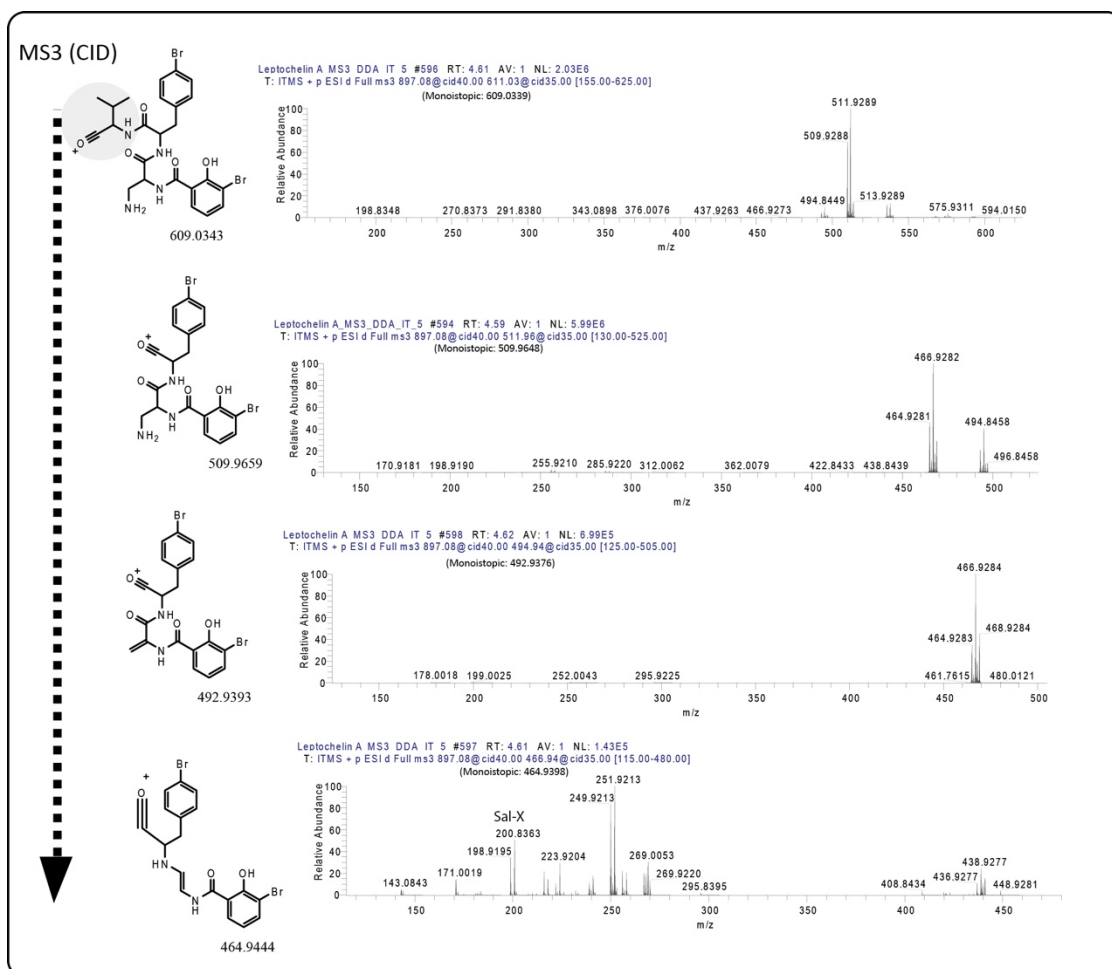


Fig. S14. MS<sup>3</sup> fragmentation series of the N-terminal fragments from leptochelin A (1).

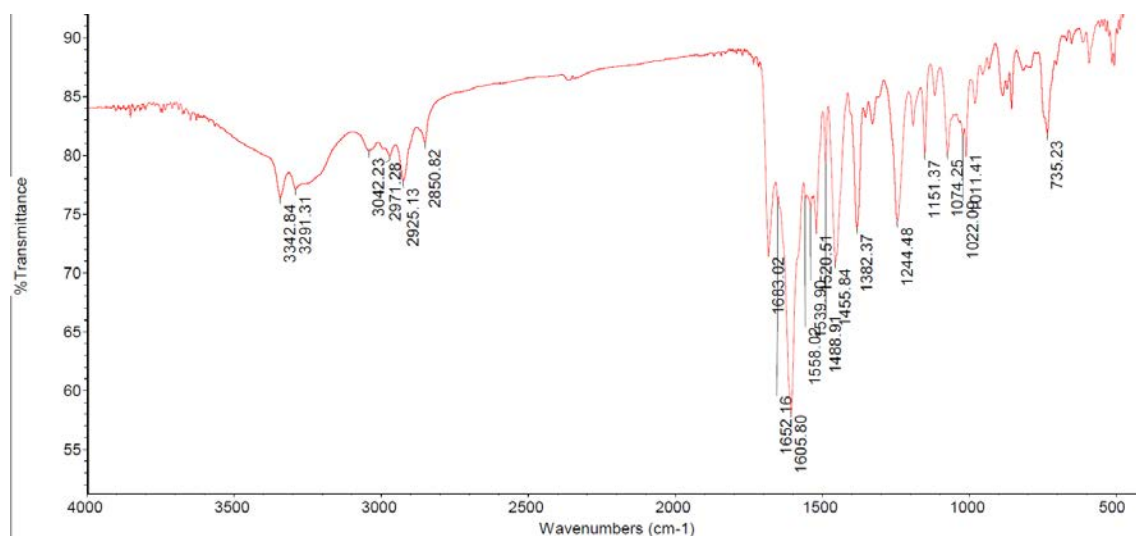


Fig. S15. IR spectrum for leptochelin A (1).

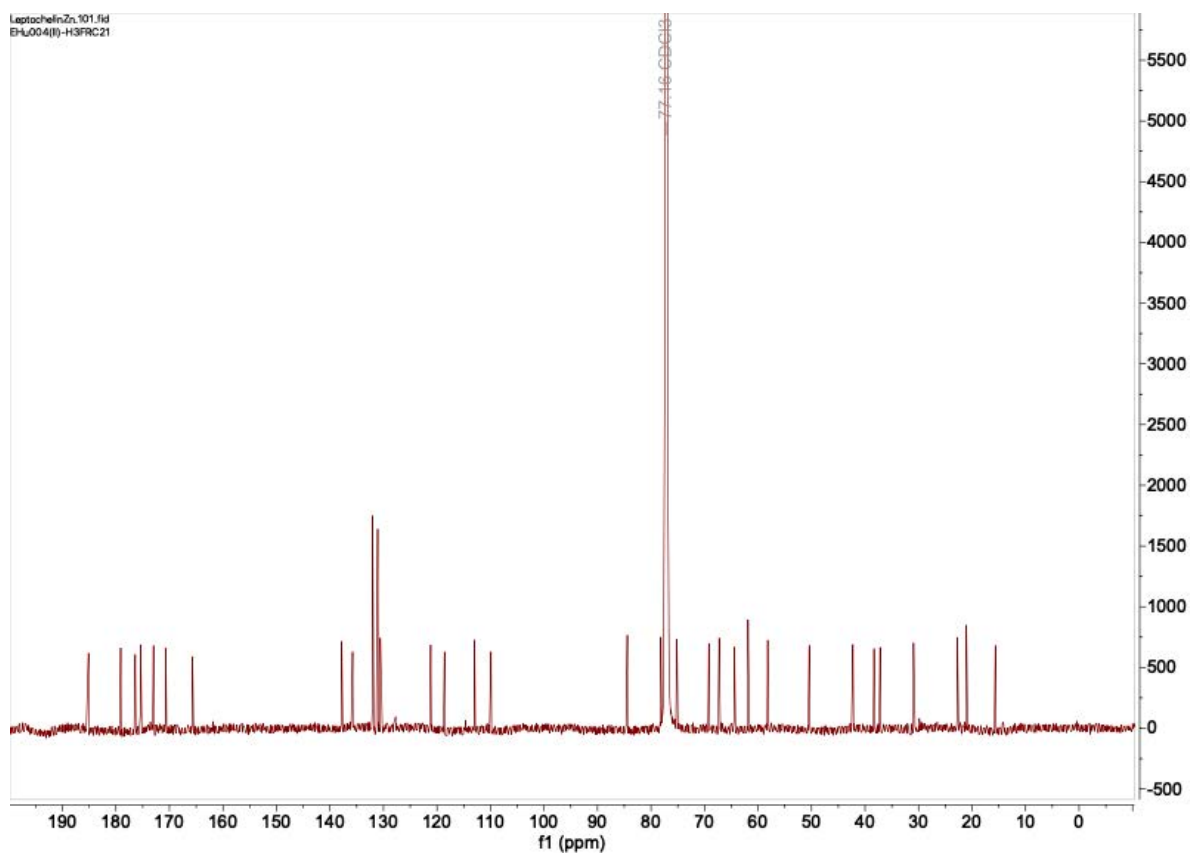


Fig. S16. <sup>13</sup>C NMR spectrum for zinc-bound leptochelin A (1) in CDCl<sub>3</sub> (150 MHz).



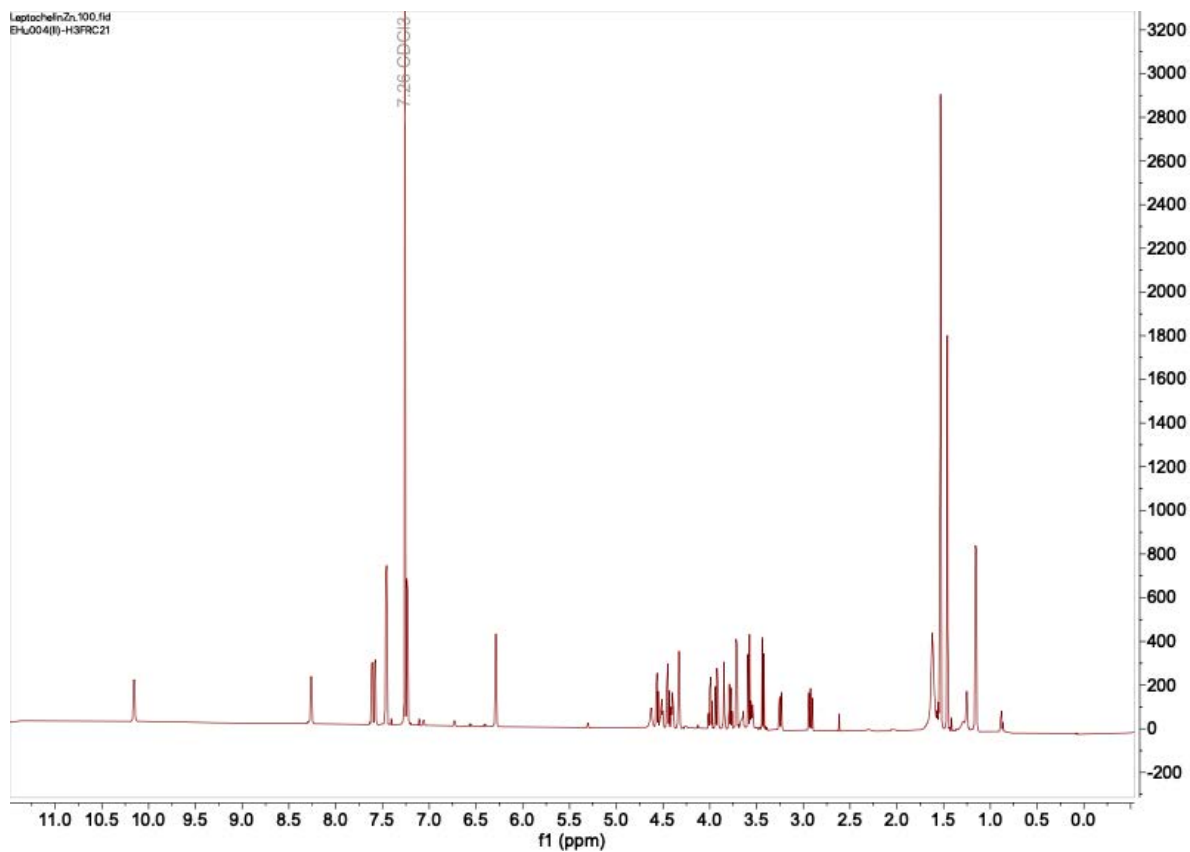


Fig. S17. <sup>1</sup>H NMR spectrum for zinc-bound leptochelin A (1) in CDCl<sub>3</sub> (600 MHz).

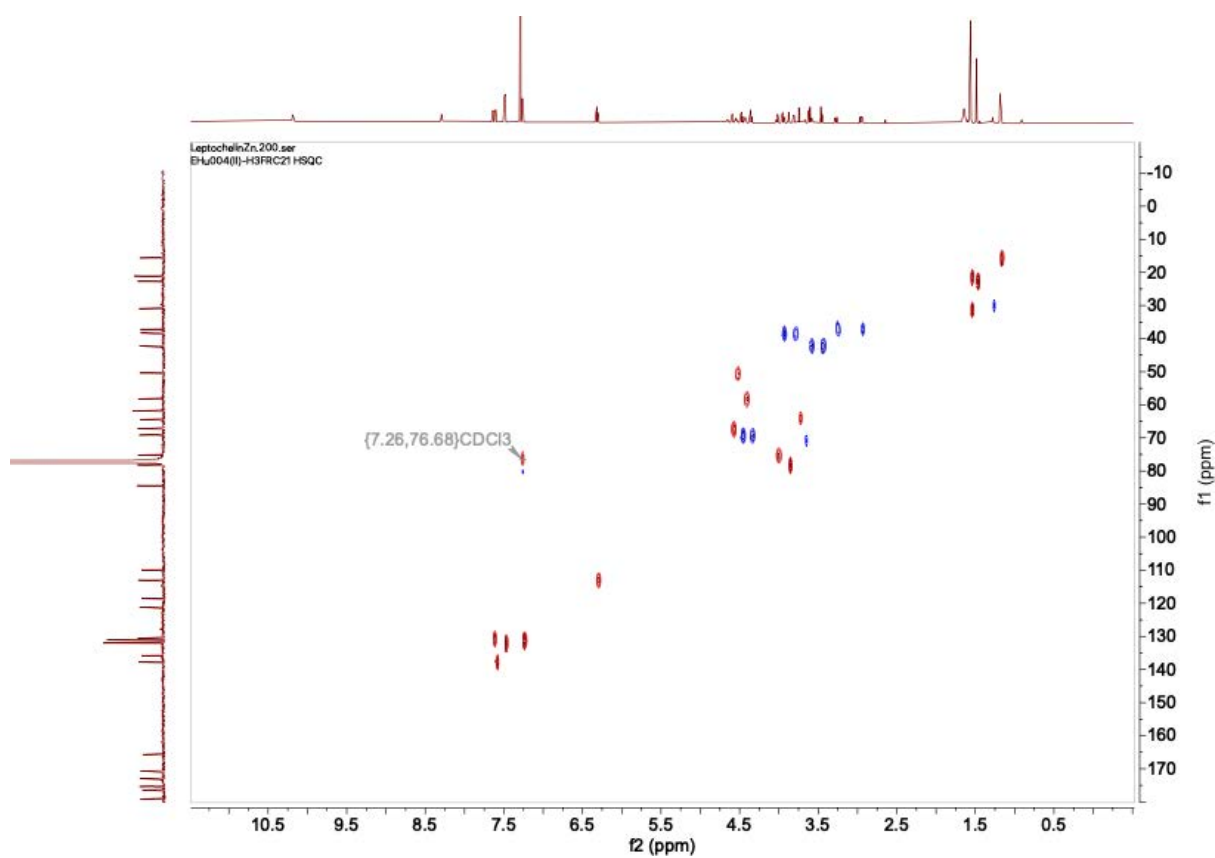
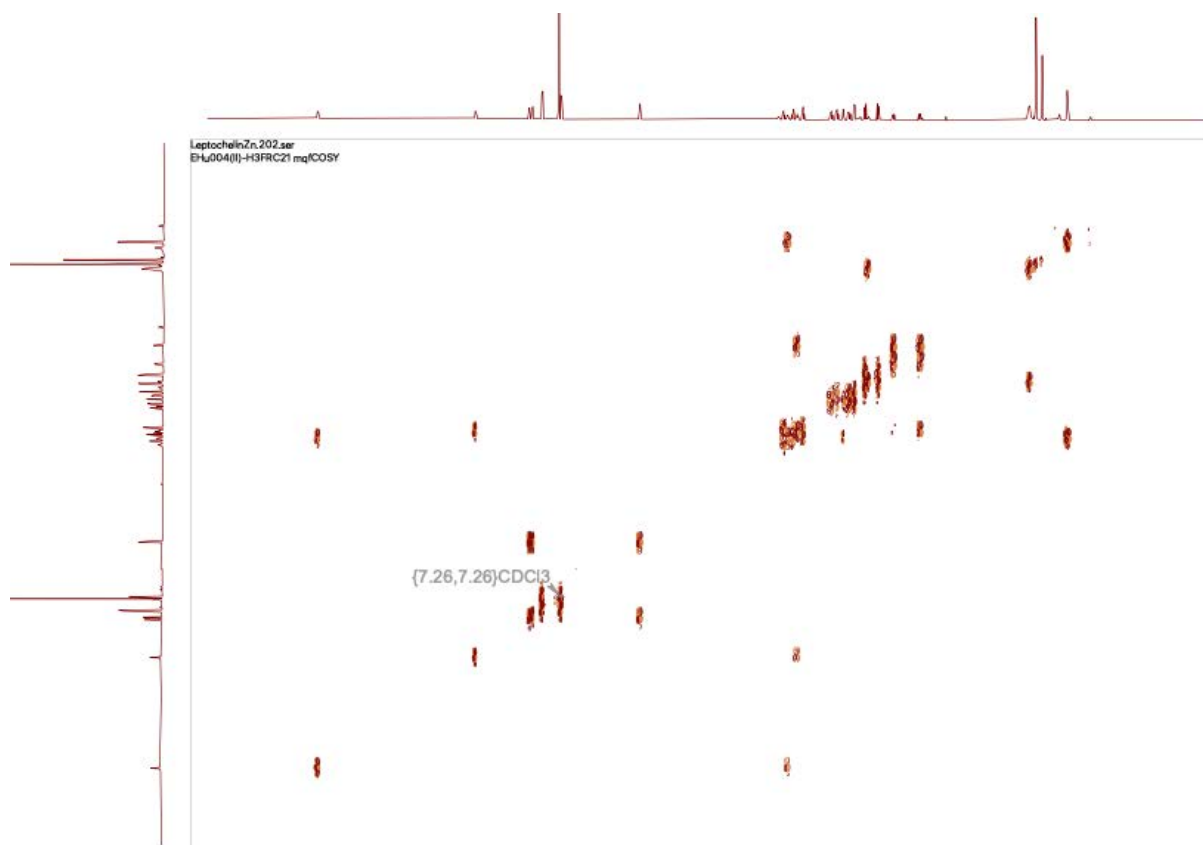
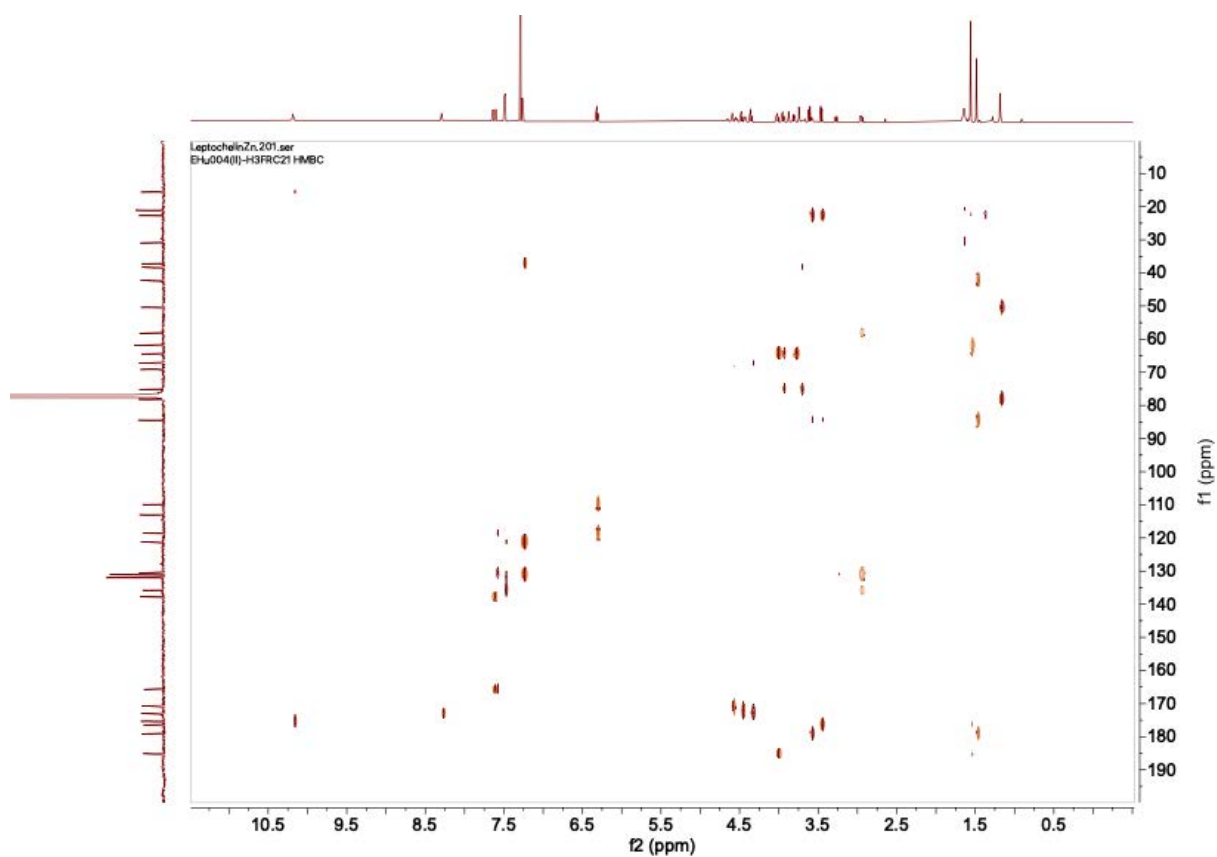


Fig. S18. Multiplicity-edited HSQC spectrum for zinc-bound leptochelin A (1) in CDCl<sub>3</sub> (600 MHz).



**Fig. S19.** <sup>1</sup>H-<sup>1</sup>H COSY spectrum for zinc-bound leptochelin A (**1**) in CDCl<sub>3</sub> (600 MHz).



**Fig. S20.** HMBC spectrum for zinc-bound leptochelin A (**1**) in CDCl<sub>3</sub> (600 MHz).

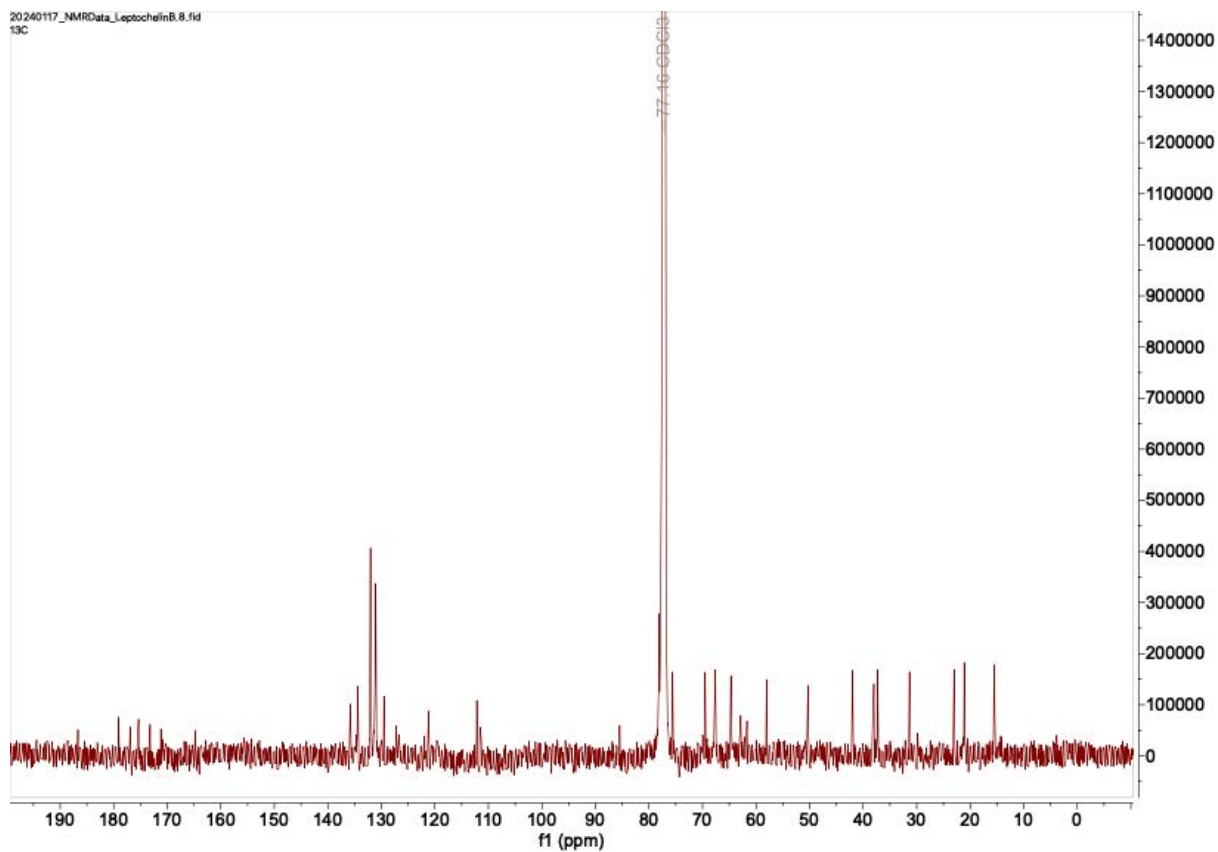


Fig. S21.  $^{13}\text{C}$  NMR spectrum for leptochelin B (**2**) in  $\text{CDCl}_3$  (200 MHz).

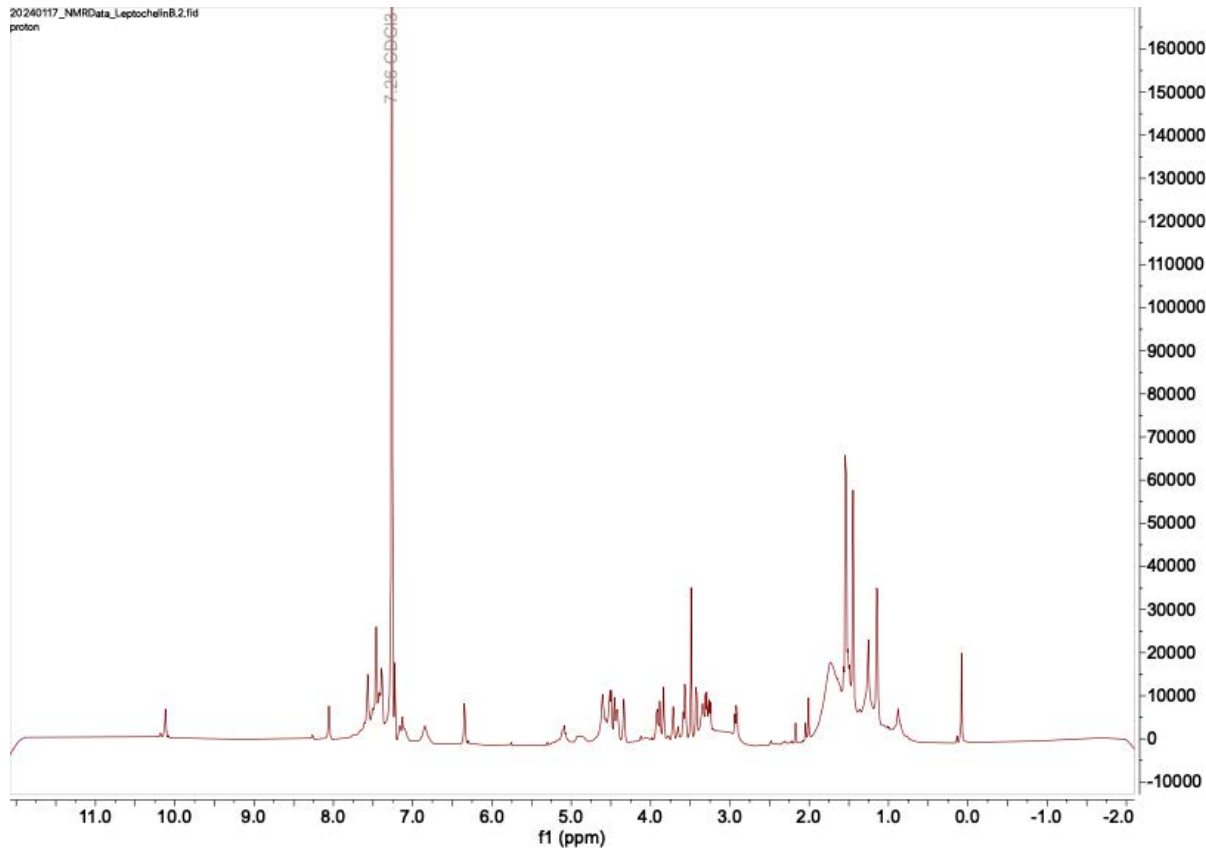


Fig. S22.  $^1\text{H}$  NMR spectrum for leptochelin B (**2**) in  $\text{CDCl}_3$  (800 MHz).

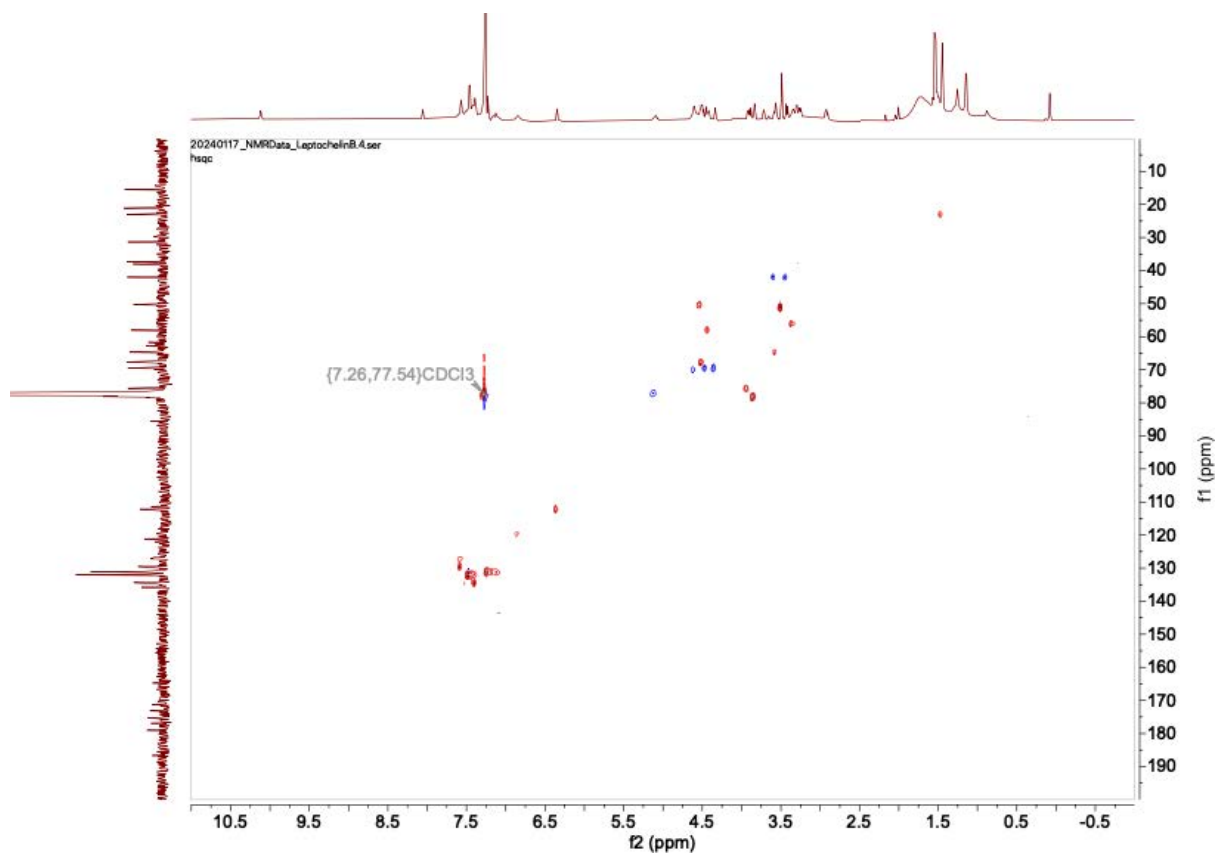


Fig. S23. Multiplicity-edited HSQC spectrum for leptochelin B (**2**) in CDCl<sub>3</sub> (800 MHz).

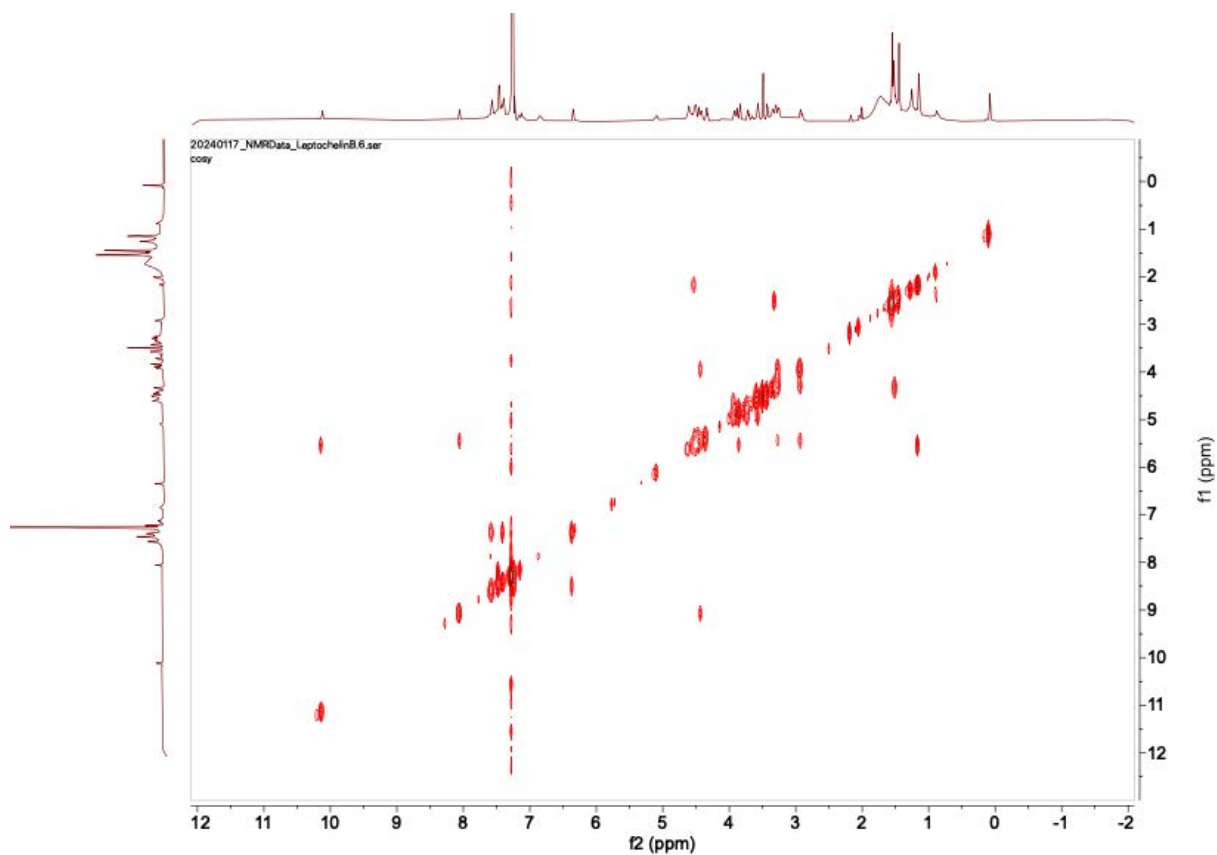


Fig. S24. <sup>1</sup>H-<sup>1</sup>H COSY spectrum for leptochelin B (**2**) in CDCl<sub>3</sub> (800 MHz).

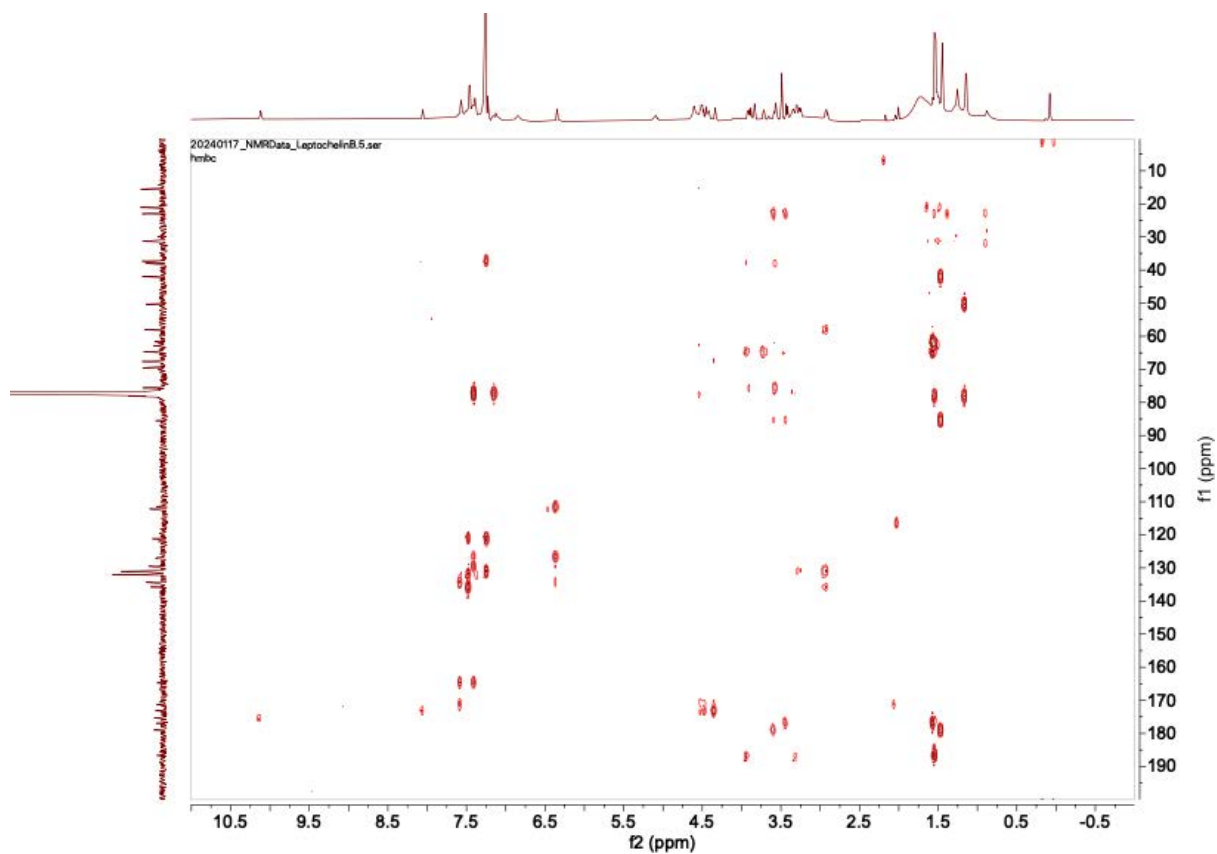


Fig. S25. HMBC spectrum for leptochelin B (**2**) in  $\text{CDCl}_3$  (800 MHz).

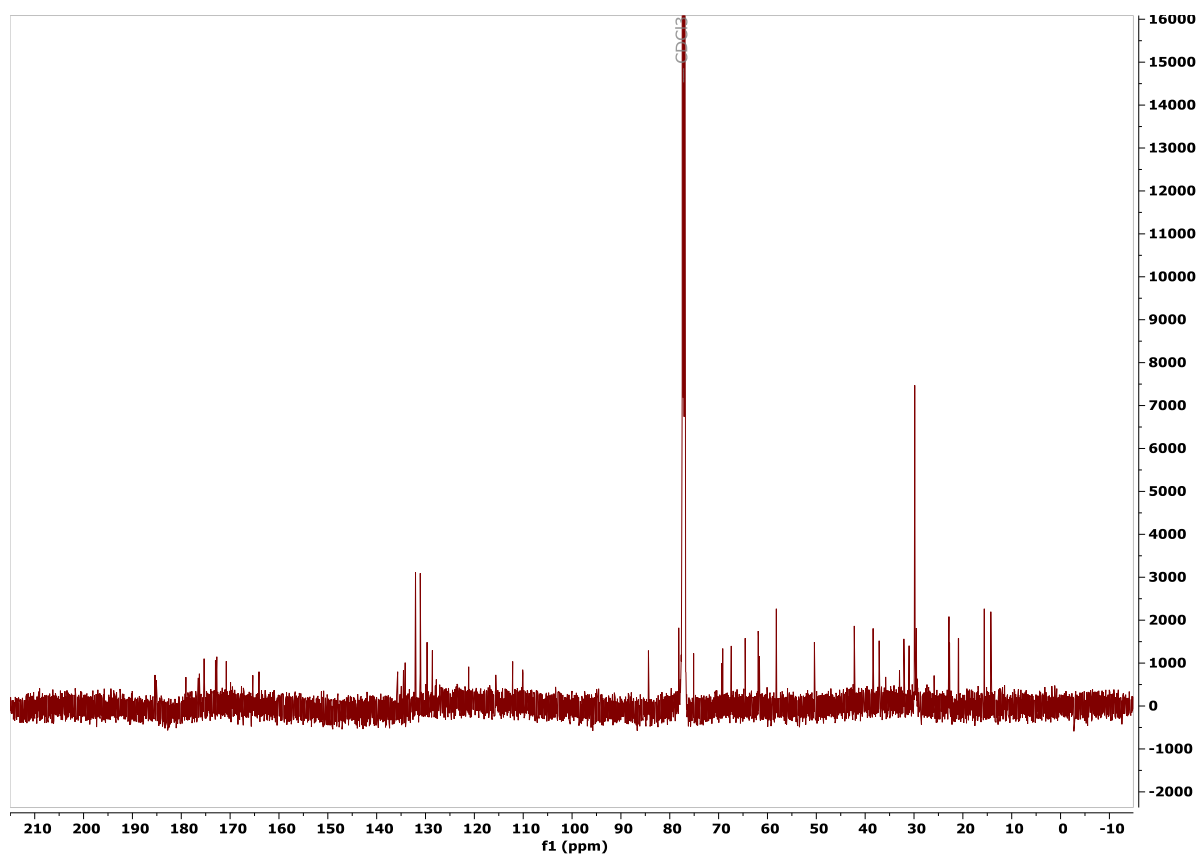


Fig. S26.  $^{13}\text{C}$  NMR spectrum for zinc-bound leptochelin B (**2**) in  $\text{CDCl}_3$  (150 MHz).

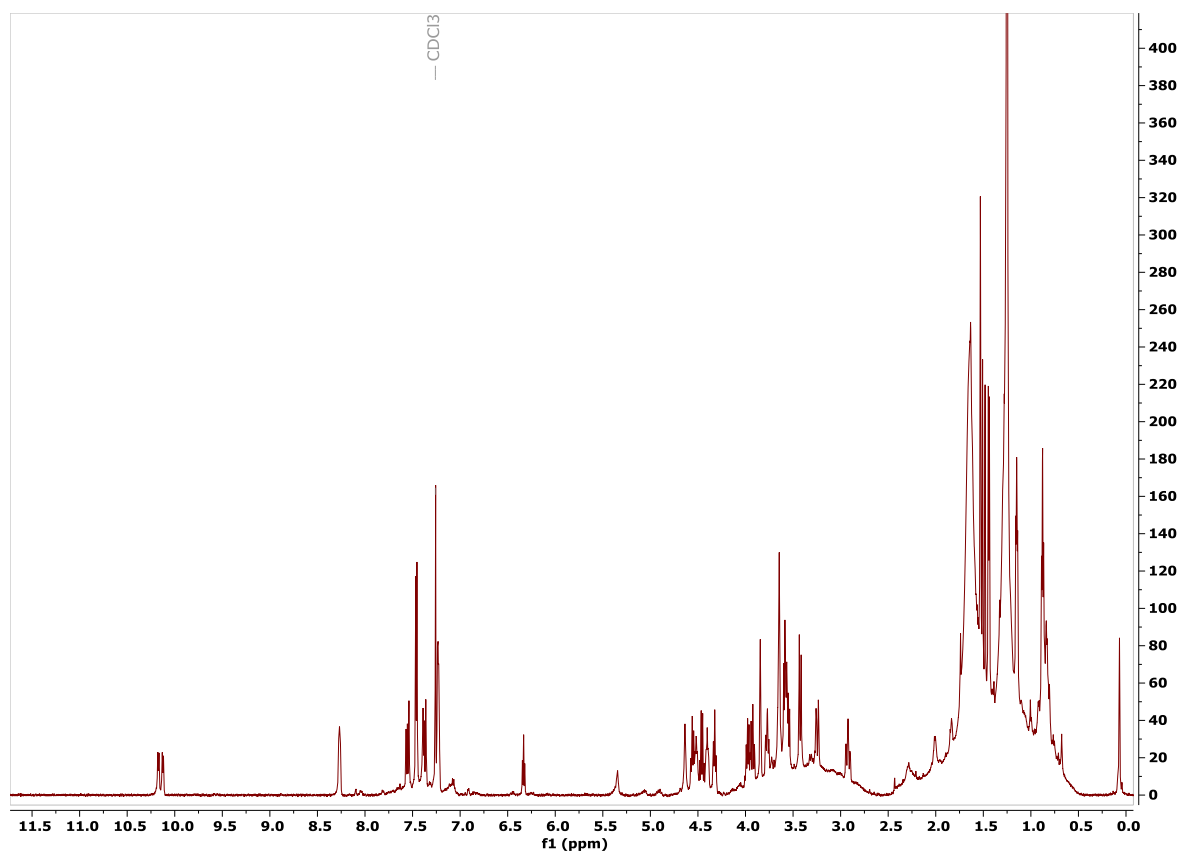


Fig. S27.  $^1\text{H}$  NMR spectrum for zinc-bound leptochelin B (**2**) in  $\text{CDCl}_3$  (600 MHz).

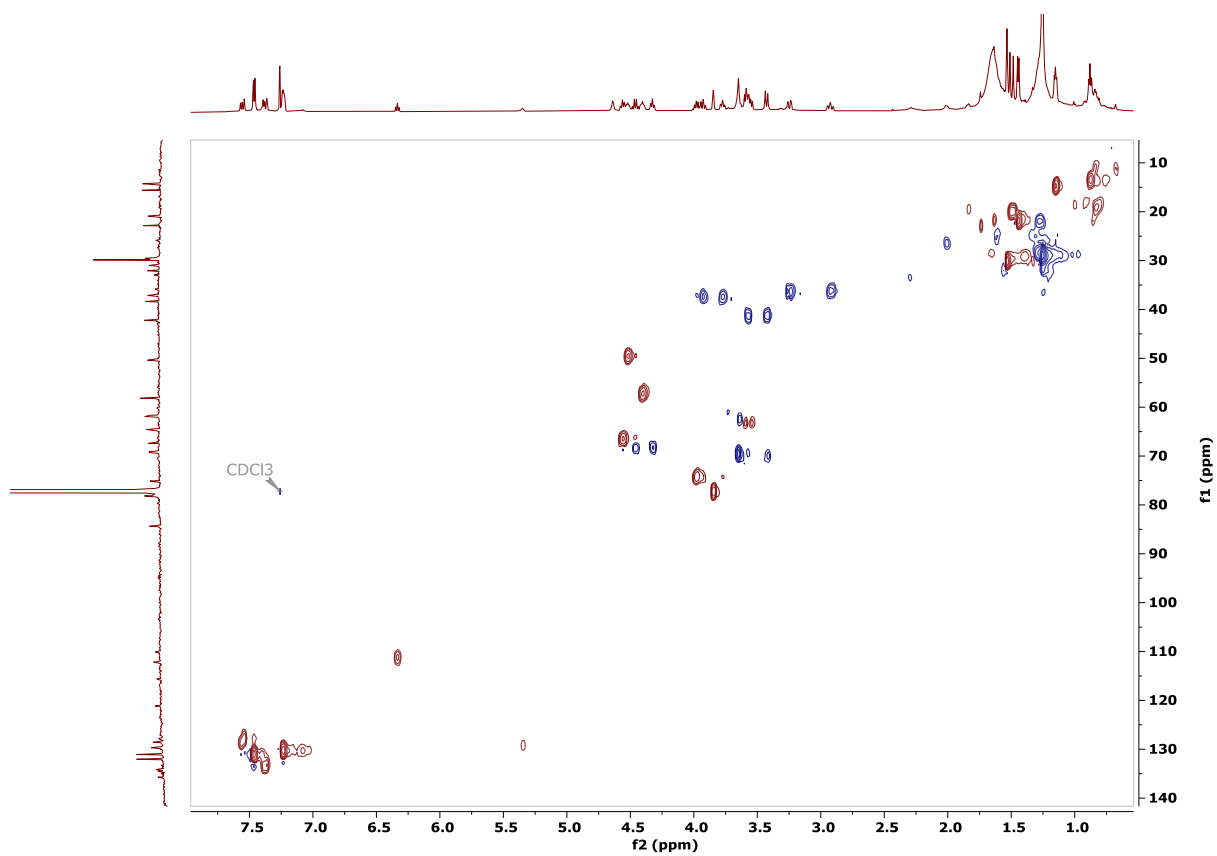


Fig. S28. Multiplicity-edited HSQC spectrum for zinc-bound leptochelin B (**2**) in  $\text{CDCl}_3$  (600 MHz).

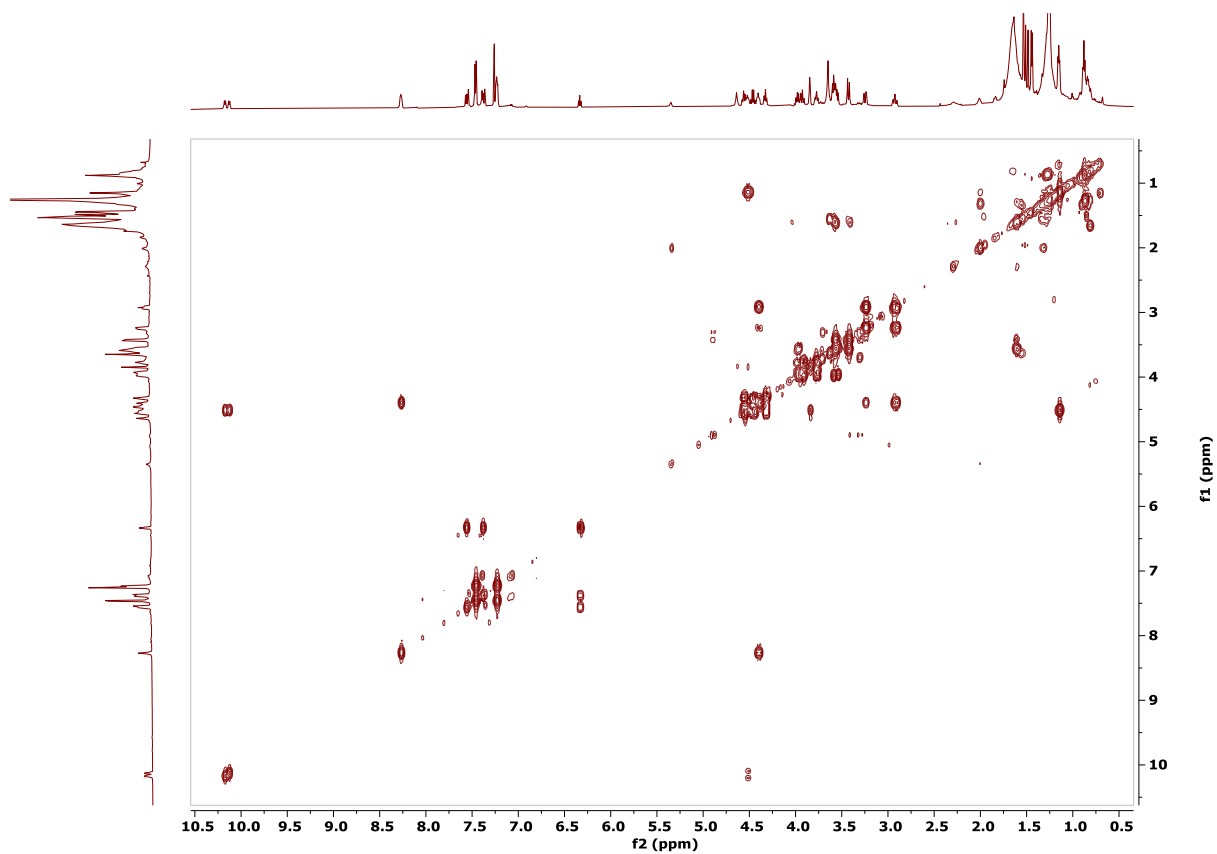


Fig. S29.  $^1\text{H}$ - $^1\text{H}$  COSY spectrum for zinc-bound leptochelin B (**2**) in  $\text{CDCl}_3$  (600 MHz).

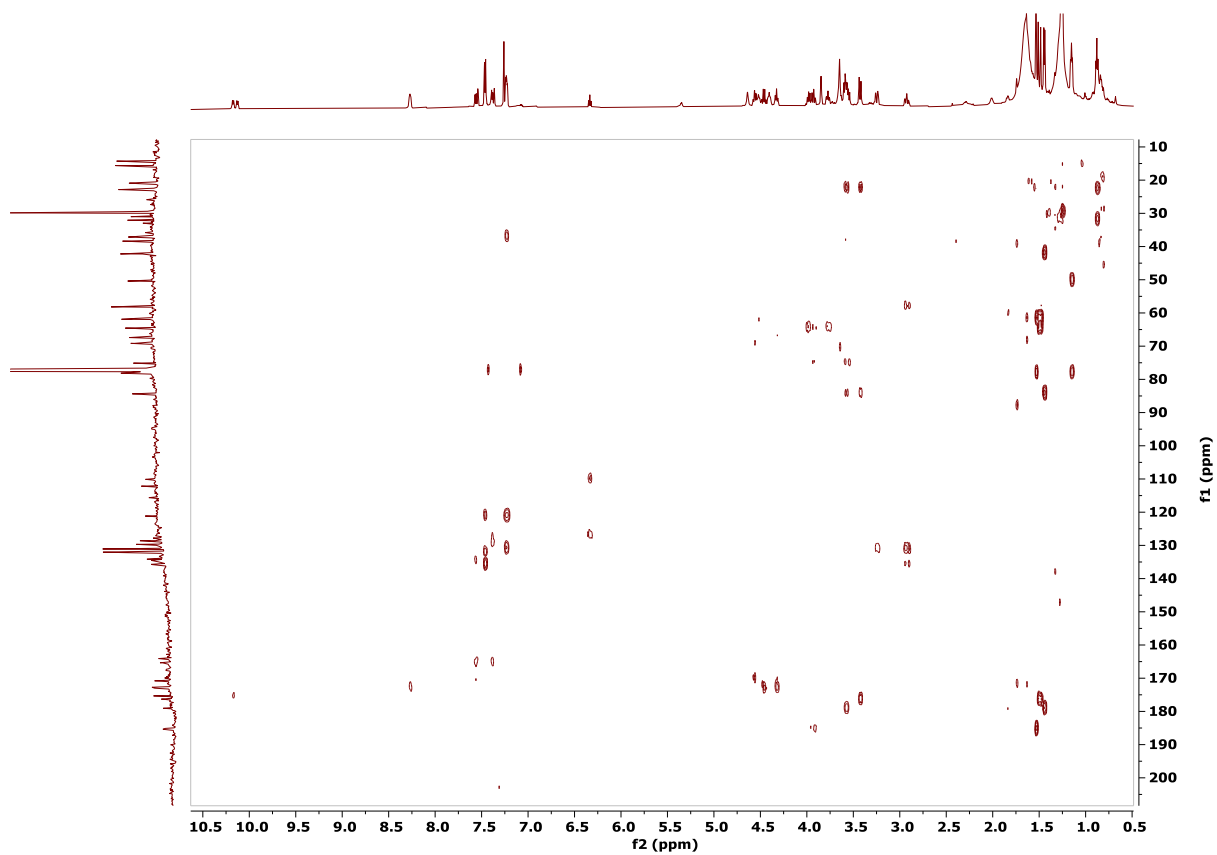


Fig. S30. HMBC spectrum for zinc-bound leptochelin B (**2**) in  $\text{CDCl}_3$  (600 MHz).

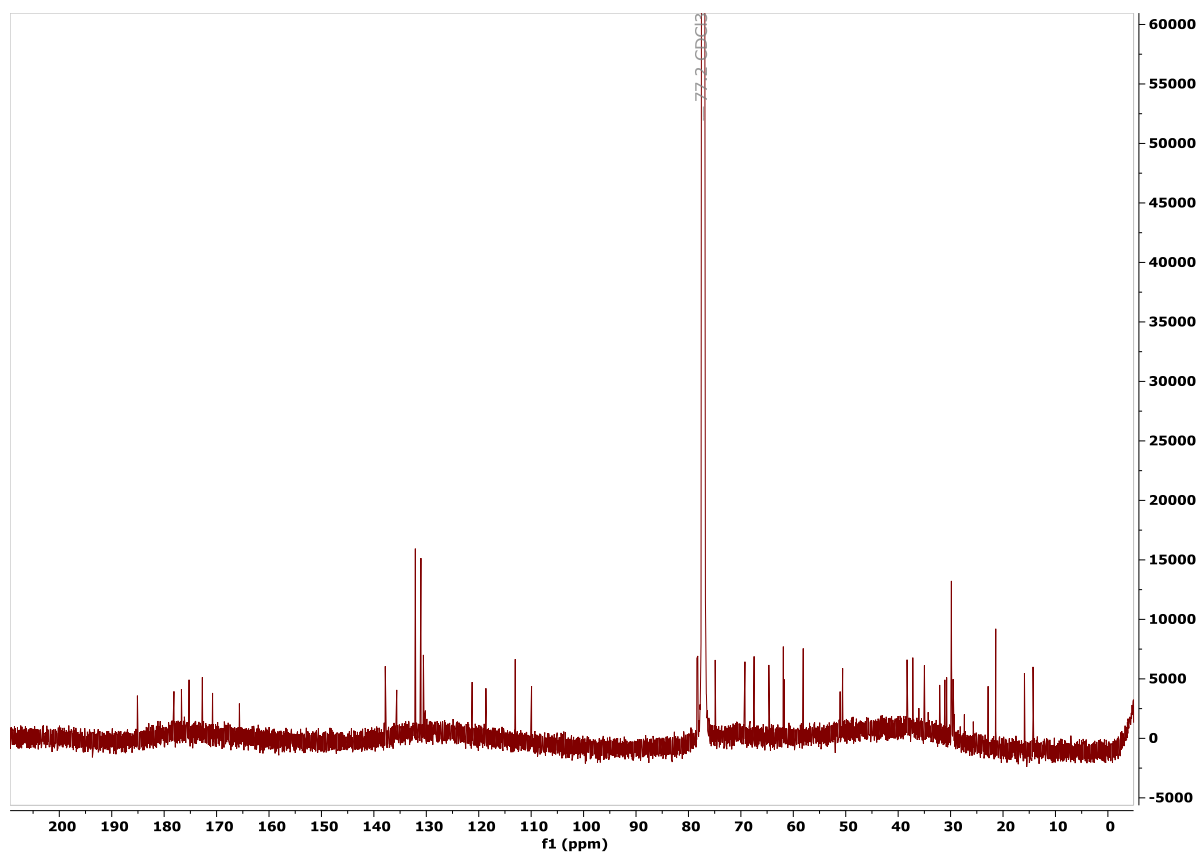


Fig. S31.  $^{13}\text{C}$  NMR spectrum for leptochelin C (**3**) in  $\text{CDCl}_3$  (150 MHz).

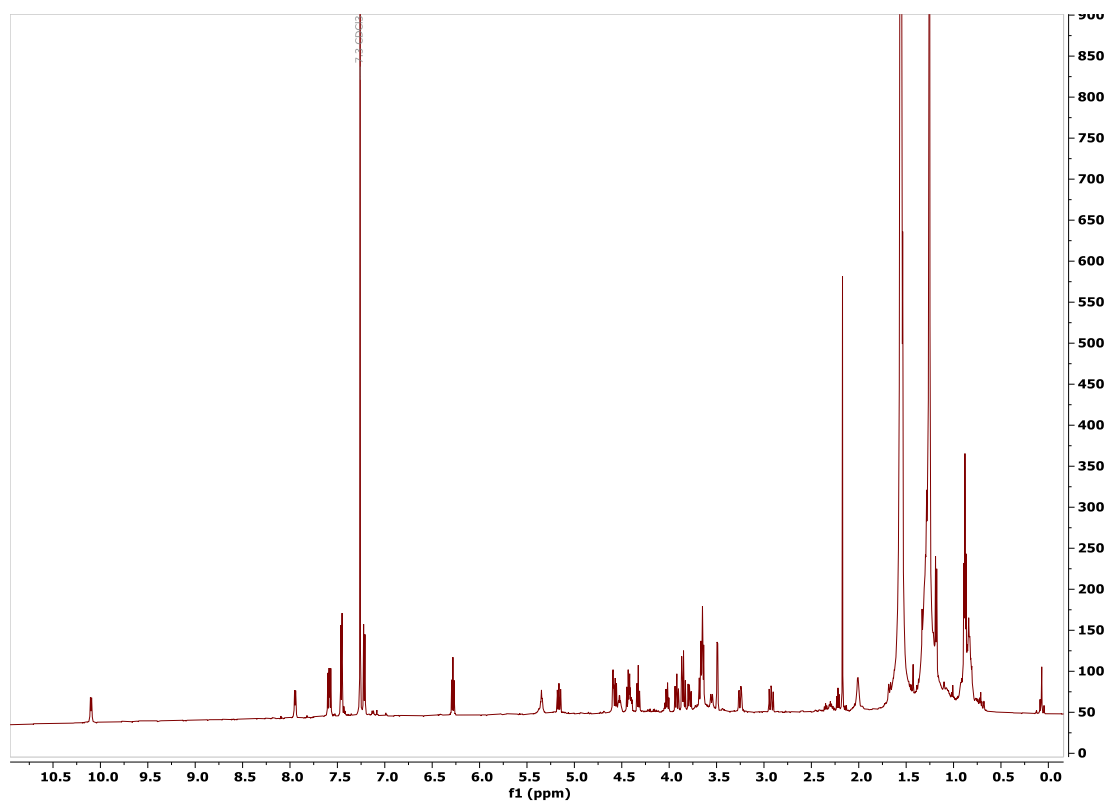


Fig. S32.  $^1\text{H}$  NMR spectrum for leptochelin C (**3**) in  $\text{CDCl}_3$  (600 MHz).



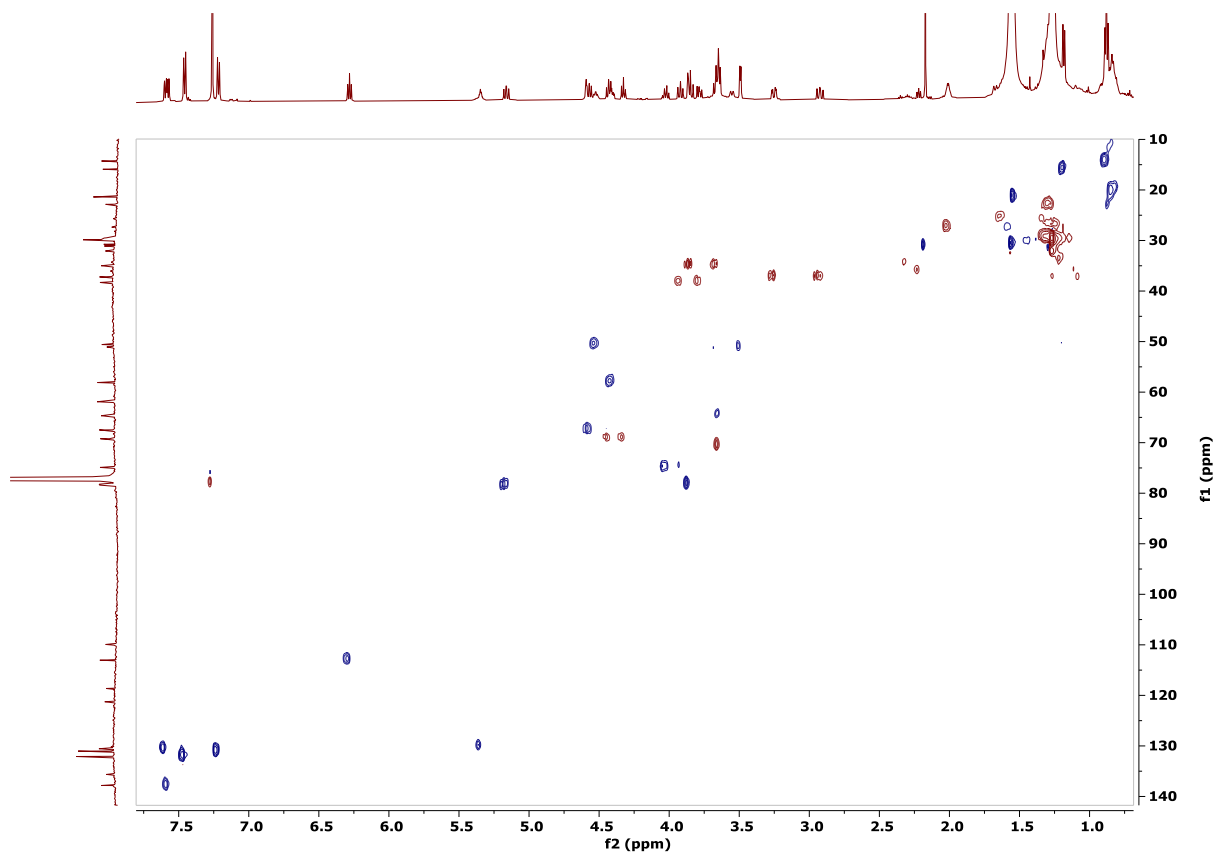


Fig. S33. Multiplicity-edited HSQC spectrum for leptochelin C (**3**) in  $\text{CDCl}_3$  (600 MHz).

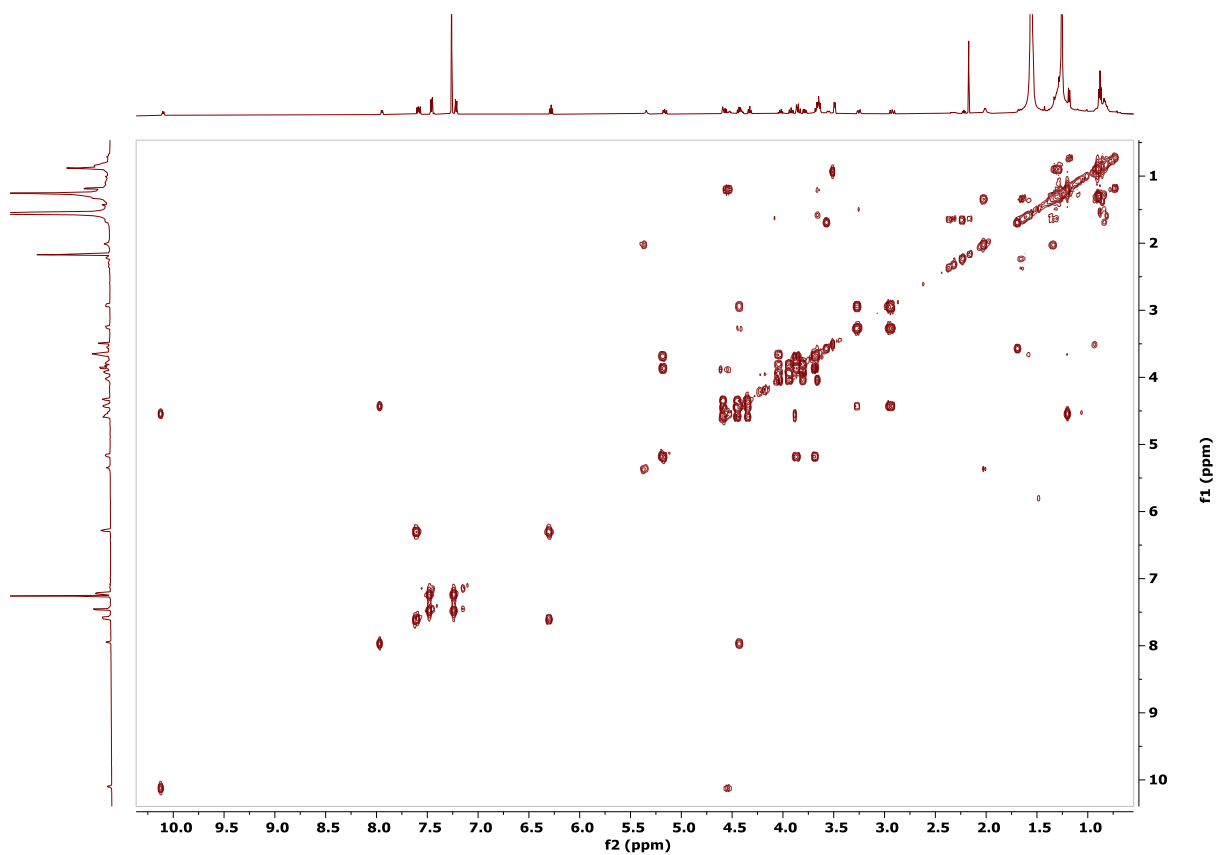


Fig. S34.  $^1\text{H}$ - $^1\text{H}$  COSY spectrum for leptochelin C (**3**) in  $\text{CDCl}_3$  (600 MHz).

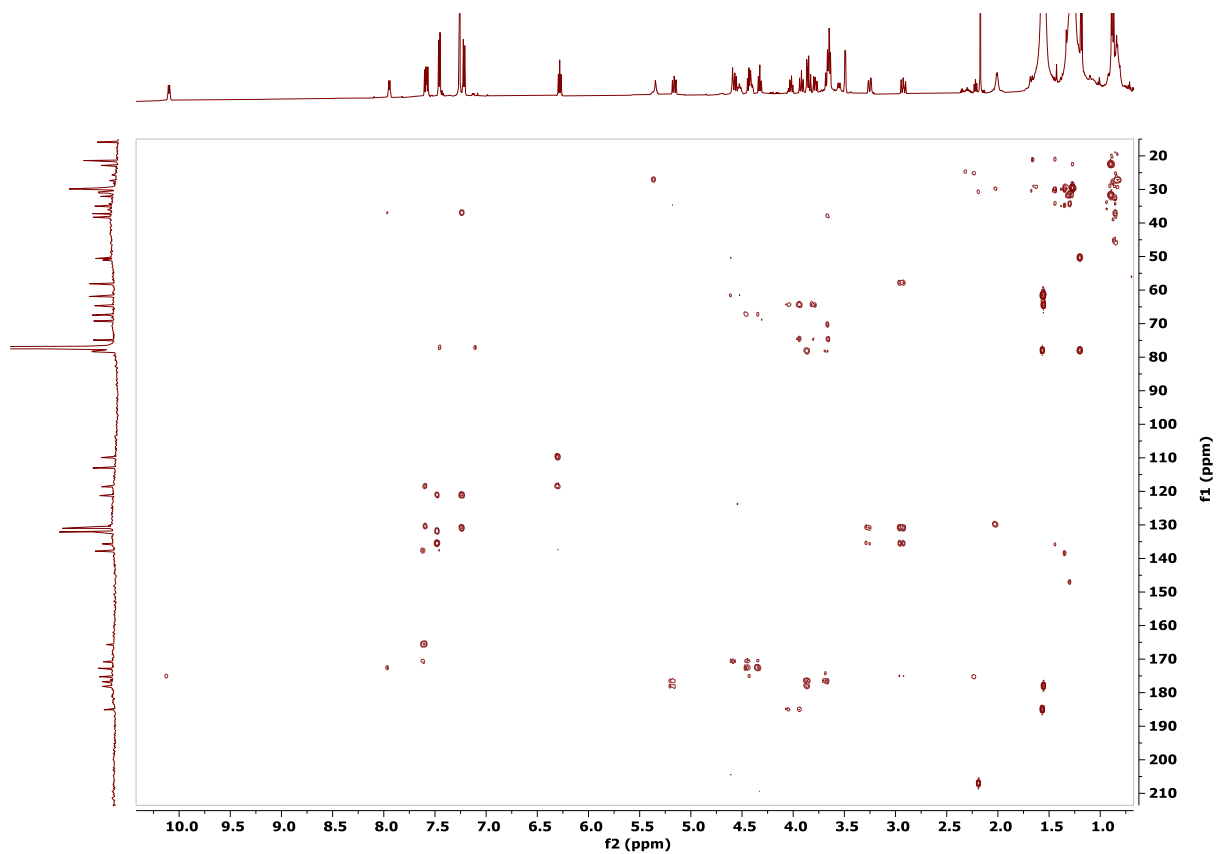


Fig. S35. HMBC spectrum for leptochelin C (**3**) in  $\text{CDCl}_3$  (600 MHz).

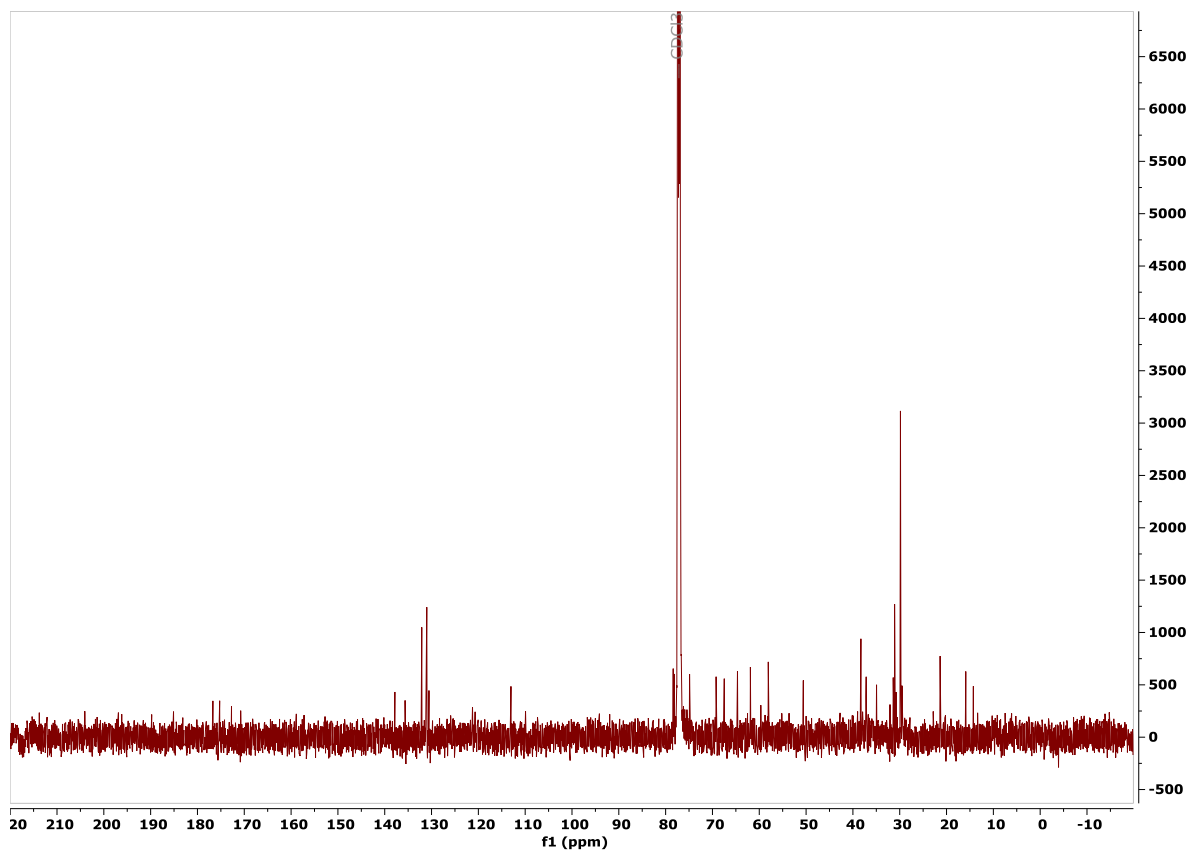


Fig. S36.  $^{13}\text{C}$  NMR spectrum for zinc-bound leptochelin C (**3**) in  $\text{CDCl}_3$  (150 MHz).

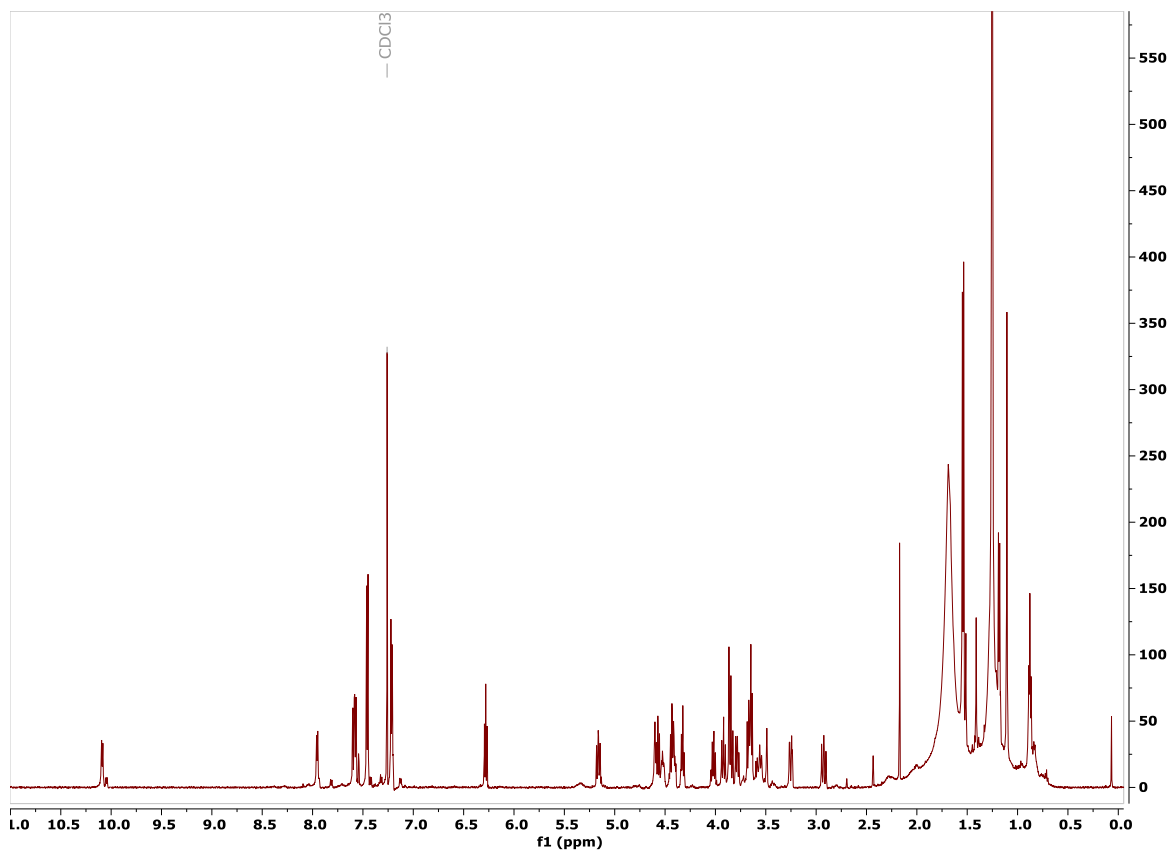


Fig. S37.  $^1\text{H}$  NMR spectrum for zinc-bound leptochelin C (**3**) in  $\text{CDCl}_3$  (600 MHz).

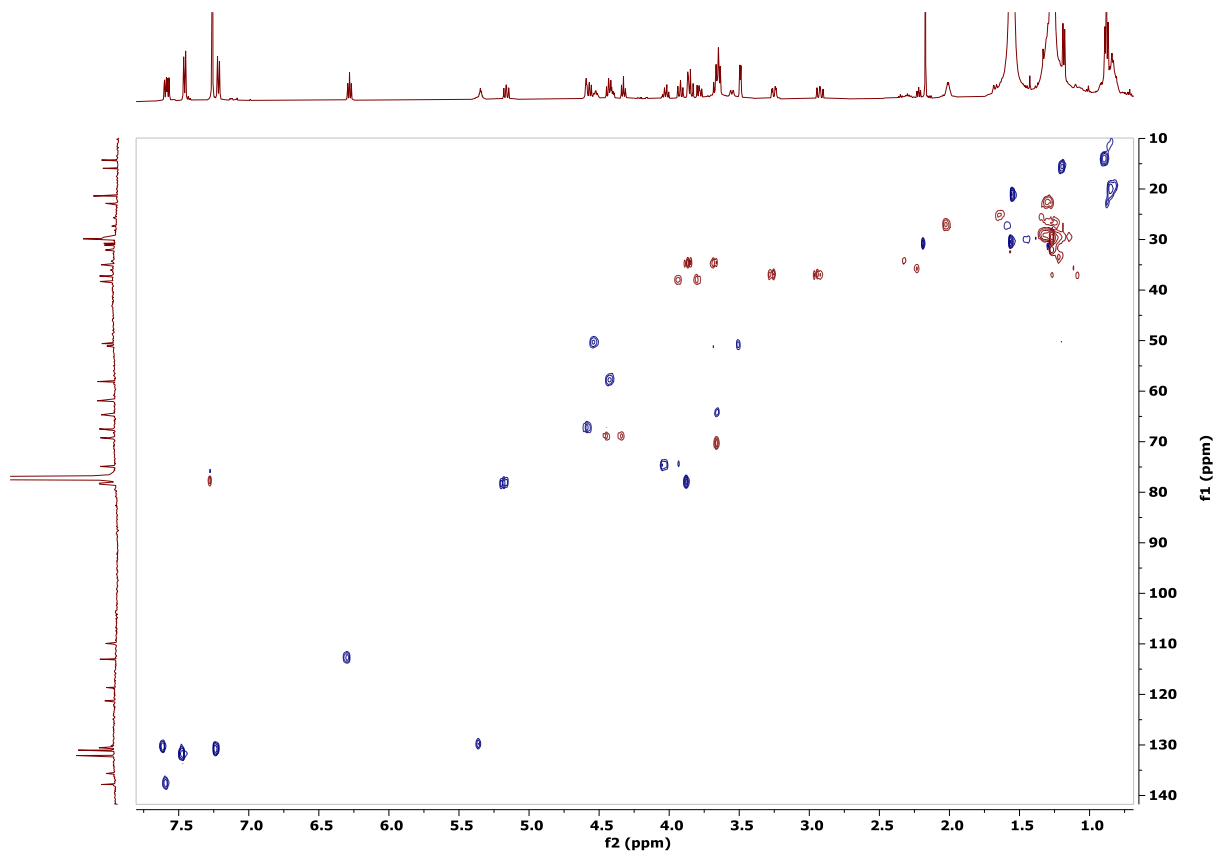


Fig. S38. Multiplicity-edited HSQC spectrum for zinc-bound leptochelin C (**3**) in  $\text{CDCl}_3$  (600 MHz).

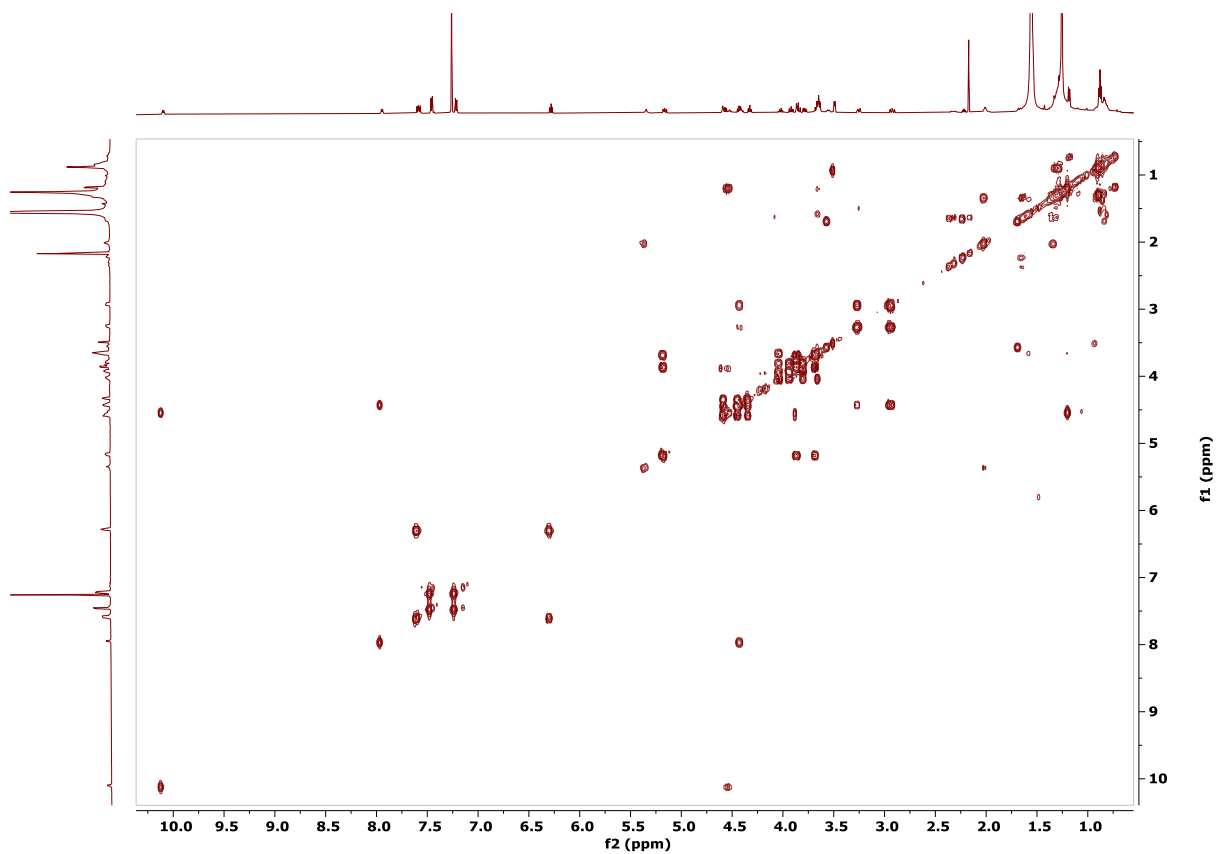


Fig. S39.  $^1\text{H}$ - $^1\text{H}$  COSY spectrum for zinc-bound leptochelin C (**3**) in  $\text{CDCl}_3$  (600 MHz).

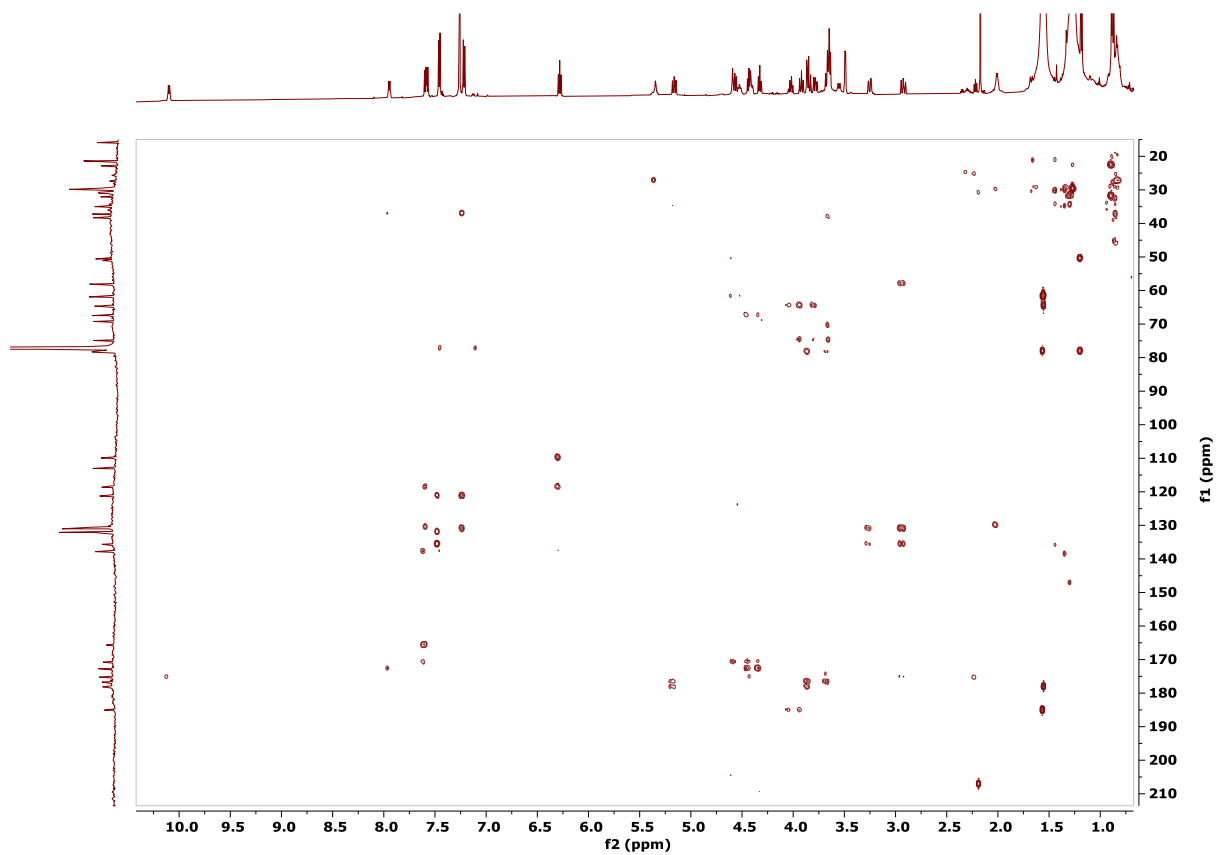
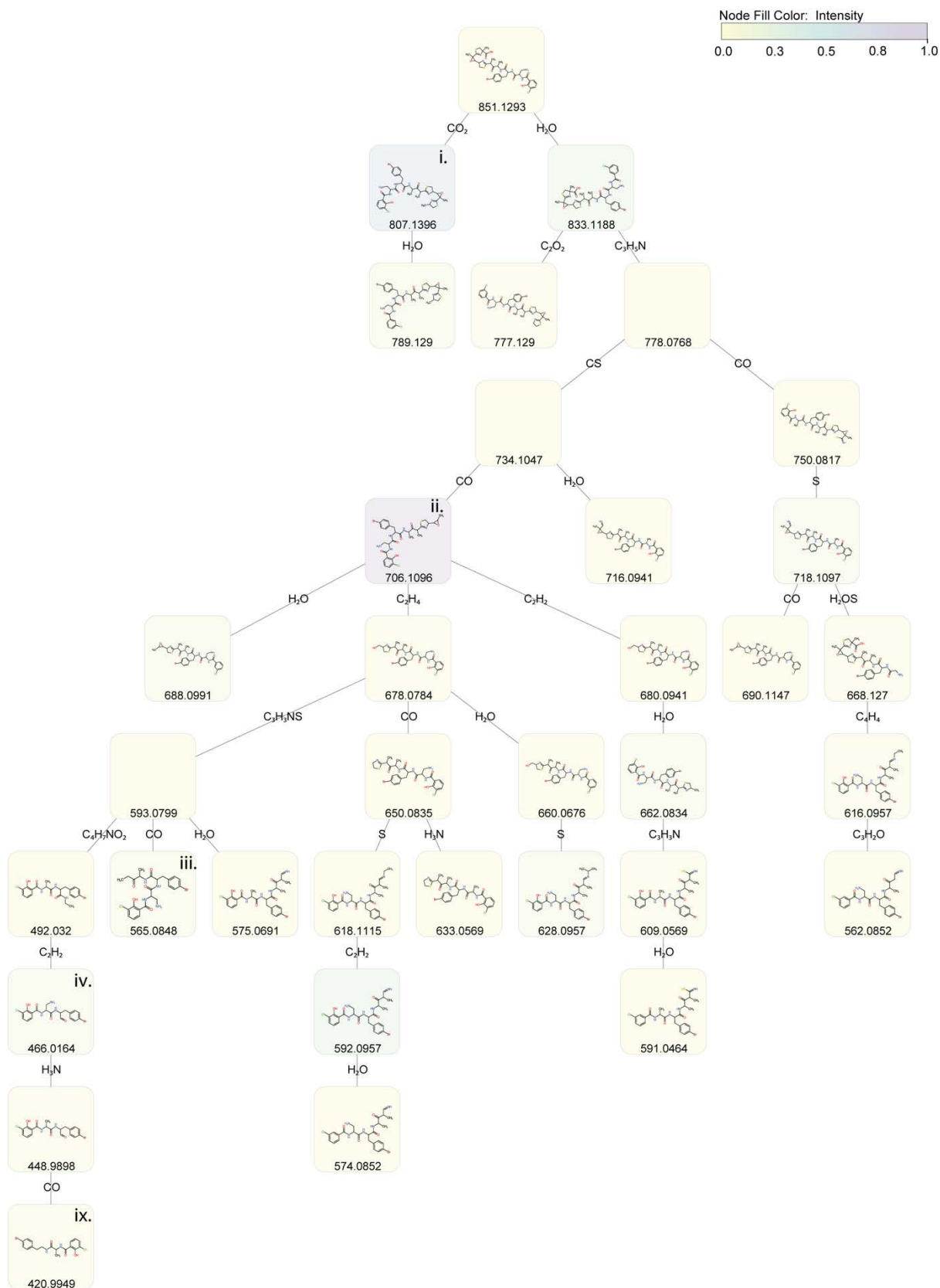
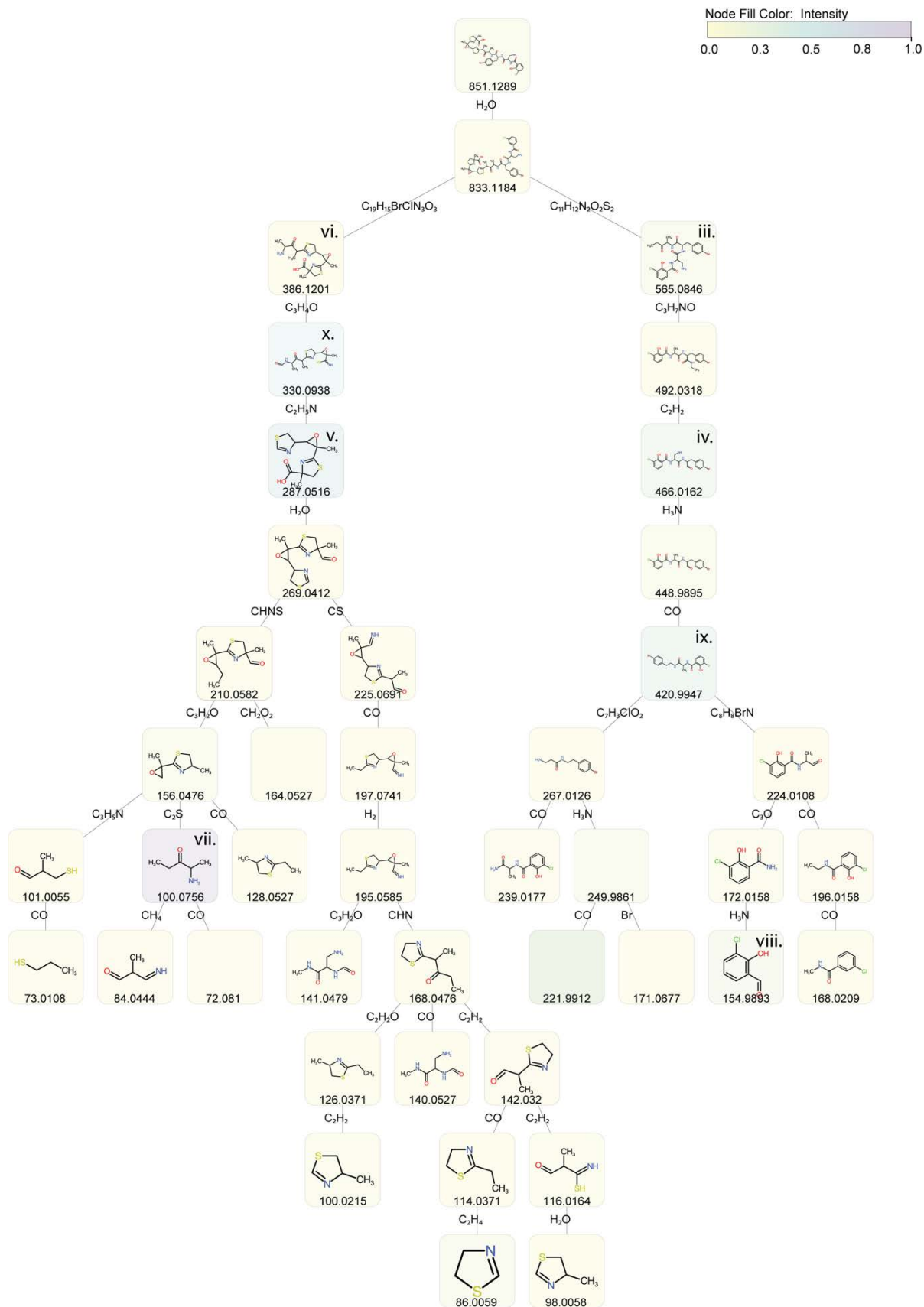


Fig. S40. HMBC spectrum for zinc-bound leptochelin C (**3**) in  $\text{CDCl}_3$  (600 MHz).



**Fig. S41.** Fragmentation trees of leptochelin B (**2**) CID MS<sup>2</sup> scan. Edges were labeled with the molecular formulas of neutral losses (from MS-FINDER) and nodes with the fragment *m/z*-values and annotated structures (from MS-FINDER), and roman numerals referencing the respective structures in **Fig. 3**. It should be noted that MS-FINDER structures do not account for hydrogen losses and might differ from manually annotated structures given in **Fig. 3**. Nodes were colored by the respective fragment intensity.



**Fig. S42.** Fragmentation trees of leptochelin B (**2**) HCD MS<sup>2</sup> scan. Edges were labeled with the molecular formulas of neutral losses (from MS-FINDER) and nodes with the fragment *m/z*-values and annotated structures (from MS-FINDER), and roman numerals referencing the respective structures in Fig. 3. It should be noted that MS-FINDER structures do not account for hydrogen losses and might differ from manually annotated structures given in Fig. 3. Nodes were colored by the respective fragment intensity.

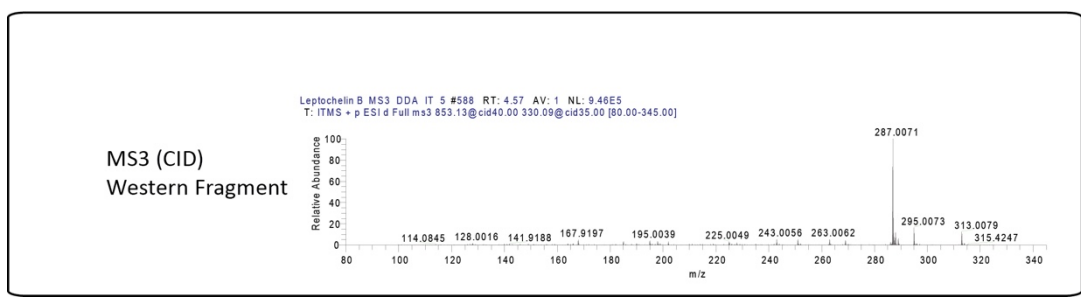
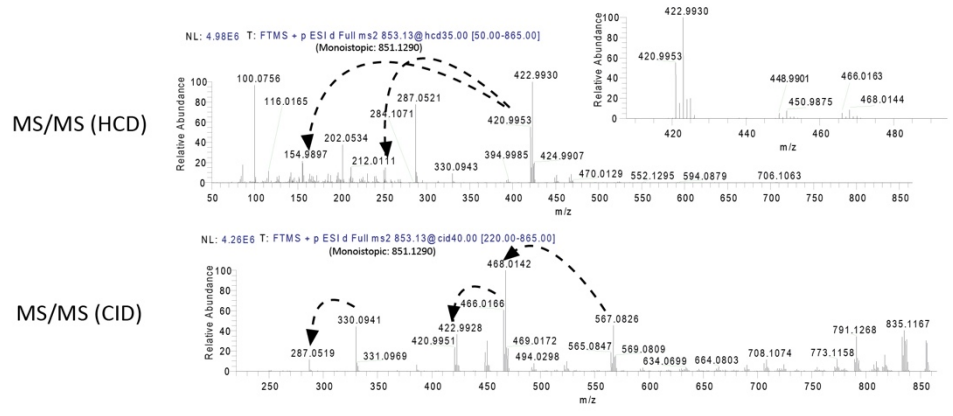
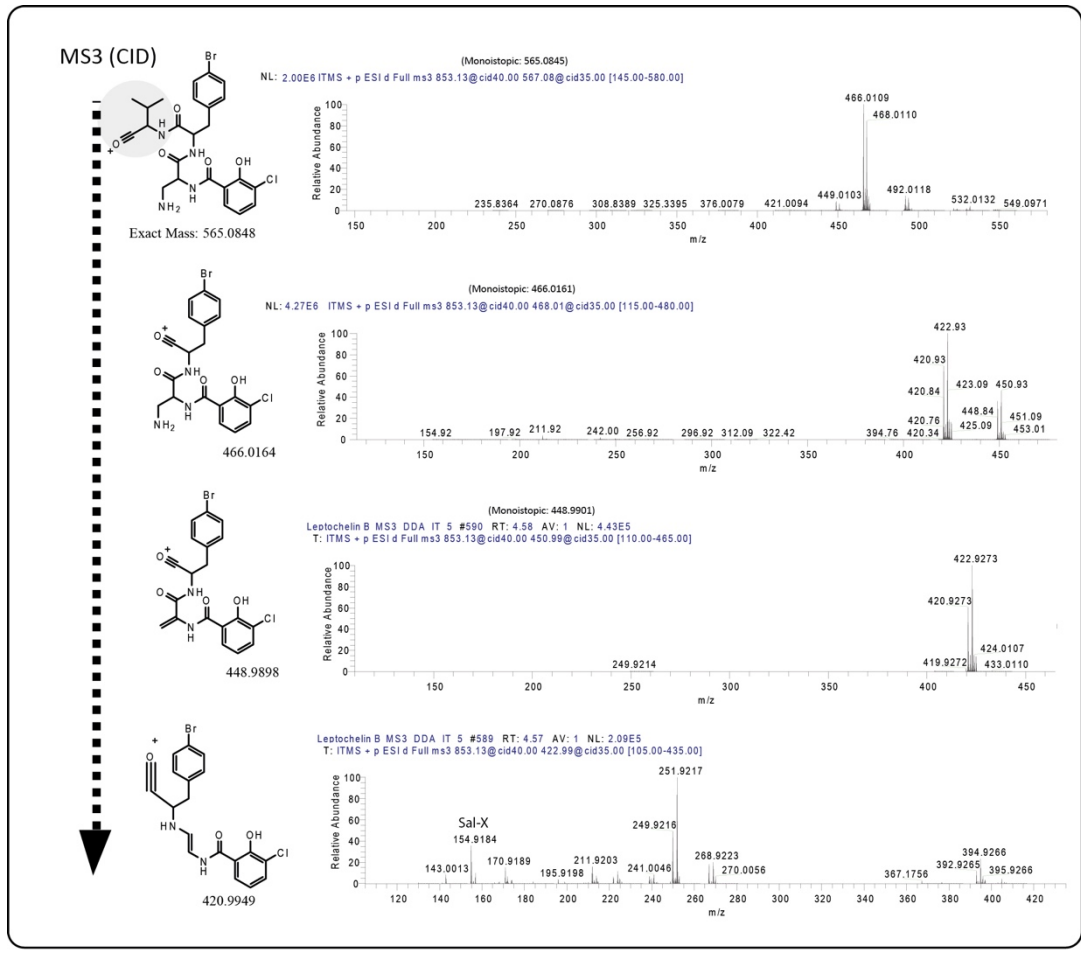
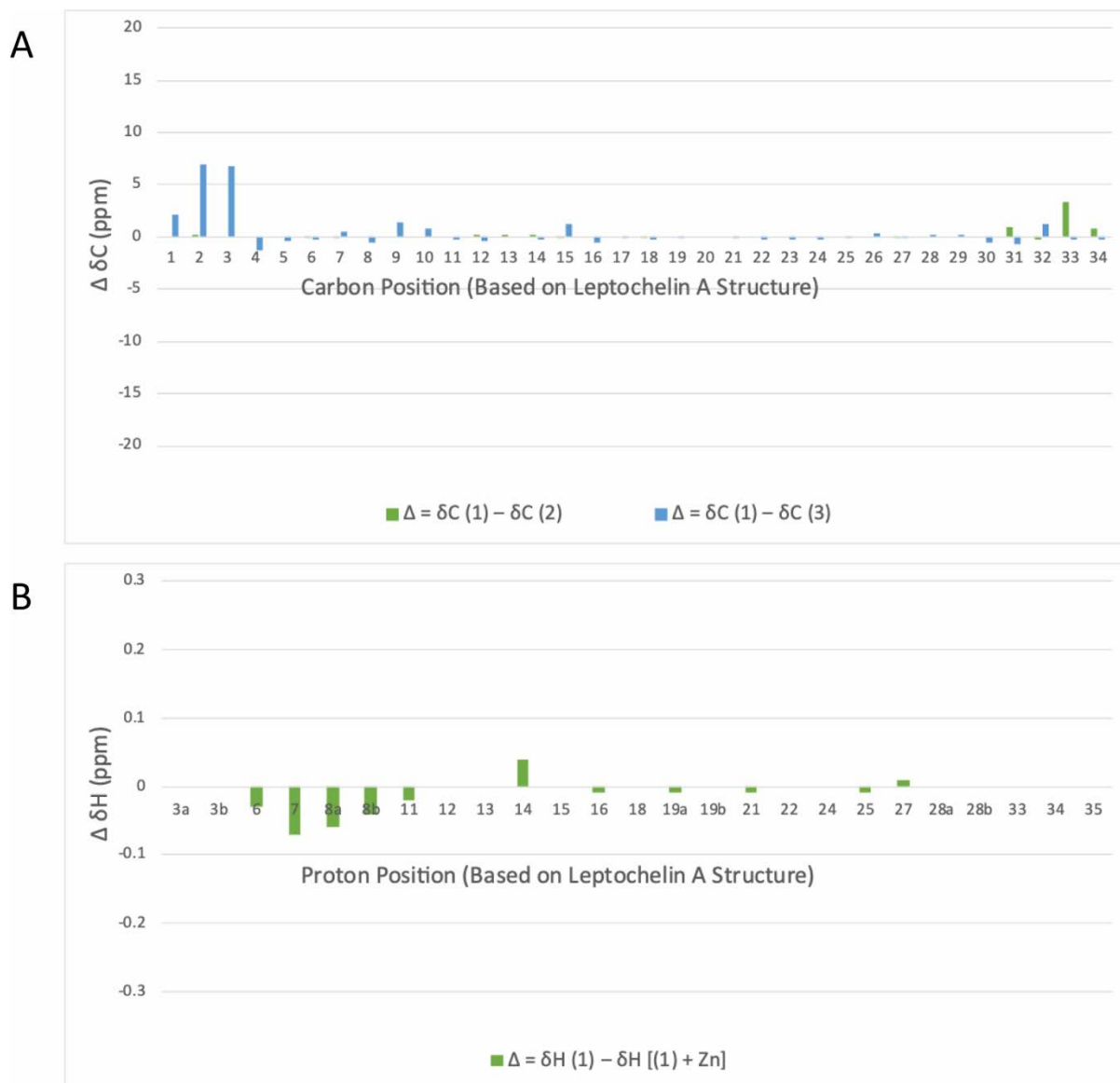
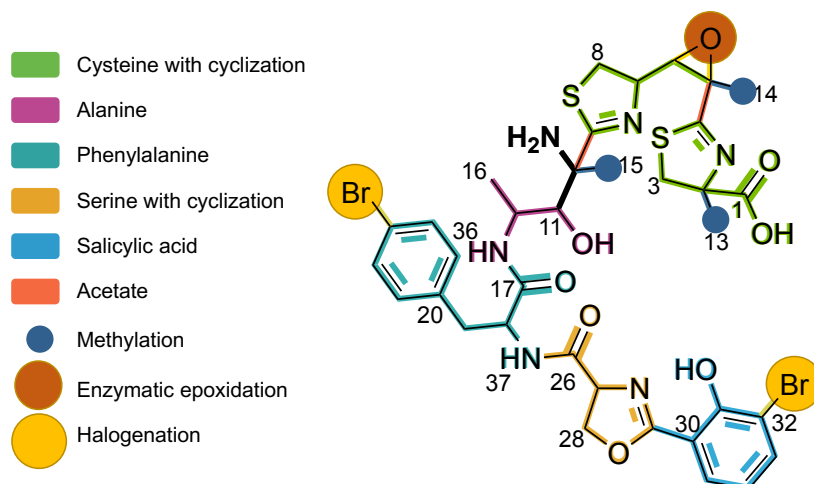


Fig. S43. MS<sup>3</sup> fragmentation series of the N-terminal fragments for leptocheilin B (2).



**Fig. S44.** Differences in  $^{13}\text{C}$  chemical shifts between metal-free leptochelins and differences in  $^1\text{H}$  chemical shifts of free and Zn-bound leptochelin A (1). **(A)** Differences of  $^{13}\text{C}$  NMR chemical shifts of leptochelin B (2) and C (3) relative to metal-free leptochelin A (1). In green, the chemical shift differences in metal-free leptochelin B (2) compared to metal-free leptochelin A (1) are notable due to chlorination rather than bromination of the phenol group. In blue, the chemical shift differences are prominent for C1 – C3, reflecting the difference in methylation at C2 between metal-free leptochelin A (1) and metal-free leptochelin C (3). The carbons at remaining stereocenters and adjacent carbon atoms show minimal differences in chemical shifts (C-5 through C-30), supporting the hypothesis that the absolute configuration at these chiral centers is consistent across all three compounds. Note that the carbon position is based on the numbering designations for leptochelin A (1). **(B)** Differences of  $^1\text{H}$  NMR chemical shifts of Zn-bound leptochelin A relative to metal-free leptochelin A (1). Small differences in chemical shift are observed, reflecting the changes that occur when the compound is coordinated to zinc.





**Fig. S45.** Retrosynthetic analysis of leptochelin A (**1**). The retrosynthetic analysis includes a hybrid NRPS-PKS system including genes responsible for core biosynthetic enzymes for salicylic acid production. This is followed by addition of a serine residue with heterocyclization, incorporation of phenylalanine, alanine, elongation by a PKS module with reduction of the  $\beta$ -carbonyl and other secondary reactions, then cysteine incorporation with heterocyclization, a PKS elongation and enzymatic methylation and epoxidation, and a final cysteine incorporation with methylation and cyclization. There are also two brominations, both occurring on aromatic rings, possibly due to a *trans*-acting halogenase.

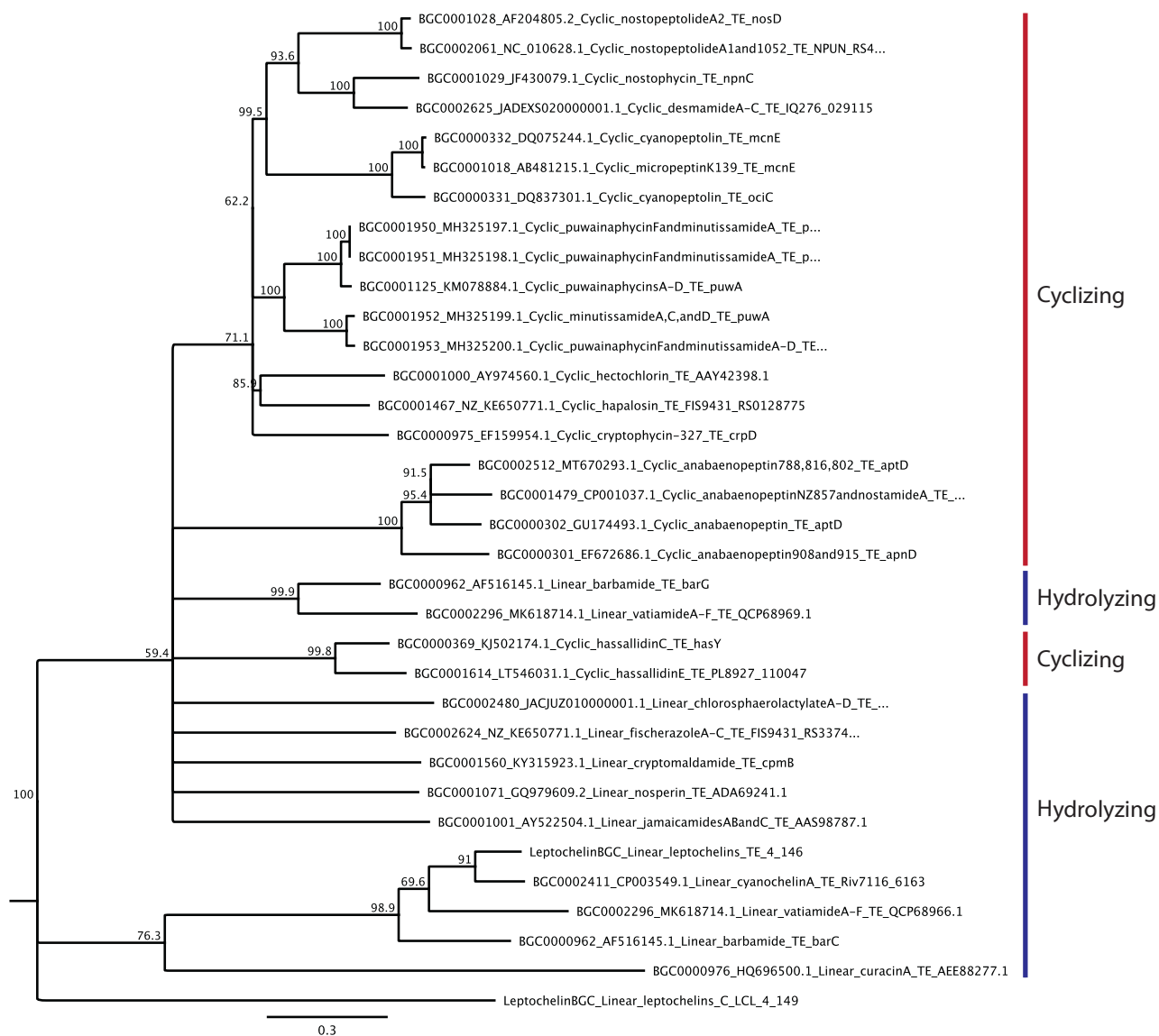


**Fig. S46.** Phylogenetic tree of the *lec* TE domain with select TE domains from BGCs linked to known natural products. Phylogenetic tree reveals that the terminating thioesterase domain in the *lec* biosynthetic gene cluster (LeptocheilinBGC\_Linear\_leptocheilins\_TE\_4\_146) clades with other TE domains that hydrolytically release a linear molecule and is distinct from TE domains that lead to cyclization before release of the newly biosynthesized molecule. MIBiG Accession Numbers, (22) NCBI Accession Numbers, linked compound, and gene names are included. The outgroup is a condensation domain from the putative leptocheilin BGC (ctg 4\_149).

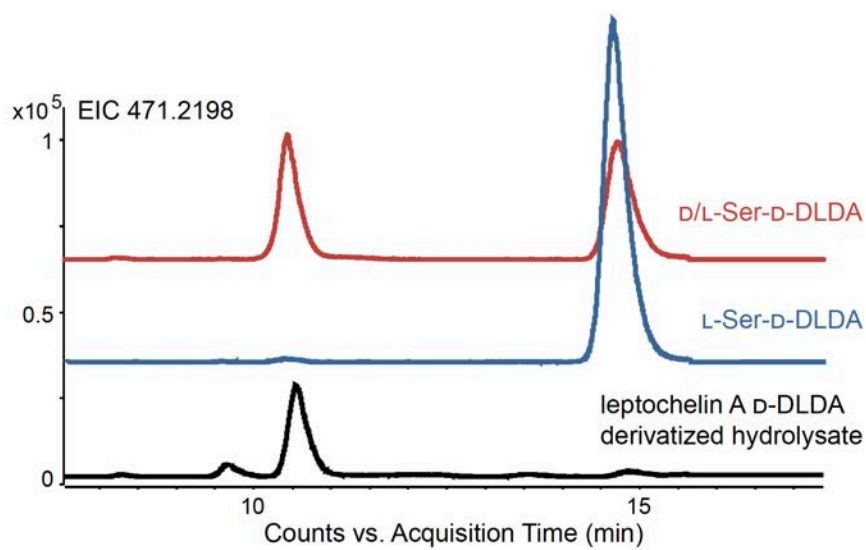


**Fig. S47.** Determination of the absolute configuration of the D-serine residue in leptochelin A (**1**). Overlaid EICs (471.2198  $m/z$ ) for the D-DLDA derivatized hydrolysate of leptochelin (black), L-Ser (blue), and D/L-Ser (red).

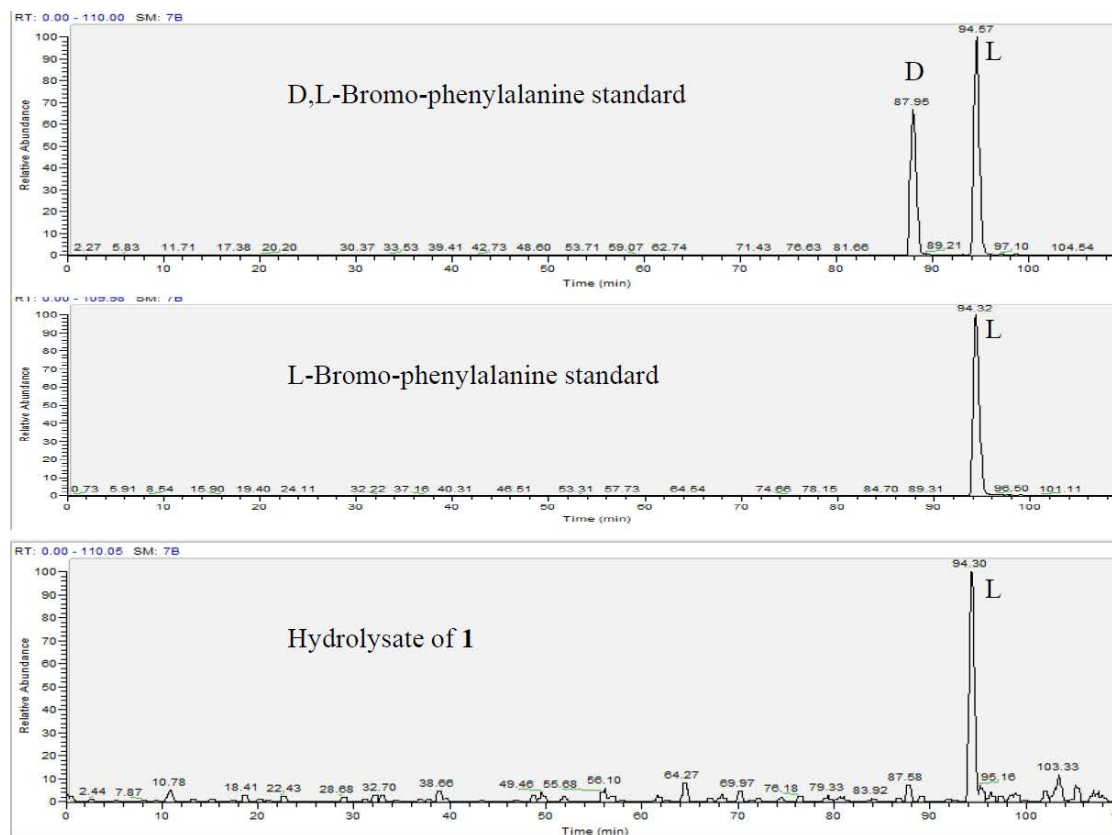


**Fig. S48.** Determination of the absolute configuration of the L-bromophenylalanine residue in leptochelin A (**1**).

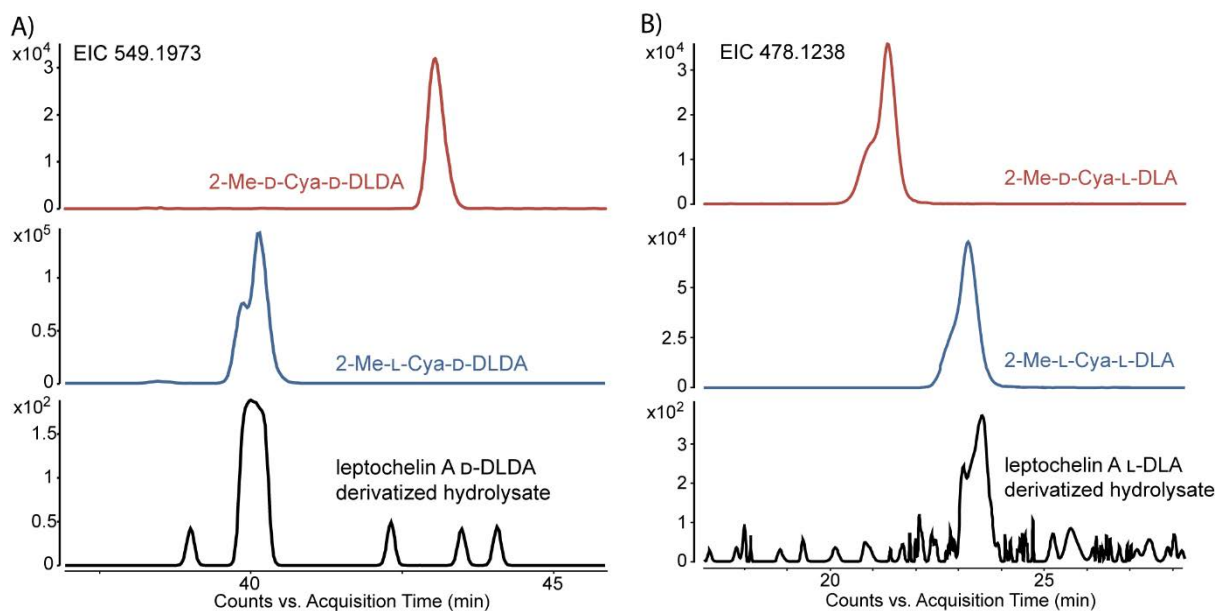


**Fig. S49.** Determination of the absolute configuration of the 2-Me-L-cysteine residue in leptochelin A (1). **(A)** Overlaid EICs (549.1973  $m/z$ ) for the D-DLDA derivatized hydrolysate of oxidized leptochelin (black), 2-Me-L-cysteic acid (Cya, blue), and 2-Me-D-Cya (red). **(B)** Overlaid EICs (478.1238  $m/z$ ) for the L-DLA derivatized hydrolysate of oxidized leptochelin (black), 2-Me-L-Cya (blue), and 2-Me-D-Cya (red).

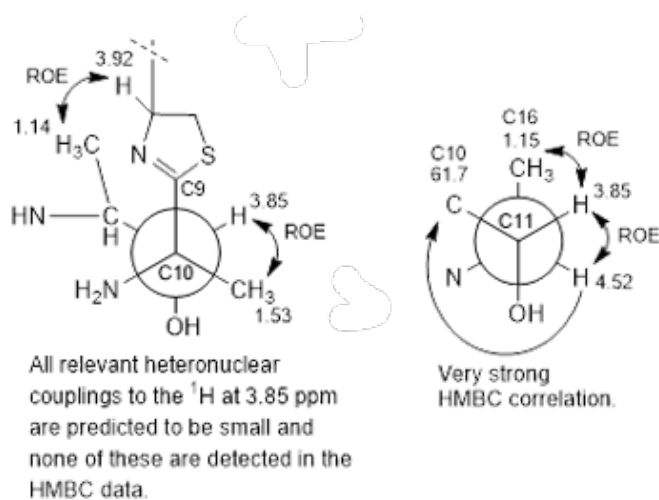


**Fig. S50.** Newman projections reflecting the NOE correlations that were key in determining the relative configuration from C-9 to C-11 in leptochelin A (1).

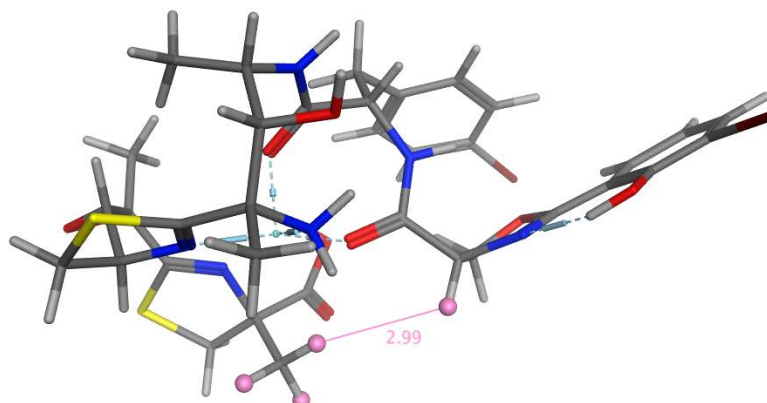


**Fig. S51.** Molecular modeling of zinc-bound leptochelin A (**1**). This modeling demonstrates the pseudo-cyclic conformation and the proximity of H<sub>3</sub>-13 and H-27 (2.99 angstroms). This proximity is consistent with the through-space correlations observed by ROESY NMR.

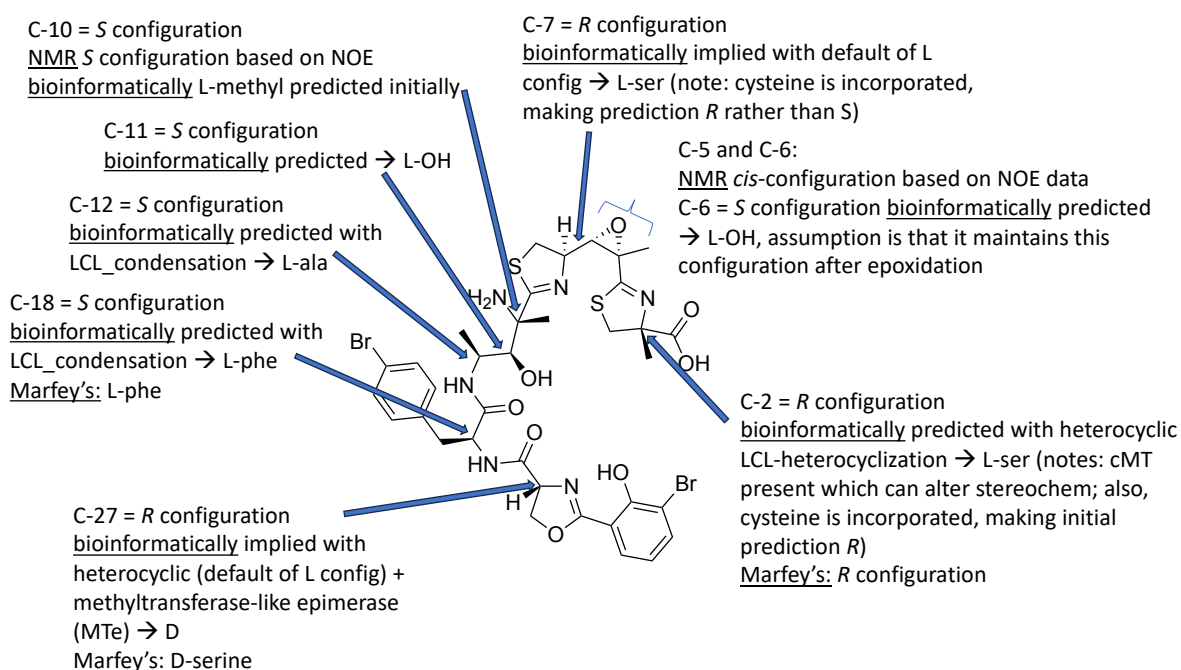


**Fig. S52.** Overview of the methods used to determine the absolute configuration of leptochelin A (**1**).

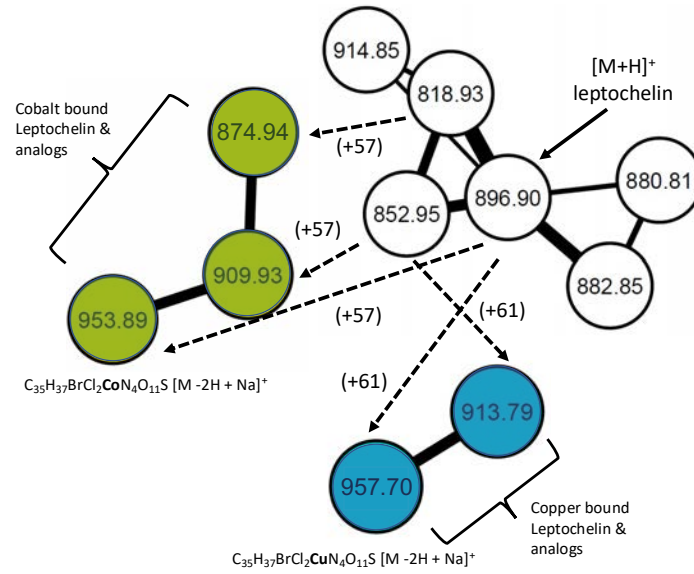


**Figure S53.** Early molecular network from GNPS revealing the potential for leptocheilin analogues with metal binding properties.

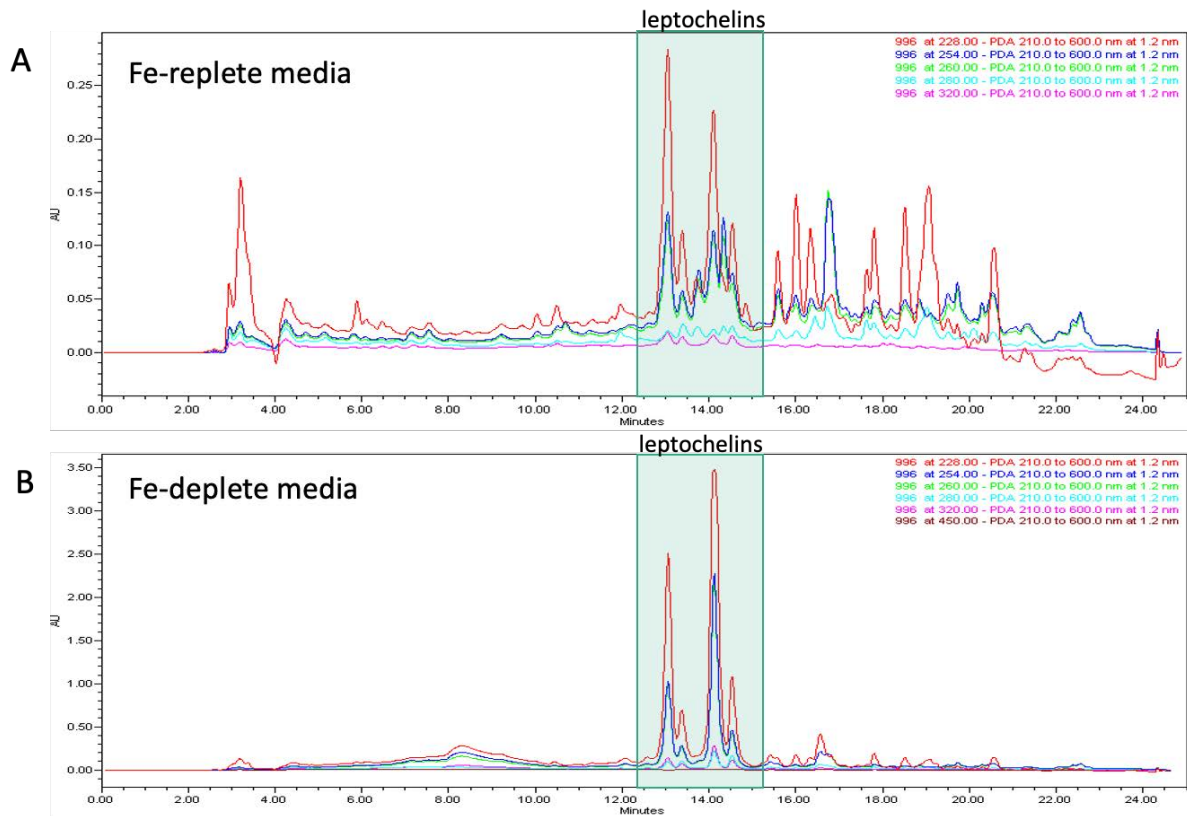


**Fig. S54.** UV chromatogram of *Leptothoe* extracts in iron replete and iron deplete media. This comparison demonstrates a substantial increase in the production of the leptocheilins when iron levels in the media are reduced.

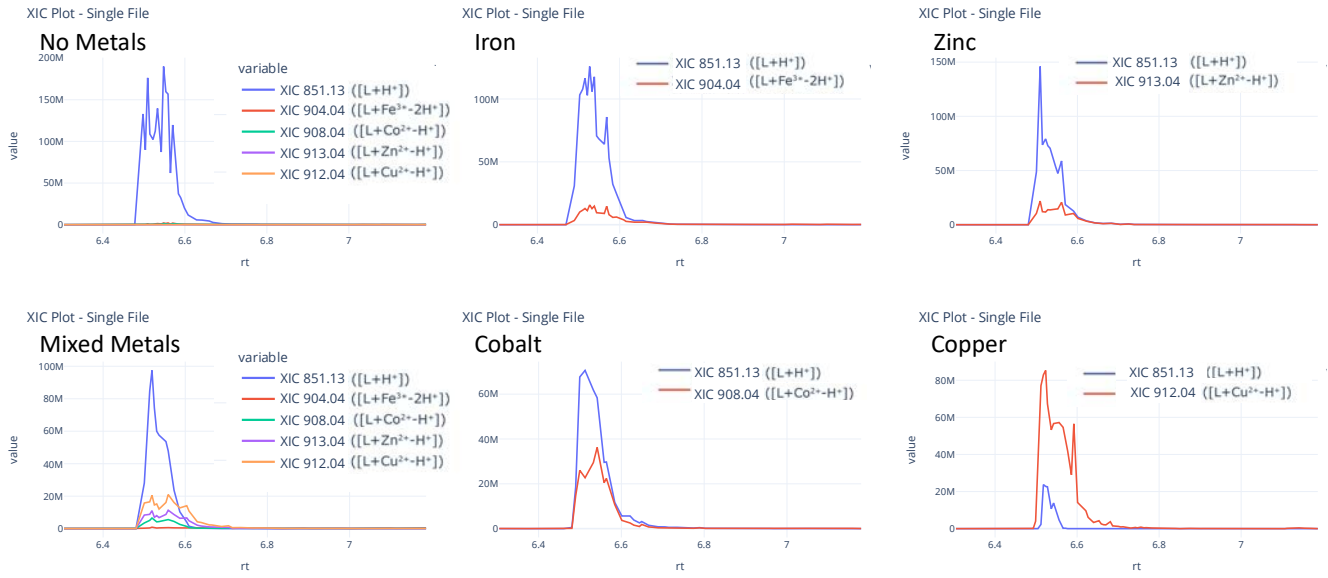


**Fig. S55.** Extracted ion chromatograms from metal-binding studies using pure leptochelin B (2).

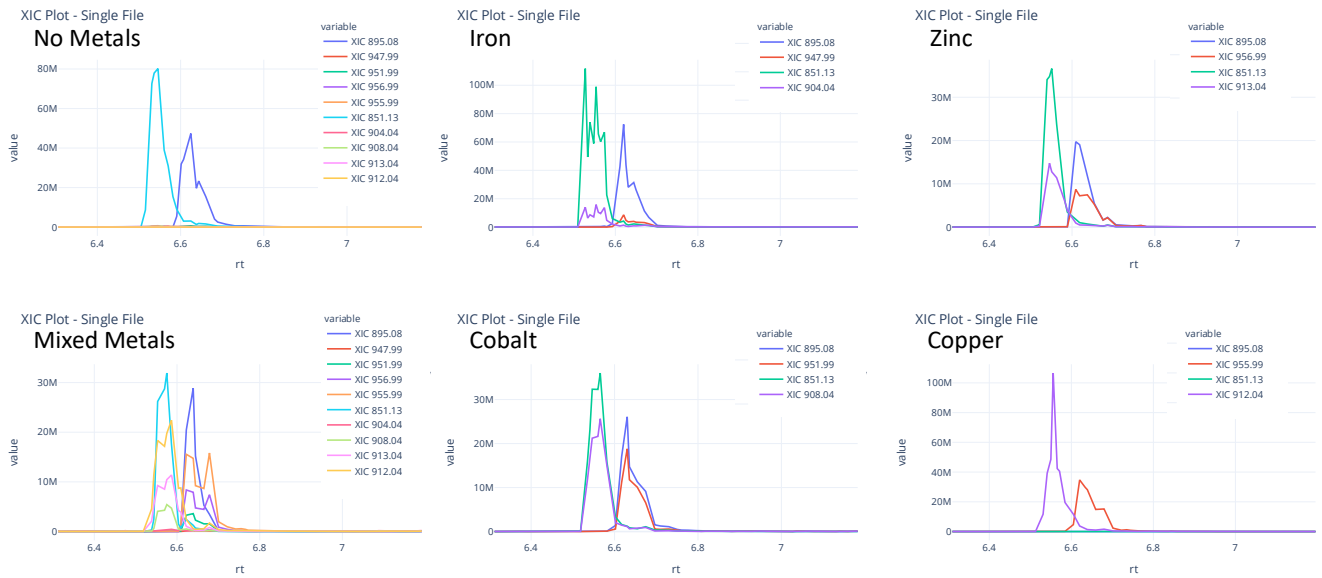


**Fig. S56.** Extracted ion chromatograms from metal-binding studies using a mixture of leptochelins A (1) and B (2).

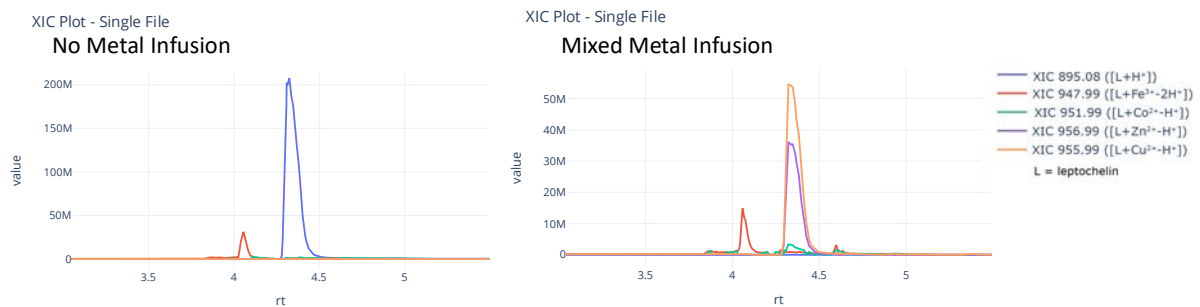


**Fig S57.** Extracted ion chromatograms from metal-binding studies using semipure leptochelin A (1) under pH adjusted conditions. This demonstrates that the leptochelin A coordination with iron in this semipure fraction persists. With metal infusion, there is post-column conversion of free leptochelin A to metal bound species even under pH adjusted conditions using a native metabolomics approach.

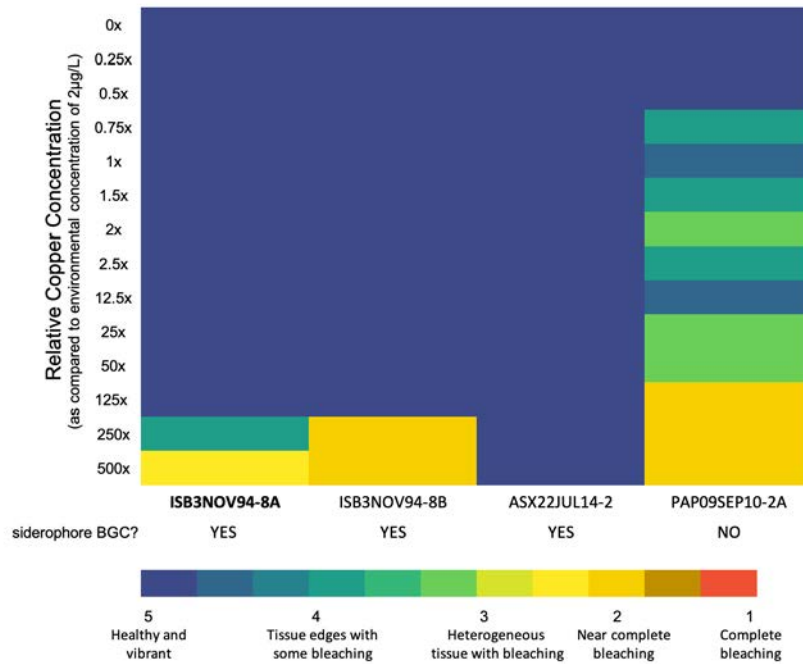


**Fig. S58.** Summary of copper toxicity assay reflecting organism health at Day 14 post-inoculation for *Leptothoe* sp. ISB3NOV94-8A and four *Leptolyngbya* spp. Relative concentrations are calculated based on an average coastal seawater concentration of  $\sim 2 \mu\text{g/L}$ . (34, 35) Color coding was based on visual inspection of culture health on a scale from Grade 1 (complete bleaching and death) to Grade 5 (healthy and vibrant) on Days 0, 2, 4, 7, 9, 10, and 14. The genome assemblies of each organism were evaluated for the presence of siderophore-producing genes. The three organisms showing resilience to increases in copper concentrations possessed genes associated with siderophore production.

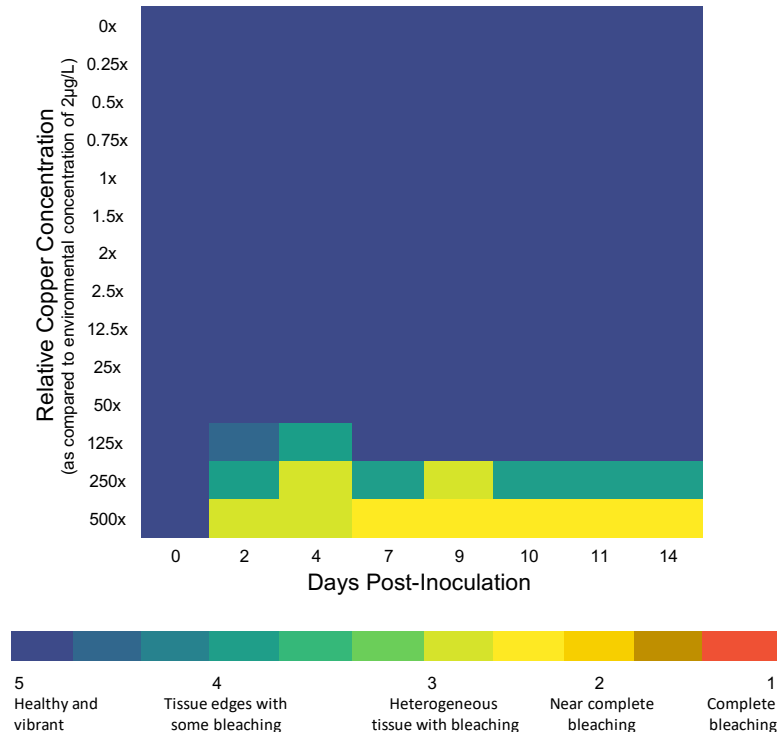


**Fig. S59.** Copper toxicity assay results for *Leptothoe* sp. ISB3NOV94-8A. Color coding was based on visual inspection of culture health on a scale from Grade 1 (complete bleaching and death) to Grade 5 (healthy and vibrant) on Days 0, 2, 4, 7, 9, 10, and 14 (**SI Appendix, Table S12**). It is notable that the cultures remained healthy appearing until the cultures were exposed to medium that was between 125x – 250 times the copper concentration of average coastal seawater. The genome of *Leptothoe* sp. ISB3NOV94-8A contains the *lec* BGC.



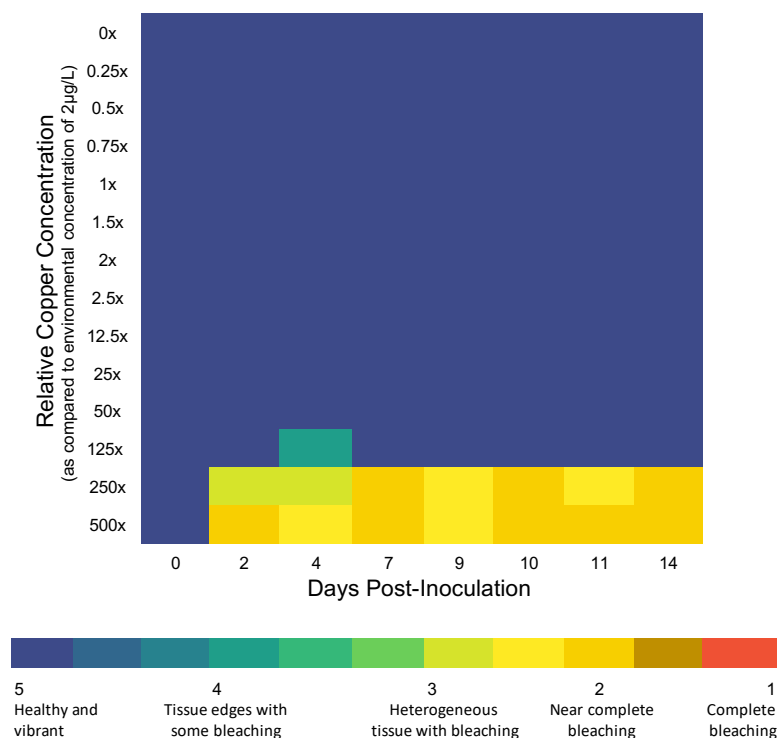


**Fig. S60.** Copper toxicity assay results for *Leptolyngbya* sp. ISB3NOV94-8B. Color coding was based on visual inspection of culture health on a scale from Grade 1 (complete bleaching and death) to Grade 5 (healthy and vibrant) on Days 0, 2, 4, 7, 9, 10, and 14 (*SI Appendix, Table S12*). The genome assembly from *Leptolyngbya* sp. ISB3NOV94-8B has a siderophore BGC and also demonstrates resistance to elevated copper concentrations.

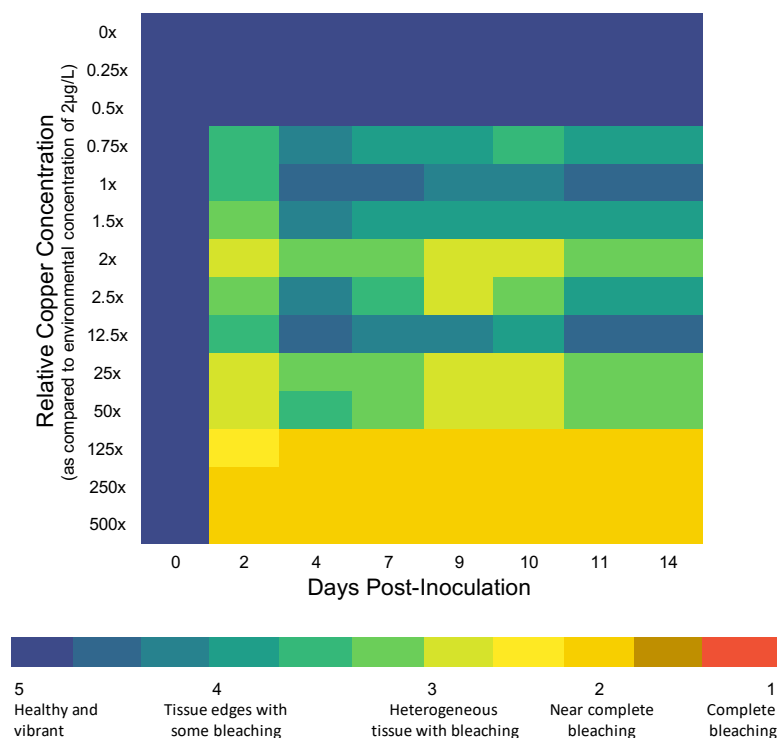


**Fig. S61.** Copper toxicity assay results for *Leptolyngbya* sp. PAP09SEP10-2A. Color coding was based on visual inspection of culture health on a scale from Grade 1 (complete bleaching and death) to Grade 5 (healthy and vibrant) on Days 0, 2, 4, 7, 9, 10, and 14 (*SI Appendix, Table S12*). The genome from *Leptolyngbya* sp. PAP09SEP10-2A shows no evidence for a siderophore biosynthetic gene cluster and is negatively impacted by elevated copper concentrations.

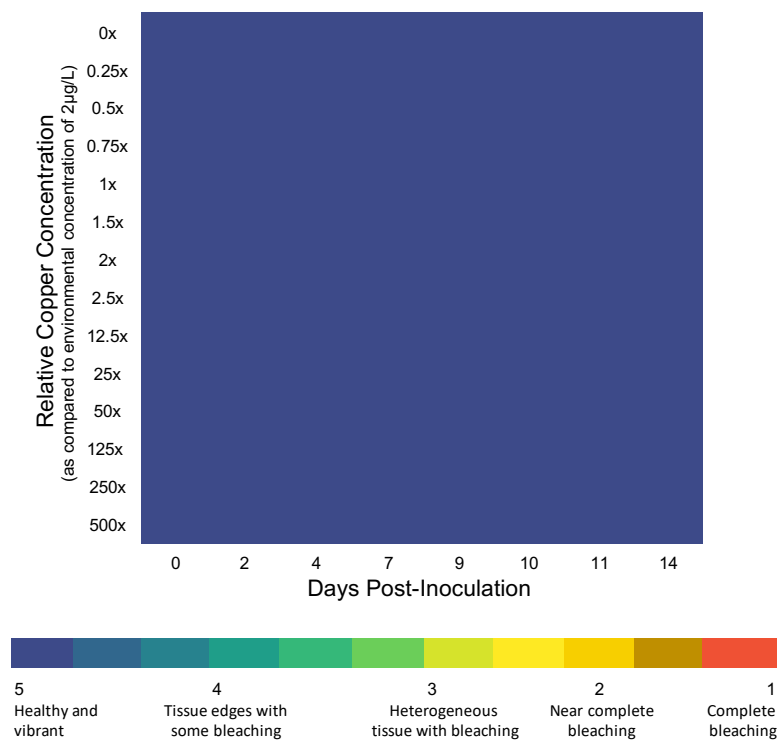


**Fig. S62.** Copper toxicity assay results for *Leptolyngbya* sp. ASX22JUL14-2. Color coding was based on visual inspection of culture health on a scale from Grade 1 (complete bleaching and death) to Grade 5 (healthy and vibrant) on Days 0, 2, 4, 7, 9, 10, and 14 (**SI Appendix, Table S12**). The genome assembly from *Leptolyngbya* sp. ASX22JUL14-2 showed the presence of a siderophore biosynthetic gene cluster. This strain also shows a remarkable resistance to elevated copper concentrations.

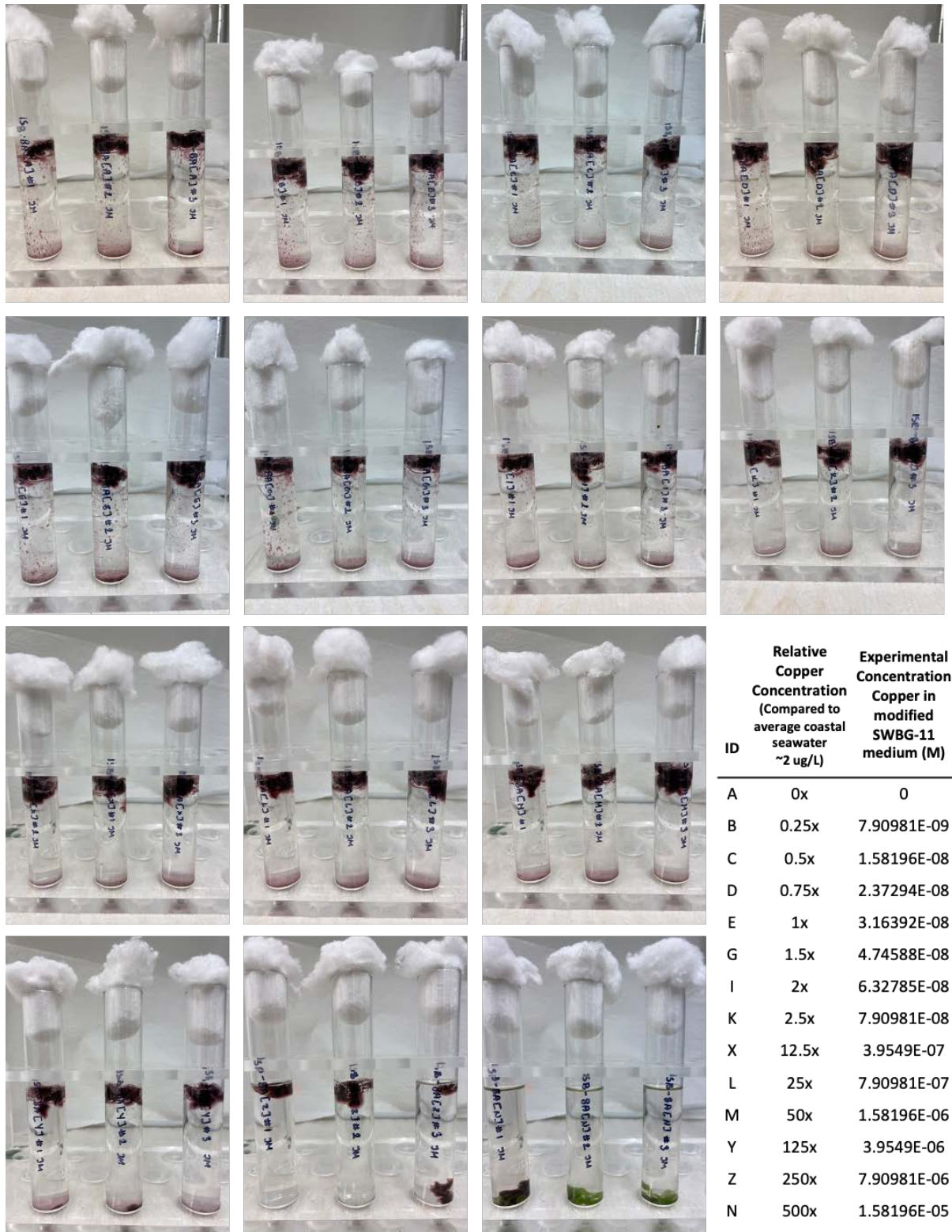
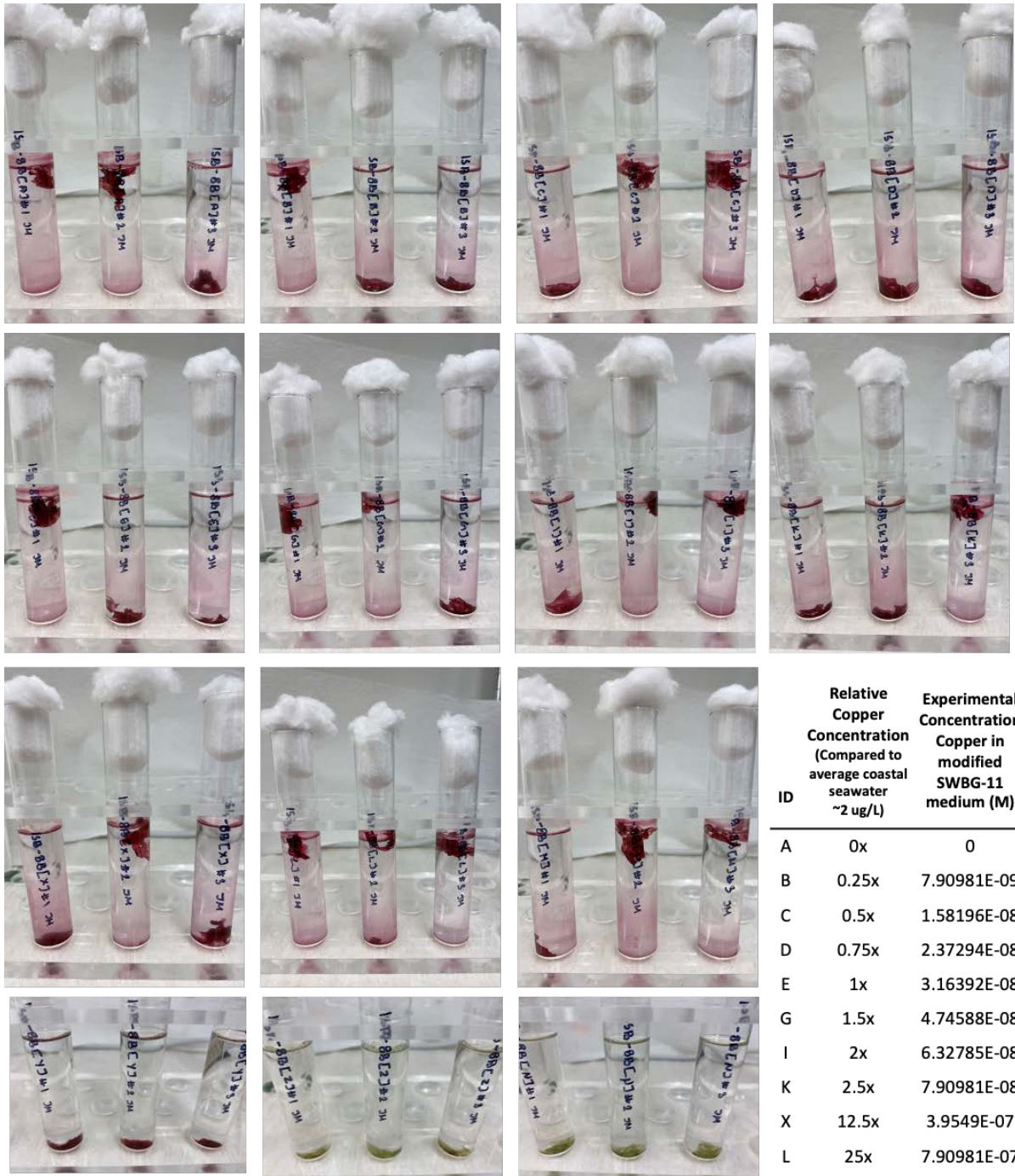


**Fig. S63.** Photographs of *Leptothoe* sp. ISB3NOV94-8A cultures on Day 14 of the copper toxicity assays. Healthy cultures maintain a deep purple pigmentation, while unhealthy cultures begin to show signs of heterogeneity with light green appearing at the edges of the biomass, and the dying cultures lose the red pigmentation and become light green. It is notable that the cultures remained healthy appearing until the cultures were exposed to medium that contained between 125x – 250x the copper concentration of average coastal seawater. This genome of *Leptothoe* sp. ISB3NOV94-8A contains the *lec* BGC.



ID	Relative Copper Concentration (Compared to average coastal seawater ~2 ug/L)	Experimental Copper Concentration in modified SWBG-11 medium (M)
A	0x	0
B	0.25x	7.90981E-09
C	0.5x	1.58196E-08
D	0.75x	2.37294E-08
E	1x	3.16392E-08
G	1.5x	4.74588E-08
I	2x	6.32785E-08
K	2.5x	7.90981E-08
X	12.5x	3.9549E-07
L	25x	7.90981E-07
M	50x	1.58196E-06
Y	125x	3.9549E-06
Z	250x	7.90981E-06
N	500x	1.58196E-05

**Fig. S64.** Photographs of *Leptolyngbya* sp. ISB3NOV94-8B cultures on Day 14 of the copper toxicity assays. Healthy cultures maintain a deep magenta pigmentation, while unhealthy cultures begin to show signs of heterogeneity with light green appearing at the edges of the biomass, and the dying cultures loose the red pigmentation and become light green. It is notable that the cultures remained healthy appearing until the cultures were exposed to medium that was between 125x – 250x the copper concentration of average coastal seawater. The genome assembly from *Leptolyngbya* sp. ISB3NOV94-8B has a siderophore BGC and also demonstrates resistance to elevated copper concentrations.



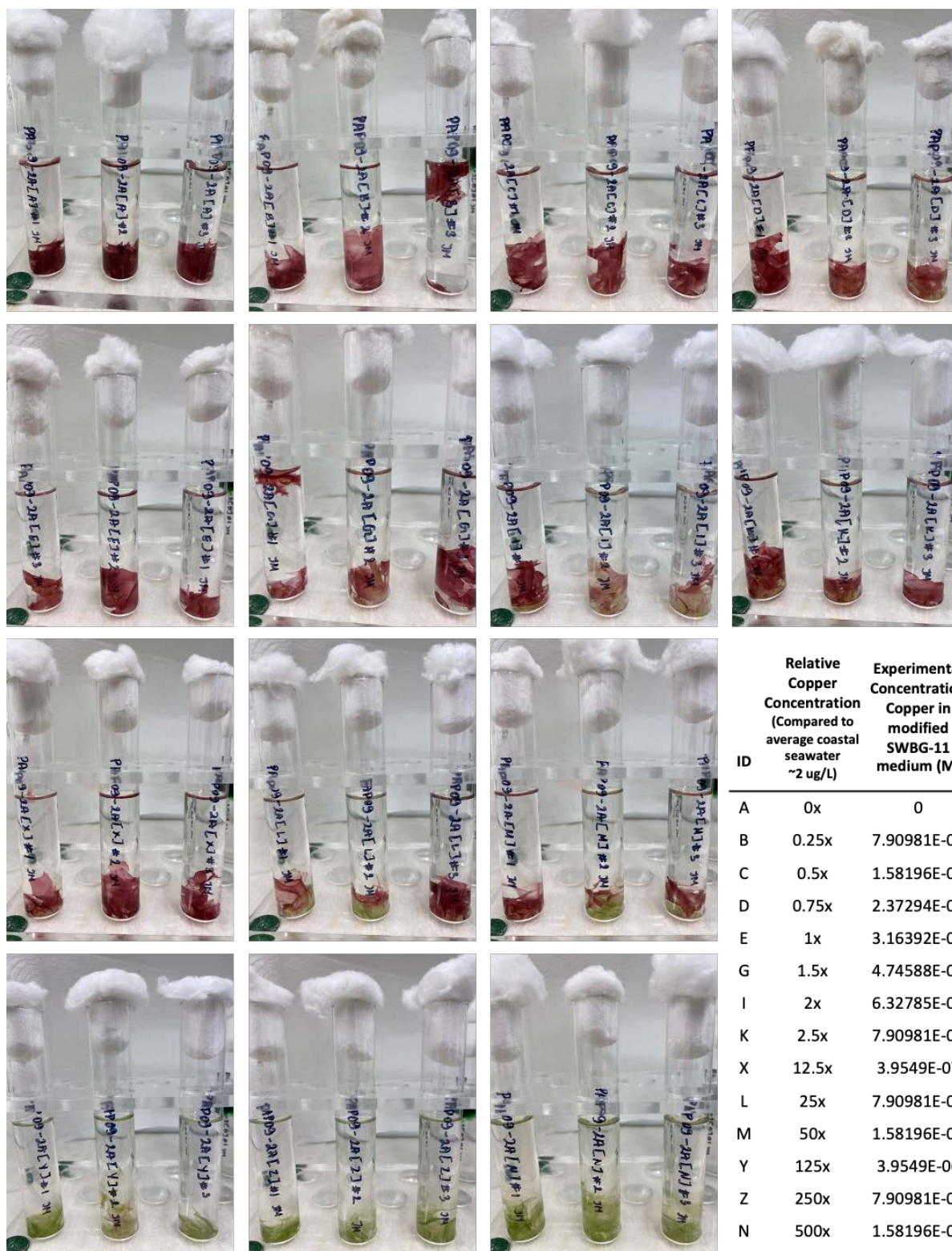


**Fig. S65.** Photographs of *Leptolyngbya* sp. PAP09SEP10-2A cultures on Day 14 of the copper toxicity assays. Healthy cultures maintain a deep magenta pigmentation, while unhealthy cultures begin to show signs of heterogeneity with light green appearing at the edges of the biomass, and the dying cultures lose the red pigmentation and become light green. It is notable that the cultures were much more sensitive to copper concentrations; however, up to a concentration of ~2x that of average coastal sea water concentrations the cultures were able to recover after an initial mild bleaching of the colony edges. Interestingly, the genome assembly from *Leptolyngbya* sp. PAP09SEP10-2A has no evidence of containing a siderophore BGC and also demonstrates susceptibility to elevations in copper concentrations.

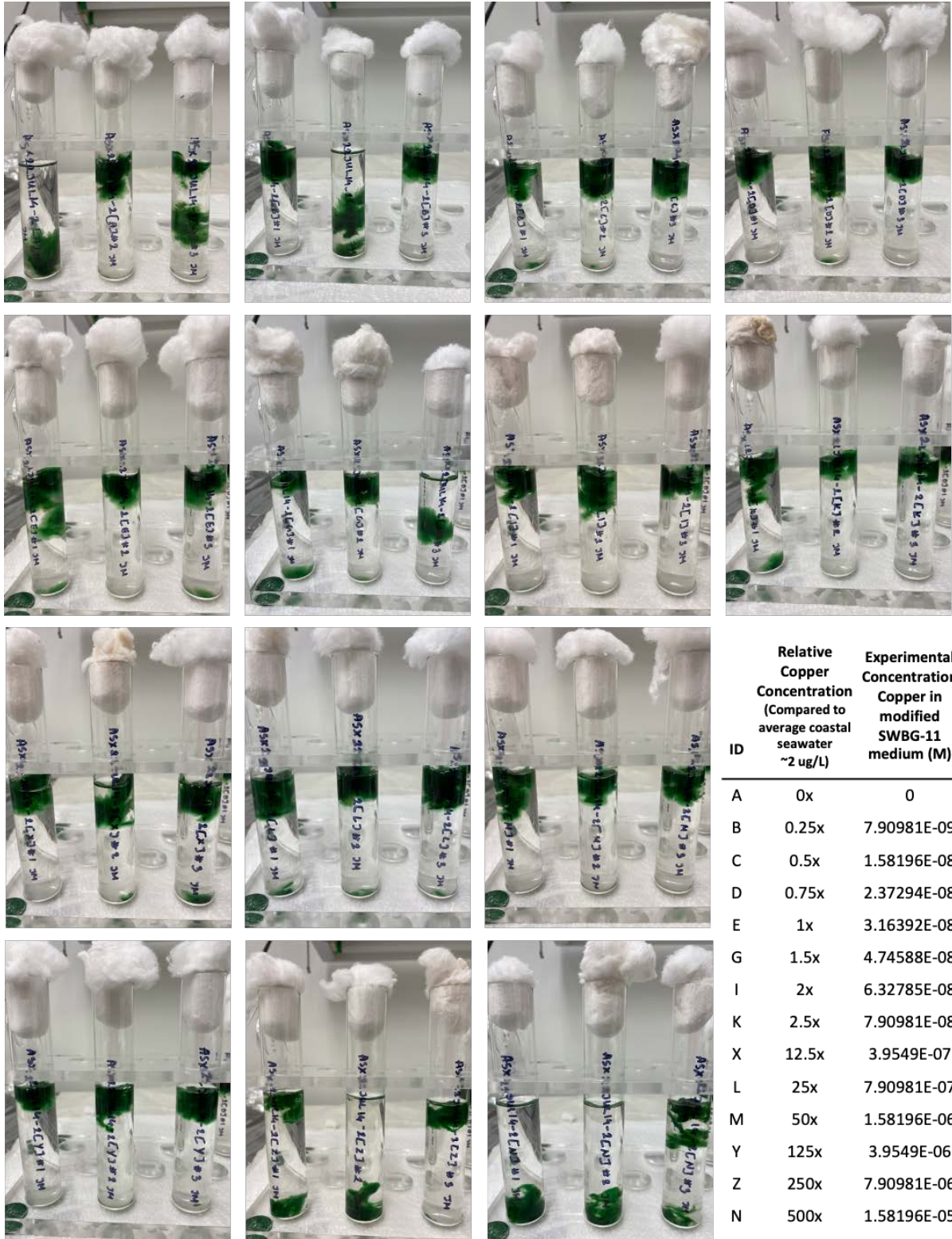


**Fig. S66.** Photographs of *Leptolyngbya* sp. ASX22JUL14-2 cultures on Day 14 of the copper toxicity assays. Healthy cultures maintain a deep green pigmentation, while unhealthy cultures begin to show signs of heterogeneity with light green appearing at the edges of the biomass, and the dying cultures lose the deep green pigmentation and become light green. It is notable that the cultures remained healthy appearing even in medium with 500x the copper concentration of average coastal seawater. The genome assembly from *Leptolyngbya* sp. ASX22JUL14-2 is predicted to contain a siderophore biosynthetic gene cluster, and also demonstrates remarkable resistance to elevated copper concentrations.



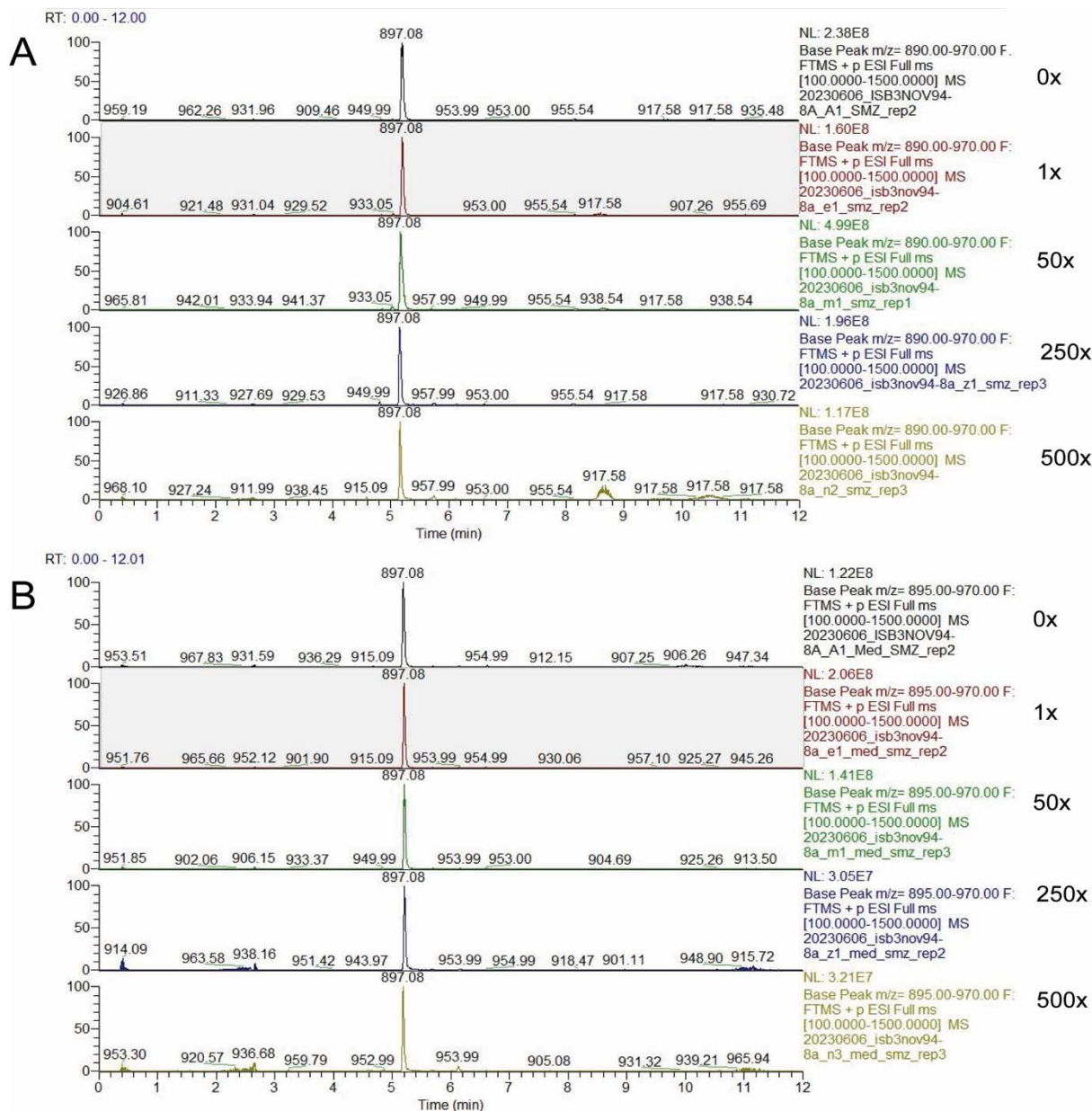


**Fig. S67.** LC-MS tracings showing no significant change in ion abundance for the  $[M + H]^+$  of leptochelin A (1) with varying concentrations of copper in the growth media. **(A)** Representative chromatograms from the cyanobacterial biomass following copper toxicity experiments. The chromatograms show results with a mass range of  $m/z$  890 – 970 from concentrations of 0x, 1x, 50x, 250x, and 500x average copper of coastal seawater concentrations. **(B)** Representative chromatograms from the culture medium following copper toxicity experiments. The chromatograms show results with a mass range of  $m/z$  890 – 970 from concentrations of 0x, 1x, 50x, 250x, and 500x average copper of coastal seawater concentrations.

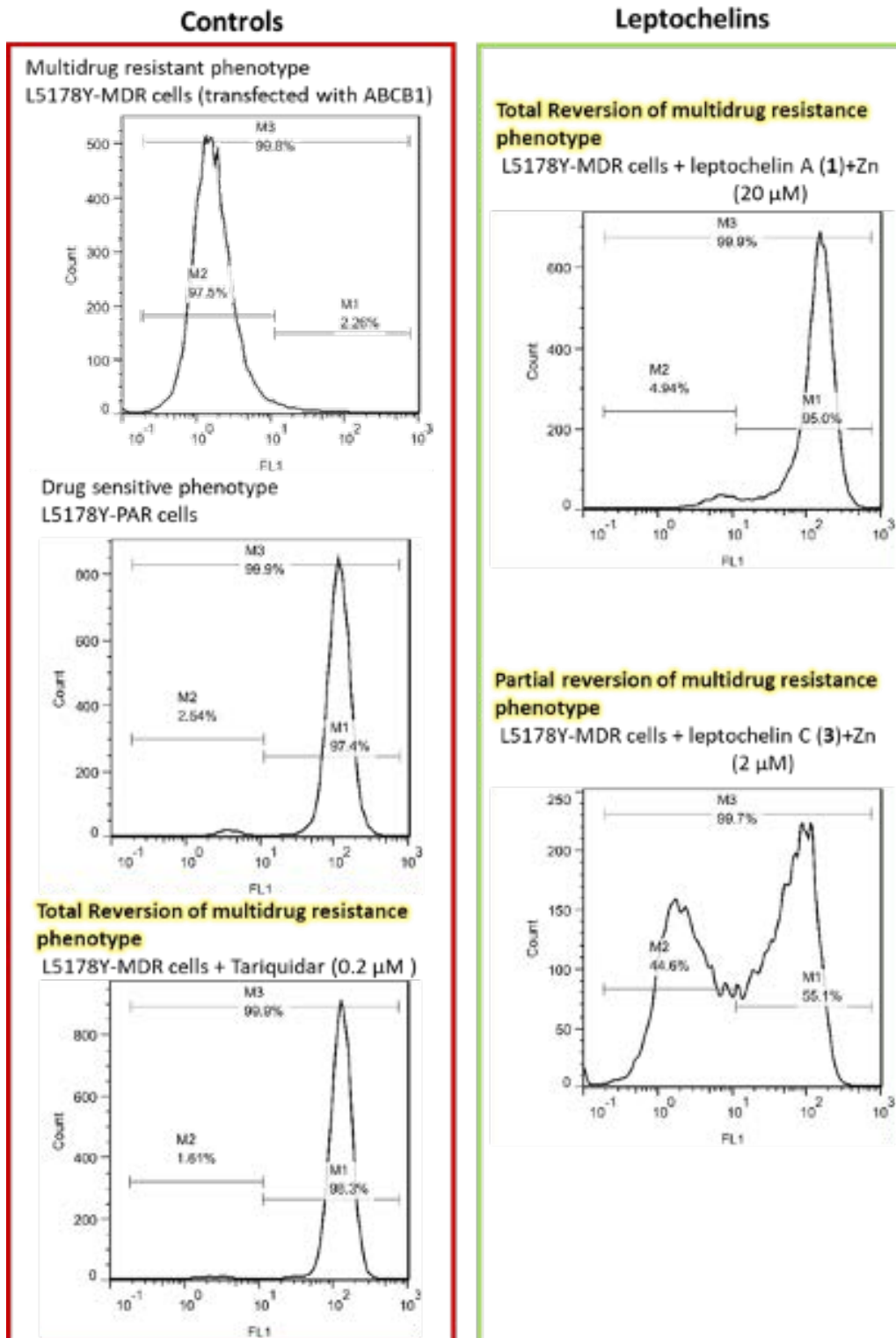


**Fig. S68.** Zinc-bound leptochelins A (1) and C (3) reverse multidrug resistance phenotype. Flow cytometry histograms illustrating the effect of the zinc-bound leptochelins A (1) at 20 μM and C (3) at 2 μM on the reversal of the multidrug resistance (MDR) phenotype through ABCB1-mediated rhodamine-123 efflux modulation. The results are compared with L5178Y-MDR chemo-resistant cells (showing low rhodamine-123 accumulation in the cytoplasm) and L5178Y-PAR parental chemo-sensitive cells (displaying high rhodamine-123 accumulation in the cytoplasm). The ABCB1 inhibitor tariquidar (0.2 μM) was used as positive control. The term "Count" on the ordinate axis is the number of individual cells belonging to the gated population M1 or M2. M3 represents the total cell count of the sample. The abscissa label "FL1" indicates the mean fluorescence intensity of rhodamine-123.



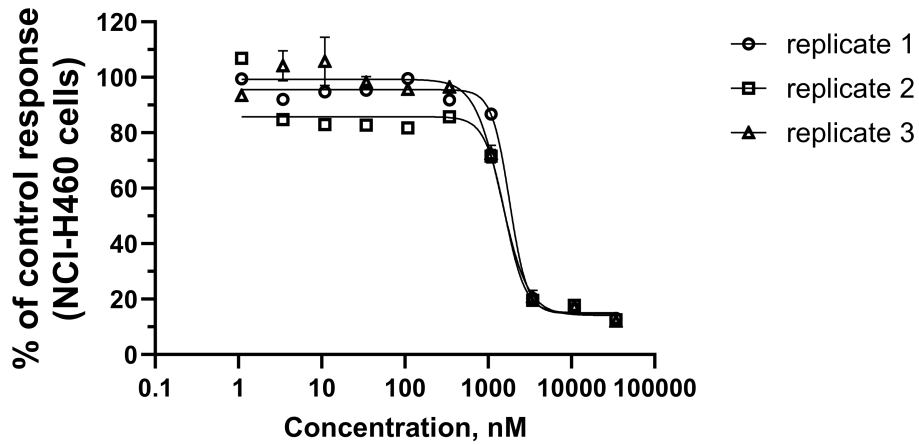


Fig. S69. The dose response curve for leptochelin A (1) in NCI-H460 cell line (3 technical replicates).

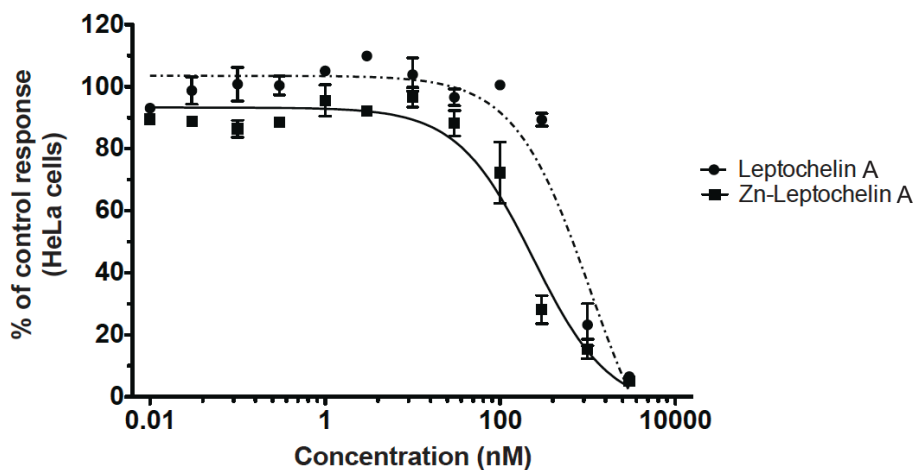
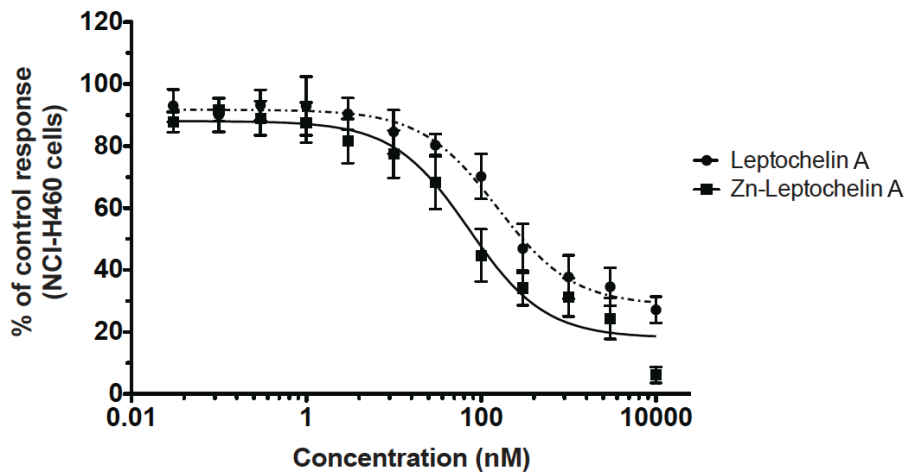
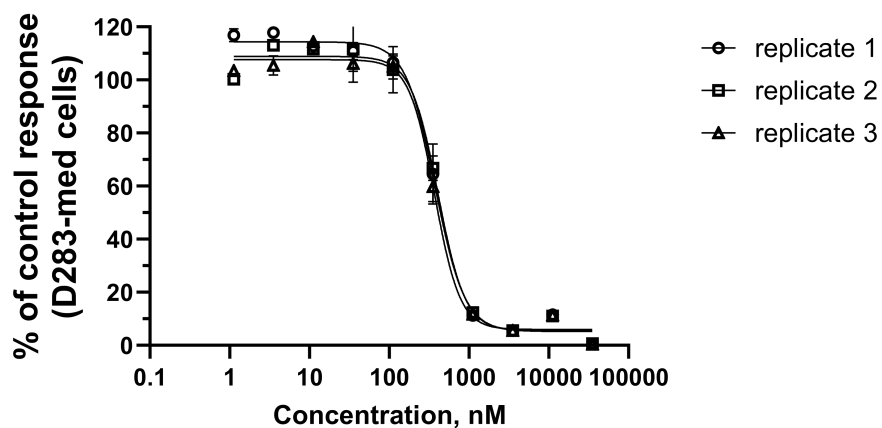
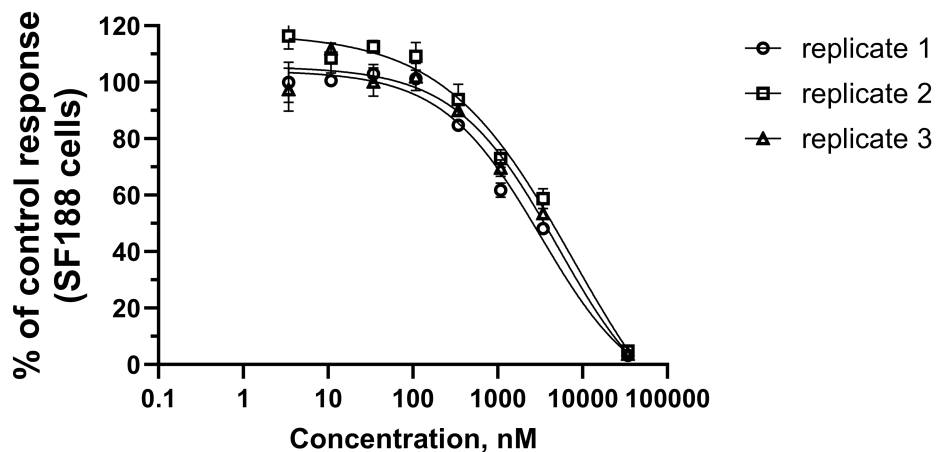


Fig. S70. The dose response curves for leptochelin A (1) and Zn-bound leptochelin A in human NCI-H460 (average of 3 technical replicates) and HeLa cervical carcinoma cell lines (average of 3 technical replicates). Cell viability was assessed after 48 hours using a colorimetric MTT cell viability assay and is reported as the percentage of viable cells relative to the vehicle control.



**Fig. S71.** The dose response curves for leptochelin A (1) in human D283-med medulloblastoma cell lines (3 technical replicates). Cell viability was assessed using a colorimetric MTT cell viability assay and is reported as a percentage of viable cells relative to the vehicle control.



**Fig. S72.** The dose response curves for leptochelin A (1) in human SF188 glioblastoma cell lines (three technical replicates). Cell viability was assessed using luminometry signals measured against a negative control and is reported as a percentage of viable cells relative to the vehicle control.

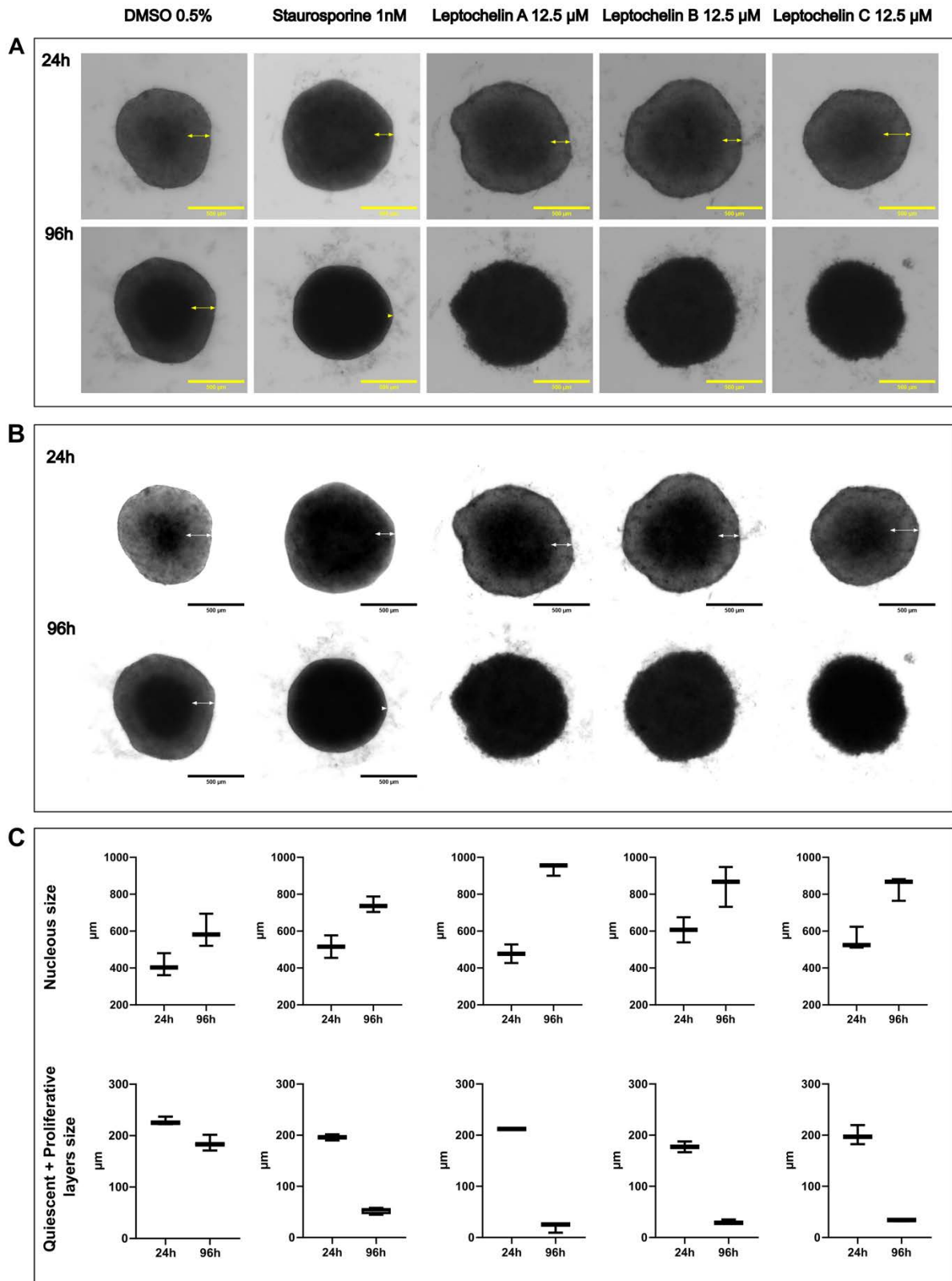


**Fig. S73.** Biological activity of the leptochelins in HCT 116 spheroids. **(A)** Brightfield micrographs of HCT 116 spheroids 24 and 96 hours after incubation with leptochelins A-C (1-3) and positive and negative controls. The size of the quiescent and proliferative layers is indicated by yellow double-headed arrows. Bars = 500  $\mu$ m. **(B)** Brightfield micrographs of HCT 116 spheroids from panel A with increased brightness of the image to visually enhance the delineation between layers. **(C)** Quantitative analysis of spheroid layers: diameter of the necrotic core and size of the quiescent and proliferative layers were measured as described in **(A and B)**. The values are given as mean sizes  $\pm$  SD for three spheroids.

## SI Appendix References:

1. C. C. Thornburg, *et al.*, Cyclic Depsipeptides, Grassypeptolides D and E and Ibu-epidemethoxylyngbyastatin 3, from a Red Sea *Leptolyngbya* Cyanobacterium. *J. Nat. Prod.* **74**, 1677–1685, (2011).
2. S. Andrews, FastQC: a quality control tool for high throughput sequence data., (2010), . Deposited 2010.
3. R. R. Wick, L. M. Judd, C. L. Gorrie, K. E. Holt, Unicycler: Resolving bacterial genome assemblies from short and long sequencing reads. *PLOS Comput. Biol.* **13**, e1005595, (2017).
4. D. D. Kang, *et al.*, MetaBAT 2: an adaptive binning algorithm for robust and efficient genome reconstruction from metagenome assemblies. *PeerJ* **7**, e7359, (2019).
5. D. H. Parks, M. Imelfort, C. T. Skennerton, P. Hugenholtz, G. W. Tyson, CheckM: assessing the quality of microbial genomes recovered from isolates, single cells, and metagenomes. *Genome Res.* **25**, 1043–1055, (2015).
6. K. Blin, *et al.*, antiSMASH 7.0: new and improved predictions for detection, regulation, chemical structures and visualisation. *Nucleic Acids Res.* **51**, W46–W50, (2023).
7. R. R. Wick, L. M. Judd, K. E. Holt, Performance of neural network basecalling tools for Oxford Nanopore sequencing. *Genome Biol.* **20**, 129, (2019).
8. W. De Coster, S. D'Hert, D. T. Schultz, M. Cruts, C. Van Broeckhoven, NanoPack: visualizing and processing long-read sequencing data. *Bioinformatics* **34**, 2666–2669, (2018).
9. R. R. Wick, Porechop, (2022), . Deposited 2022.
10. M. Kolmogorov, J. Yuan, Y. Lin, P. A. Pevzner, Assembly of long, error-prone reads using repeat graphs. *Nat. Biotechnol.* **37**, 540–546, (2019).
11. Y.-W. Wu, B. A. Simmons, S. W. Singer, MaxBin 2.0: an automated binning algorithm to recover genomes from multiple metagenomic datasets. *Bioinformatics* **32**, 605–607, (2016).
12. A. P. Arkin, *et al.*, KBase: The United States Department of Energy Systems Biology Knowledgebase. *Nat. Biotechnol.* **36**, 566–569, (2018).
13. K. Katoh, D. M. Standley, MAFFT Multiple Sequence Alignment Software Version 7: Improvements in Performance and Usability. *Mol. Biol. Evol.* **30**, 772–780, (2013).
14. K. Katoh, MAFFT: a novel method for rapid multiple sequence alignment based on fast Fourier transform. *Nucleic Acids Res.* **30**, 3059–3066, (2002).
15. D. Darriba, G. L. Taboada, R. Doallo, D. Posada, jModelTest 2: more models, new heuristics and parallel computing. *Nat. Methods* **9**, 772–772, (2012).
16. B. Q. Minh, *et al.*, IQ-TREE 2: New Models and Efficient Methods for Phylogenetic Inference in the Genomic Era. *Mol. Biol. Evol.* **37**, 1530–1534, (2020).
17. I. Letunic, P. Bork, Interactive Tree Of Life (iTOL) v5: an online tool for phylogenetic tree display and annotation. *Nucleic Acids Res.* **49**, W293–W296, (2021).
18. Inkscape Project, (2020), . Deposited 2020.
19. C. Prieto, C. García-Estrada, D. Lorenzana, J. F. Martín, NRPSsp: non-ribosomal peptide synthase substrate predictor. *Bioinformatics* **28**, 426–427, (2012).
20. G. L. Challis, J. Ravel, C. A. Townsend, Predictive, structure-based model of amino acid recognition by nonribosomal peptide synthetase adenylation domains. *Chem. Biol.* **7**, 211–224, (2000).
21. C. L. M. Gilchrist, Y.-H. Chooi, clinker & clustermap.js: automatic generation of gene cluster comparison figures. *Bioinformatics* **37**, 2473–2475, (2021).
22. B. R. Terlouw, *et al.*, MIBiG 3.0: a community-driven effort to annotate experimentally validated biosynthetic gene clusters. *Nucleic Acids Res.* **51**, D603–D610, (2023).
23. D. Petras, *et al.*, GNPS Dashboard: collaborative exploration of mass spectrometry data in the web browser. *Nat. Methods* **19**, 134–136, (2022).

24. J. B. Shaw, *et al.*, 21 Tesla Fourier Transform Ion Cyclotron Resonance Mass Spectrometer Greatly Expands Mass Spectrometry Toolbox. *J. Am. Soc. Mass Spectrom.* **27**, 1929–1936, (2016).
25. L. A. Dietz, Electrostatic Field Correction Using Tapered Rose Shims. *Rev. Sci. Instrum.* **32**, 859–860, (1961).
26. B. Morandi, E. M. Carreira, Iron-Catalyzed Cyclopropanation in 6 M KOH with in Situ Generation of Diazomethane. *Science* **335**, 1471–1474, (2012).
27. T. Kuranaga, *et al.*, Highly Sensitive Labeling Reagents for Scarce Natural Products. *ACS Chem. Biol.* **15**, 2499–2506, (2020).
28. K. Taori, V. J. Paul, H. Luesch, Structure and Activity of Largazole, a Potent Antiproliferative Agent from the Floridian Marine Cyanobacterium *Symploca* sp. *J. Am. Chem. Soc.* **130**, 13506–13506, (2008).
29. A. T. Aron, *et al.*, Native mass spectrometry-based metabolomics identifies metal-binding compounds. *Nat. Chem.* **14**, 100–109, (2022).
30. R. W. Castenholz, “[3] Culturing methods for cyanobacteria” in *Methods in Enzymology*, (Elsevier, 1988), , pp. 68–93.
31. N. A. Moss, T. Leao, E. Glukhov, L. Gerwick, W. H. Gerwick, “Collection, Culturing, and Genome Analyses of Tropical Marine Filamentous Benthic Cyanobacteria” in *Methods in Enzymology*, (Elsevier, 2018), , pp. 3–43.
32. M. L. Sousa, T. Ribeiro, V. Vasconcelos, S. Linder, R. Urbatzka, Portoamides A and B are mitochondrial toxins and induce cytotoxicity on the proliferative cell layer of in vitro microtumours. *Toxicon* **175**, 49–56, (2020).
33. M. L. Sousa, M. Preto, V. Vasconcelos, S. Linder, R. Urbatzka, Antiproliferative Effects of the Natural Oxadiazine Nocuolin A Are Associated With Impairment of Mitochondrial Oxidative Phosphorylation. *Front. Oncol.* **9**, 224, (2019).
34. A. G. Lewis, P. H. Whitfield, The biological importance of copper in the sea. A literature review., (1974).
35. R. N. McNeely, V. P. Neimanis, L. Dwyer, *Water Quality Sourcebook: A Guide to Water Quality Parameters* (Inland Waters Directorate, Water Quality Branch, 1979).